Characterization of dopaminergic innervation and receptor expression in mouse models and patients with Focal Cortical Dysplasia

Doctoral thesis

to obtain a doctorate (PhD)

from the Faculty of Medicine

of the University of Bonn

Norisa Meli

Vlore, Albania

2025

Written with authorization of
the Faculty of Medicine of the University of Bonn

First reviewer: Prof. Dr. Sandra Blaess

Second reviewer: Prof. Dr. Albert Becker

Day of oral examination: 24.04.25

From the Institute of Reconstructive Neurobiology
Director: Prof. Dr. Oliver Brüstle

Table of contents

List of abbreviations

4E-BP1	Eukaryotic Translation Initiation Factor 4E-Binding Protein 1
5-HT	Serotonin
AC	Anterior Cingulate
ADHD	Attention Deficit/Hyperactivity Disorder
AKT	Protein Kinase B
ANOVA	Analysis of Variance
ASD	Autism Spectrum Disorder
cAMP	Cyclic Adenosine Monophosphate
CB	Calbindin
DA	Dopamine
DARPP-32	Dopamine- and cAMP-Regulated Neuronal Phosphoprotein
DAT	Dopamine Transporter
DBH	Dopamine β-Hydroxylase
DCC	Deleted in Colorectal Cancer
DEPDC5	DEP Domain Containing 5
DISC1	Disrupted-In-Schizophrenia 1
DOPAC	3,4-dihydroxyphenylacetic acid
DRD	Dopaminergic Receptor
E	Embryonic day
E/I	Excitation/Inhibition
EEG	Electroencephalography
EGFP	Enhanced Green Fluorescent Protein
EZ	Epileptic Zone
FCD	Focal cortical dysplasia
FDG	Fluorodeoxyglucose Positron Emission Tomography
FFPE	Formalin-Fixation Paraffin-Embedding
FISH	Fluorescence *In Situ* Hybridization
FS	Fast-Spiking
GABA	Gamma Amino Butyric Acid
GAP	GTPase-activating proteins
GATOR1	GAP Activity Toward Rags

GFP	Green Fluorescent Protein
GW	Gestational Week
H&E	Haematoxylin and Eosin
HME	Hemimegalencephaly
HPLC	High-Performance Liquid Chromatography
HSD	Honestly Significant Difference
HVA	Homo-Vanillic Acid
IHC	Immunohistochemistry
IL	Infralimbic Cortex
ILAE	International League Against Epilepsy
IQ	Intelligence Quotient
IRS1	Insulin Receptor Substrate 1
IUE	*In Utero* Electroporation
LC	Locus Coeruleus
M/TLE	Mesial/Temporal Lobe Epilepsy
MCD	Malformations of Cortical Development
mDA	Midbrain Dopaminergic
MFB	Medial Forebrain Bundle
mPFC	Medial Prefrontal Cortex
MRI	Magnetic Resonance Imaging
MSN	Medium Spiny Neurons
MTORC1/2	Mammalian Target of Rapamycin Complex 1/2
NA	Noradrenaline
NDS	Normal Donkey Serum
NET	Norepinephrine Transporter
NeuN	Neuronal Nuclear Protein
NF	Neurofilament
NPRL2/3	Nitrogen Permease Regulator-Like 2/3
P	Postnatal Day
PBS-T	Phosphate-Buffered Saline-Triton/Tween-20
PDK1	3-Phosphoinositide-Dependent Kinase 1
PET	Positron Emission Tomography

PI3K	Phosphoinositide 3-Kinase
PKA	Protein Kinase A
PL	Prelimbic Cortex
pS6	phospho-S6
PTEN	Phosphatase and Tensin Homolog
PTZ	Pentylenetetrazole
PV	Parvalbumin
RFP	Red Fluorescent Protein
RHEB	Ras Homolog Enriched in Brain
ROI	Region of Interest
RRF	Retrorubral Field
RS-FISH	Radial Symmetry-FISH
SD	Standard Deviation
SEM	Standard Error of The Mean
SERT	Serotonin Transporter
SMI32	Non-phosphorylated Neurofilament H Subunit
SNc	Substantia Nigra Pars Compacta
SPECT	Single-Photon Emission Computed Tomography
TH	Tyrosine Hydroxylase
TSC1/2	Tuberous Sclerosis Complex 1/2
VTA	Ventral Tegmental Area
VZ	Ventricular zone
WT	Wild Type

1. Introduction

1.1. Cortical development

The cerebral cortex is a highly-specialized brain structure featuring various types of neurons with specific functions arranged across several distinct layers (Cadwell et al., 2019). Cortical development involves several key stages and mechanisms that lead to the formation and maturation of the cerebral cortex, which initiate during fetal growth and continue into early adulthood. Cortical excitatory neurons are generated from neural stem cells and progenitor cells located in the ventricular zone (VZ) of the brain between embryonic (E) days 11 and 17 in mice and between gestational week (gw) 6 and gw 28 in humans (Cadwell et al., 2019; Caviness et al., 1995; Malik et al., 2013; Rakic, 1995). These stem cells divide and differentiate into neurons in a tightly regulated manner, guided by intrinsic and external cues (Agirman et al., 2017; Jiang et al., 2023). Once these postmitotic neurons are generated, they migrate radially from the VZ and travel along radial glial fibers, specialized cells that serve as scaffolds for migrating neurons, towards the pial surface until they reach their final locations and organize themselves into one of the 6 distinct layers within the cortical plate (Noctor et al., 2001; Rakic, 1972, 1978). These layers are formed in an inside-out manner, with early-born neurons forming deep layers and later-born neurons forming more superficial layers (Angevine & Sidman, 1961). Cortical migration starts around E12 in mice and neurons born between E12-E13 migrate to form the deeper layers 5 and 6, whereas neurons generated between E14-E16 will migrate towards the upper layers L4 and L2/3 (Cadwell et al., 2019; Kwan et al., 2012). In humans, the majority of cortical migratory events are believed to happen between the third and fifth months of gestation and to be completed by the third trimester (Bystron et al., 2008; Gressens, 2000; Rakic et al., 1994; Sidman & Rakic, 1973). The precise organization of these layers is critical for the establishment of functional neural circuits as these neurons, once properly localized, acquire distinct morphologies and functions. This maturation process also involves the formation of synapses between neurons, facilitating communication through neurotransmitters, thus establishing functional neuronal connectivity (Bystron et al., 2008; Cadwell et al., 2019; Rakic & Lombroso, 1998). In mice, cortical organization and differentiation are largely completed around birth (Bystron et al., 2008; Subramanian, Calcagnotto, & Paredes, 2020). In humans, synaptogenesis begins

at 22 gw, but continues postnatally in a region-dependent manner e.g., for 8–12 months in the visual cortex and for 2–4 years of age in the prefrontal cortex (Huttenlocher et al.,1982; Huttenlocher, 1979).

1.2. Malformations of cortical development

Disruptions in one or more of these critical processes of cortical development leads to malformations of cortical development (MCDs) which encompass a broad spectrum of structural abnormalities associated with developmental delay and epilepsy (Barkovich et al., 1996; Desikan & Barkovich, 2016; Subramanian et al., 2020). These malformations can arise from germline or somatic genetic mutations or environmental insults which affect the cortical structural organization and circuitry. Analysis of 9,523 brain specimens collected from patients who underwent surgery for drug-resistant epilepsies show that MCDs are found in around 20% of these patients and are thus third most common histopathological disease diagnosed in these patients, after hippocampal sclerosis and tumors (Blümcke et al., 2017). Moreover, MCDs were the most common histopathological diagnosis among pediatric cohorts making up for about 40% of the diagnosis (Blümcke et al., 2017).

There are a number of possible mechanisms resulting in MCDs. Abnormal progenitor proliferation and apoptosis might result in microcephaly, a disorder caused primarily due to reduced progenitor numbers. Alternatively, if such events occur in a more localized manner they can cause cortical dysplastic malformations like Focal Cortical Dysplasias (FCD), Tuberous Sclerosis (TSC), or Hemimegalencephaly (HME) (Desikan & Barkovich, 2016; Subramanian et al., 2020). The latter disorders, are often characterized by causative mosaic mutations that primarily affect the mammalian target of rapamycin (mTOR) signaling pathway and are then termed “mTORopathies" (Crino, 2015; Iffland & Crino, 2017). The mTOR-signaling cascade is a major regulator of essential cellular processes such as homeostasis, energy metabolism, cell proliferation, differentiation, migration, cytoskeletal organization, and autophagy (Dobashi et al., 2011; Laplante & Sabatini, 2009; Zoncu et al., 2011). Key genes implicated in “mTORopathies” include *PIK3*, *AKT1/3*, *TSC1/2*, *DEPDC5*, and *MTOR* (D’Gama et al., 2015, 2017; Hoelz et al., 2018; Lee et al., 2012; Lim et al., 2017; Poduri et al., 2012). Mutations in these genes lead

to hyperactivation of mTOR signaling, which can impact cell proliferation, differentiation, and cell size. Finally, altered neuronal migration is the underlying cause for disorders like lissencephalies, which are characterized by a smooth brain and heterotopias. Heterotopias form when neurons accumulate in abnormal locations due to incomplete migration (Desikan & Barkovich, 2016; Subramanian et al., 2020).

1.3. Focal cortical dysplasia

Focal Cortical Dysplasia (FCD) is one of the most common types of MCDs and is characterized by focally-localized malformed structures in the cerebral cortex (Blümcke et al., 2011). FCDs are a major cause of pharmacorefractory epilepsies (Baldassari et al., 2019a). Based on the histopathological features, the International League Against Epilepsy (ILAE) classifies FCDs in 3 main types and additional subtypes: FCD Type 1 is characterized by disrupted cortical layering. This condition manifests in two variants: Type 1a, which affects the radial migration and maturation of neurons, and Type 1b, which disrupts the 6-layered tangential structure of the neocortex. When both abnormalities are present, the condition is classified as Type 1c (Blümcke et al., 2011; Najm et al., 2022). FCD Type 2 is associated with disrupted cortical layering with additional distinctive cytological abnormalities such as dysmorphic neurons and balloon cells. Type 2a features only dysmorphic neurons without the presence of balloon cells, and Type 2b includes both dysmorphic neurons and balloon cells **(Fig. 1A)** (Blümcke et al., 2011; Najm et al., 2022). Dysmorphic neurons are characterized by a markedly enlarged cell body (16-43µm) and nucleus (15-28µm), disorientation and the accumulation of neurofilament (NF) proteins within the cytoplasm **(Fig. 1B)** (Blümcke et al., 2011). They can be found in any cortical layer or also white matter. Balloon cells are characterized by a large cell body and can contain multiple nuclei. They are identified with H&E staining as their cytoplasms appear as opalescent, glassy eosinophilic **(Fig. 1C)** and can also accumulate intermediate filaments, such as nestin and vimentin. Balloon cells can also be located throughout the cortical layers, but are frequently found in the white matter (Blümcke et al., 2011). FCD Type 3 occurs when the cortical malformation is associated with a principal lesion, typically adjacent to or in the same cortical area. This malformation is further categorized into four subtypes: Type 3a is associated with hippocampal sclerosis; 3b is associated with tumors;

Type 3c is associated with vascular malformations and Type 3d is linked to other primary lesions that develop early in life (Blümcke et al., 2011; Najm et al., 2022).

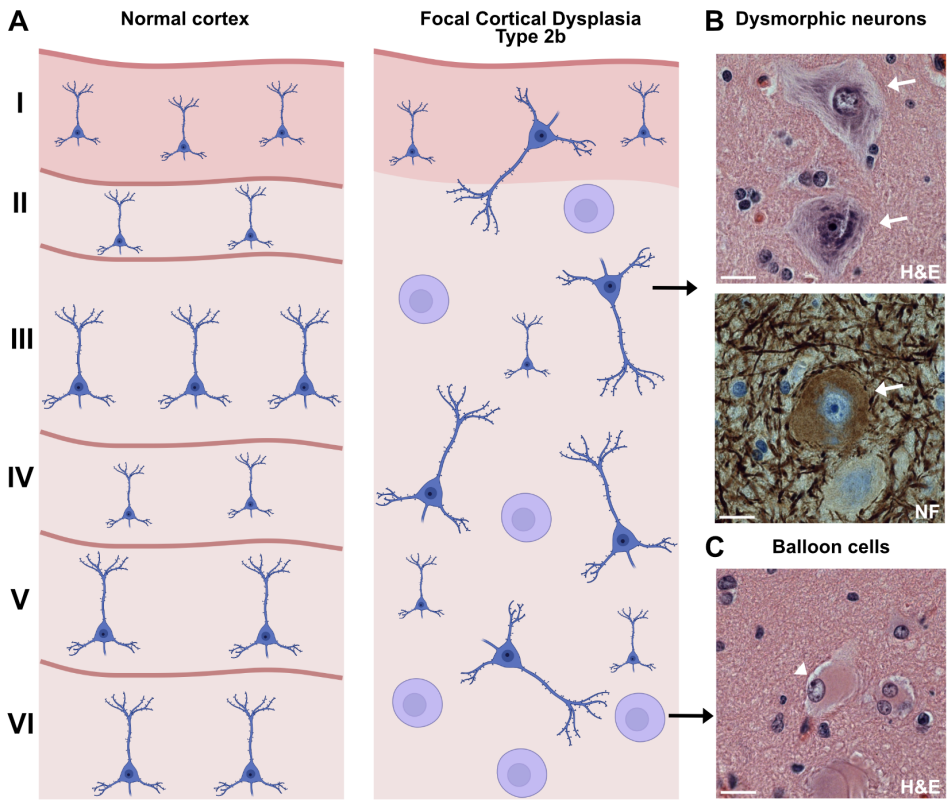

Fig. 1. Neuropathological markers of FCD type 2b in humans. **A)** Schematic comparison between a normally-developed cortex (left), showing proper formation of the six cortical layers, and disrupted cortical layering in FCD patients (right), with cytological abnormalities characteristic of FCD type 2b. Created with BioRender.com **B)** H&E and NF (clone 2F11) staining highlighting dysmorphic neurons (white arrows) in human FCD type 2b specimen. **C)** Identification of balloon cells (white arrowheads) with H&E staining in human FCD type 2b specimen. Scale bar: 20 µm.

To diagnose FCDs and the extent of the epileptic zone (EZ), a combination of multiple advanced imaging techniques can be implemented: magnetic resonance imaging (MRI) to detect structural abnormalities associated with FCD and electroencephalography (EEG) to detect epileptiform discharges present in FCD patients (Kim et al., 2011; Seifer et al., 2012; Sierra-Marcos et al., 2013). Additional tools can be employed such as fluorodeoxyglucose positron emission tomography (FDG-PET) to detect hypometabolism in the dysplastic cortex, since the hypometabolic area is thought to correspond to the EZ in FCD patients. Ictal and interictal single-photon emission computed tomography

(SPECT) is used to identify changes in cerebral blood flow related to seizure activity in the dysplastic region (Kim et al., 2011; Krsek et al., 2013; Schur et al., 2018). These tools aid in identifying neuropathological hallmarks associated with FCDs like focal cortical thickening, blurring of the gray-white matter boundary, which is caused by abnormal neuronal migration and proliferation, and other abnormal white matter features such as reduced myelination or dysplastic white matter tracts (Falco-Walter et al., 2017; Seifer et al., 2012).

Patients with drug-resistant epilepsy often have to undergo surgery to alleviate seizure activity. FCD is the most common etiology in children and adolescents (under 18 y.o.) and the third most common one in adults (above 18 y.o.) after other etiologies like hippocampal sclerosis and tumors in patients undergoing epilepsy surgeries (Lerner et al., 2009). According to the same study, seizure onset in FCD patients is at a younger age (2.6 y.o.) and occurs with higher frequency than in the other epilepsy etiologies that result in surgery (Lerner et al., 2009). Some studies report that around 60% of the patients achieve seizure freedom after surgery (Alexandre et al., 2006; Hauptman & Mathern, 2012; Kim et al., 2009; Kloss et al., 2002). This surgical outcome largely depends on the extent of lesion resection, with complete resections leading to seizure freedom in up to 80% of patients, compared to only 20% in cases of incomplete resections (Hauptman & Mathern, 2012; Krsek et al., 2009).

Furthermore, patients with FCD often experience additional symptoms and comorbidities. Studies found that around 51% of children (0-17 y.o.) with FCD suffered from cognitive impairments and also observed that younger epilepsy onset patients performed weaker cognitive functioning in neuropsychological intelligence quotient (IQ) tests (Veersema et al., 2019). Furthermore, in one study, 22% of FCD patients were diagnosed with psychiatric disorders, and approximately 37% of the patients exhibited psychiatric symptoms, a higher rate than in any other MCD group analyzed in the study (Ho et al., 2019). Among these psychiatric symptoms, anxiety-related symptoms were the most prevalent (60%), but other symptoms like irritability (40%) and depression (27%) were also observed (Ho et al., 2019).

1.3.1. FCD type 2 and mTOR pathway

FCD type 2 is the most common type of MCD, particularly in pediatric individuals, accounting for 17% of the cases in children under 18 years old (Blümcke et al., 2017). Additionally, it is the most severe type of FCD with patients experiencing earlier age onset of epilepsy seizures, typically around 6 years old, compared to other histopathological conditions like hippocampal sclerosis (age onset around 11 years old) and ganglioglioma (age onset around 12 years old) in patients who undergo epilepsy surgery (Blümcke et al., 2017). FCD type 2 might arise due to mosaic somatic mutations occurring in neural progenitor cells during early stages of development affecting progenitor proliferation and/or neuronal migration (Desikan & Barkovich, 2016; Subramanian et al., 2020). Several of these mutations are in genes that encode for proteins in the mTOR signaling pathway. Hence FCD type 2 is part of the group of neurodevelopmental disorders known as "mTORopathies" (See above 1.2.). mTOR signaling is a prominent pathway involved in cell proliferation, growth, metabolism and autophagy. The mTOR protein is a 289-kDa serine-threonine kinase and can be part of mTOR complex 1 (mTORC1) and mTOR complex 2 (mTORC2) (Laplante & Sabatini, 2009, 2012; Loewith et al., 2002). The mTOR pathway is regulated by growth factors, hormones and other metabolic components. For example, when insulin is bound to receptors like IRS1 (Insulin Receptor Substrate 1) on the cell surface, it signals through the PI3K (Phosphoinositide 3-Kinase) pathway. This leads to the activation of PDK1 (3-Phosphoinositide-Dependent Kinase 1), which in turn activates the protein kinase AKT (also known as Protein Kinase B) **(Fig. 2)** (Laplante & Sabatini, 2009; Lawlor & Alessi, 2001). AKT plays a key role in inhibiting the TSC1/TSC2 complex (Inoki et al., 2002; Laplante & Sabatini, 2009; Potter et al., 2002), which consists of the proteins TSC1 (Tuberous Sclerosis Complex 1 or known as hamartin) and TSC2 (Tuberous Sclerosis Complex 2 or tuberin) **(Fig. 2)**. Generally, TSC1/TSC2 act as GTPase-activating proteins (GAP) for the Ras homolog enriched in brain (Rheb) GTPase. In its GTP-bound form, Rheb directly engages with mTORC1, significantly enhancing its kinase activity. By functioning as a GAP, the TSC1/2 complex inhibits mTORC1 by converting Rheb into its inactive GDP-bound state (Inoki et al., 2003; Laplante & Sabatini, 2009; Tee et al., 2003). Thus, when AKT inhibits the TSC1/TSC2 complex, Rheb becomes active and thus activates mTORC1 **(Fig. 2)**. When mTORC1 is activated, it

phosphorylates downstream targets. Phosphorylation of S6K (Ribosomal Protein S6 Kinase) results in S6K activation and in phosphorylation of the ribosomal protein S6. Phosphorylation of 4E-BP1 (Eukaryotic Translation Initiation Factor 4E-Binding Protein 1) leads to its inhibition. Since 4E-BP1 is a repressor of cap-dependent translation, this inhibition results in the release of the translation initiation factor eIF4E, allowing the initiation of cap-dependent translation **(Fig. 2)**. These signaling cascades lead to increased protein synthesis and regulation of processes like cell growth and proliferation (Laplante & Sabatini, 2009, 2012; Ma & Blenis, 2009).

Other proteins that affect the mTOR signaling pathway are (1) PTEN (Phosphatase and Tensin Homolog), a tumor suppressor protein, which acts as a negative regulator of the PI3K/PDK1/AKT pathway, thus preventing the activation of AKT and resulting in suppression of the mTORC1 (Crino, 2011; Kwon et al., 2003) **(Fig. 2)** and (2) the GATOR1 (GAP Activity Toward Rags) complex, which consists of the proteins NPRL3 (Nitrogen Permease Regulator-Like 3), NPRL2 (Nitrogen Permease Regulator-Like 2), and DEPDC5 (DEP Domain Containing 5). GATOR1 regulates mTORC1 activity in response to amino acid availability. Specifically, GATOR1 acts as negative regulator and inhibits mTORC1 under conditions of amino acid deprivation (Bar-Peled et al., 2013; Panchaud et al., 2013) **(Fig. 2)**. Somatic and germline mutations in various components of this pathway such as *PTEN*, *TSC1/2, GATOR1* complex *and MTOR* have been associated with FCD type 2 (all reviewed in Crino, 2015; Iffland & Crino, 2017; Mühlebner et al., 2019) **(Fig. 2)**. These mutations generally cause a downstream activation of mTORC1 thus leading to dysregulated cell growth and signaling. Among these, brain somatic missense *MTOR* mutations are the most commonly reported, particularly in patients with FCD Type 2 (Baldassari et al., 2019b; D'Gama et al., 2015; Jesus-Ribeiro et al., 2021; Leventer et al., 2015; Lim et al., 2015; Mirzaa et al., 2016) **(Fig. 2)**. The identified mutations cause mTOR hyperactivation. This hyperactivation might contribute to the emergence of dysmorphic neurons and balloon cells, the cell types typically associated with FCD type 2 like. Indeed, a study performing laser-capture microdissection in FCD type 2 patients confirmed the presence of the mTOR hyperactivating mutations in these cells (Baldassari et al., 2019b).

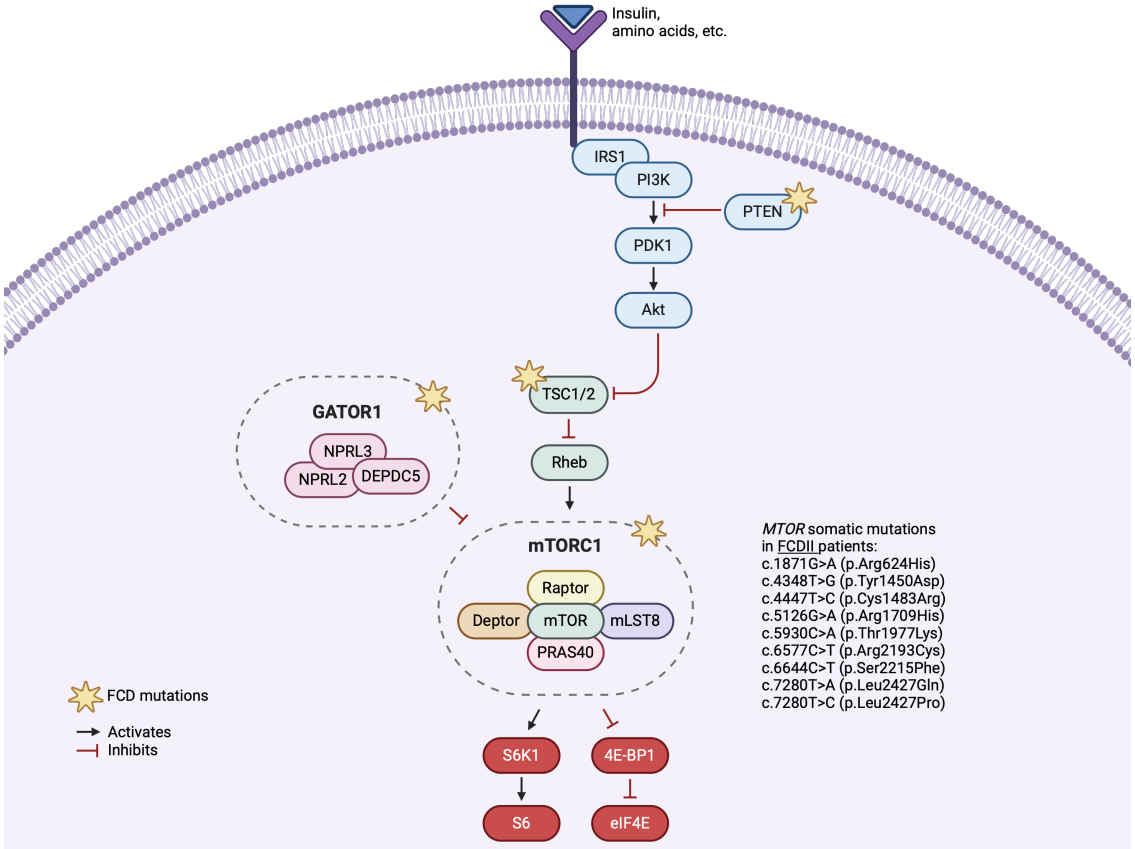

Fig. 2. mTOR signaling pathway and causative mutations in FCD type 2. Proteins or complexes for which mutations have been identified in FCD patients are marked with a star. Abbreviations: IRS1, insulin receptor substrate 1; PI3K, PI3kinase; PDK1, phosphoinositide-dependent kinase-1; PTEN, phosphatase and tensin homologue; AKT, protein kinase B; TSC1/2, Tuberous Sclerosis Complex 1/2; RHEB, ras homolog enriched in brain; mTORC1, mammalian target of rapamycin complex 1; GATOR1, Gap Activity TOward Rag 1; DEPDC5, DEP Domain Containing 5; NPRL2, NPR2 Like, GATOR1 Complex Subunit; NPRL3, NPR3 Like, GATOR1 Complex Subunit; S6K1, p70S6kinase; S6, ribosomal S6 protein; 4EBP1, eIF4E-binding protein 1; eIF4E, binding of eukaryotic translation. Modified from (Mühlebner et al., 2019). List of MTOR somatic mutations from FCD type 2 patients is based on (Lim et al., 2015). Created with BioRender.com

Given the complexity of this type of neurodevelopmental malformation and the necessity to elucidate the underlying mechanisms of FCD type 2, several *in vivo* mouse models were developed by introducing some of the above-mentioned mutations in the mTOR pathway. A comprehensive summary of these models is provided by Nguyen & Bordey, 2021. For example, introducing a mutated *MTOR* (p.Leu2427Pro) construct into the developing cortex of E14 mice *via* in utero electroporation resulted in impaired neuronal migration, formation of enlarged neurons and also induced spontaneous seizures (Lim et al., 2015). Treatment with rapamycin, an mTOR inhibitor, effectively reduced the enlarged

neuron sizes and the frequency of epileptic seizures (Lim et al., 2015). Overall, this model was able to recapitulate some of the major molecular and pathological hallmarks of FCD type 2. These kinds of *in vivo* models serve as important tools to investigate the underlying mechanisms of FCD Type 2 and to evaluate potential therapeutic interventions targeting the molecular and cellular dysregulations associated with the disorder.

1.4. Long-range monoaminergic inputs in the PFC

Epileptic activity in FCD type 2 patients is often associated with abnormal intrinsic electrophysiological properties of dysmorphic neurons and balloon cells. Dysmorphic neurons have electrophysiological properties that make them hyperexcitable, whereas balloon cells are unable to generate action potentials (Cepeda et al., 2005, 2006, 2003). The presence of these abnormally developed cells and/or their interaction with normal neurons in the FCD type lesion can affect the excitation/inhibition (E/I) balance in the lesion area and be the underlying cause of the epileptic activity (Cepeda et al., 2006). The E/I balance of cortical circuits, in particular in frontal areas, is modulated be monoaminergic systems like the dopaminergic (DA), noradrenergic (NA) and serotonergic (5-HT) that innervate the frontal cortex (Cools & Arnsten, 2022; Kalsbeek et al.,1988; Lidov et al., 1980; Waterhouse & Chandler, 2016) **(Fig. 3)**. The effect of monoaminergic modulators on cortical function has been studied in detail for the prefrontal cortex (PFC). The PFC is the hub of higher cognitive functions such as working memory, goal-directed behavior, planning and problem-solving in both primates and rodents, but there are important anatomical and functional distinctions to consider. The PFC covers the most rostral part of the frontal cortex. There is still no consensus on the definition of the PFC, largely due to ongoing disagreements about the subdivisions of prefrontal cortical areas across different species. In humans, the PFC is divided into several specialized regions, including the dorsolateral (dlPFC), dorsomedial (dmPFC), ventrolateral (vlPFC), ventromedial (vmPFC), and orbital (OFC) prefrontal cortices **(Fig. 3)**. Most of these regions are granular, displaying a 6-layered cortical structure. Some areas of the primate PFC, such as the anterior cingulate cortex, are dysgranular, with a less defined layer IV, or agranular, where layer IV is absent. In rodents, the prelimbic (PL), infralimbic (IL), and anterior cingulate (AC) cortices constitute the medial PFC (mPFC) **(Fig. 3)** and even though is agranular, is considered functionally analogous to human PFC regions (Carlén,

2017; Laubach et al., 2018). While the development of the PFC follows the general stages of cortical development, it is among the last cortical regions to fully mature, continuing to develop into adulthood in both humans and rodents (Kolk & Rakic, 2022; Petanjek et al., 2011).

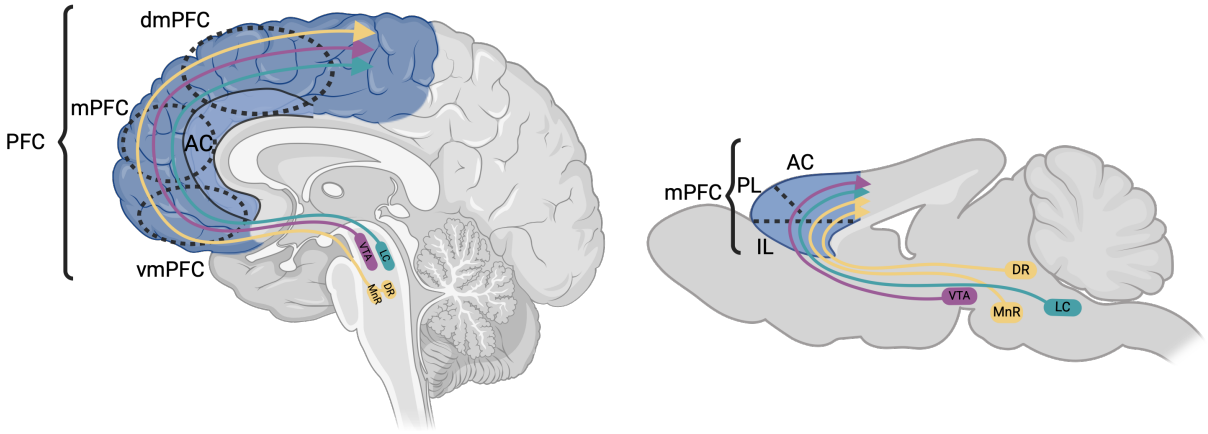

Fig. 3. Anatomical distinction of the PFC and long-range monoaminergic modulation pathways in human and mouse PFC. Sagittal view of human (left) and mouse (right) PFC regions. Blue area shows the whole frontal cortex. PFC is specified and distinct regions visible are: dorso-medial PFC (dmPFC), medial PFC (mPFC), ventro-medial PFC (vmPFC) and anterior cingulate cortex (AC) in human; prelimbic cortex (PL), infralimbic cortex (IL) and AC in mouse. Adapted from Mohapatra & Wagner, 2023. Areas like dorsolateral (dlPFC), ventrolateral (vlPFC), and orbital (OFC) PFC in human are not shown. DA innervation (purple) coming from the ventral tegmental area (VTA). NA innervation (green) coming from the locus coeruleus (LC). 5-HT innervation (yellow) coming from the dorsal raphe nucleus (DR) and median raphe nucleus (MnR). Adapted from Boyle et al., 2024. Created with BioRender.com

1.4.1. Dopaminergic inputs

1.4.1.1. Development of mesoprefrontal dopaminergic system

The DA system is a crucial neuromodulatory system involved in motor control, reward processing, and modulation of cognitive functions (Iversen et al., 2009). The midbrain dopaminergic (mDA) system is comprised of DA neurons that are mainly located in the retrorubral field (RRF, A8), substantia nigra pars compacta (SNc, A9) and the ventral tegmental area (VTA, A10) of the midbrain (Björklund & Dunnett, 2007). These mDA neurons send their axons toward different forebrain structures. The mesoprefrontal

/mesocortical DA system includes projections from the medial VTA to the mPFC and other frontal areas (Lammel et al., 2008) **(Fig. 3)**. This pathway plays a critical role in higher cognitive functions, including working memory, attention, and executive decision-making (Goldman-Rakic et al., 2000; Robbins & Arnsten, 2009; Seamans & Yang, 2004).

The development of mDA neurons occurs within a specialized region of the neural tube known as the ventral midbrain floor plate, which is established at early stages of embryonic development. The Sonic Hedgehog pathway is one of the signaling pathways important for establishing the mDA progenitor domain. As a ventralising factor, it is necessary from E8.0 onwards to establish the floor plate and thus the mDA progenitors cells (Blaess et al., 2011). As development continues, these mDA progenitors start to differentiate into mDA neurons. Tyrosine hydroxylase (TH), the rate-limiting enzyme in DA synthesis, is first detected in a small group of differentiated neurons around E10.5 in mice (Dumas & Wallén-Mackenzie, 2019). Neurogenesis continues until about E14.5 (Petese et al., 2022). After E10.5, differentiated mDA neurons migrate to their final location in the SN or VTA and start to extend their axons through the medial forebrain bundle (MFB), which then gradually innervates the forebrain targets like the mPFC. A subset of neurons in the VTA forms the mesocortical/mesoprefrontal system during this developmental process (Iversen et al., 2009). In rodents, the development of the mesocortical DA system begins around E11-12, with the extension of DA axons. Around E13.5 TH-expressing axons take a rostral trajectory and collectively create the MFB which then extends towards the forebrain (Islam & Meli et al., 2021; Kolk et al., 2009; Nakamura et al., 2000). While some of these axons enter the striatum, a fraction of them will reach the frontal cortical subplate and marginal zone by E15 in mice and E17 in rats. However, these axons do not immediately enter the cortical plate, instead, they appear to pause until around E18.5 in mice and E20 in rats, only after that they begin to innervate the cortex (Islam & Meli et al., 2021; Kalsbeek et al., 1988; Kolk et al., 2009). Several guidance molecules have been identified in the axonal pathfinding of mesoprefrontal DA axons, including Semaphorins, and Netrins. In early mDA development, Semaphorin 3F, via its receptor Neuropilin-2 that is expressed in mDA neurons, initially repels mDA axons away from the midbrain, but later acts as a chemoattractant guiding them to the cortical plate of the mPFC during prenatal stages (Kolk et al., 2009). Additionally, Netrin-1, an extracellular protein, and its receptor,

deleted in colorectal cancer (DCC), are crucial in guiding mesoprefrontal and mesolimbic DA axons. Netrin-1 binds to DCC receptors to attract axons. Mesolimbic mDA axons, which target the nucleus accumbens, show high DCC levels, whereas mesoprefrontal mDA axons, targeting the PFC, express low DCC levels. Reduced DCC expression, as in *Dcc* haplosufficient mice, leads to increased mDA innervation in the mPFC. Proper DCC-Netrin-1 expression during adolescence is crucial for directing mDA axons to their final targets (Hoops & Flores, 2017; Reynolds et al., 2018).

In humans, the development of the mesocortical DA system begins in early gestation. TH-positive neurons are first detected around 6 gw, and these neurons start forming axons toward the telencephalic wall of the cortex by 7-8 gw. Similar to rodents, these axons also initially remain in the intermediate and subplate domain (for 4 weeks) before innervating the cortical plate (Islam & Meli et al., 2021; Verney, 1999; Zecevic & Verney, 1995). Dense TH innervation is observed in frontal cortical areas at 20-24 gw with areas like motor and anterior cingulate cortex exhibiting higher innervation than more rostral PFC areas (Islam & Meli et al., 2021; Verney et al., 1993). This area-specific innervation density is comparable to that observed in the adult cortex (Gaspar et al., 1989), suggesting a robust prenatal innervation pattern that then continues to increase in density postnatally (Islam & Meli et al., 2021; Verney, 1999; Verney et al., 1993). Certain areas like the PFC and parietal cortex display a characteristic bi-laminar distribution of DA axons in adulthood where the upper and deeper layers exhibit denser innervation than the middle layers (Gaspar et al., 1989; Islam & Meli et al., 2021; Raghanti et al., 2008). This lamination pattern is already partially established at midgestation in prefrontal areas, where the highest density of TH-positive axons was observed in the deeper cortical plate and upper subplate areas. In contrast, sparse innervation was seen in the upper layers, such as layer I, indicating ongoing remodeling and development of DA innervation that continues until adulthood (Islam & Meli et al., 2021; Verney, 1999; Verney et al., 1993). A protracted postnatal development of the DA input is also observed in rodents, where DA innervation and DA concentration gradually increase postnatally, particularly during the juvenile (postnatal day (P)25) and adolescent (P30/P45) periods in the mPFC, until reaching full maturation in adulthood (P70) (Naneix et al., 2012). The maturation of the mesocortical DA axons also involves the formation of varicosities along the axons, which are potential

sites of DA release. These DA varicosities have been observed to form selective contacts with gamma amino butyric acid (GABA)-positive interneurons in the rat mPFC (Benes et al., 1993). Moreover, the density of varicosities adjacent to GABA-positive neurons increased gradually postnatally until it reached adult levels at P60 in the rat mPFC (Benes et al., 1996). Thus, the increase in the number of these varicosities correlates with the protracted maturation of the DA system that proceeds in parallel with the increasing functional maturation of the mPFC during this critical postnatal period. Volume transmission has been suggested for DA, however junctional complexes have been observed on 93% of DA varicosities in the rat anteromedial PFC, suggesting that DA transmission in the PFC is predominantly synaptic (Lapish et al., 2007; Séguéla et al., 1988).

1.4.1.2. Dopaminergic receptors

The effects of DA on the receiving neurons is mediated primarily through DA receptors (DRDs). DRDs are divided into two families: the D1-like family (including DRD1 and DRD5) and the D2-like family (including DRD2, DRD3, and DRD4). DRDs are G-protein-coupled receptors that modulate intracellular signaling and can be expressed pre- and also postsynaptically in nerve terminals and axonal varicosities and also in dendritic shafts and spines, respectively (Islam & Meli et al., 2021; Missale et al., 1998; Tritsch & Sabatini, 2012). Activation of D1-like receptors stimulate the activity of adenylyl cyclase (AC), leading to production of cyclic adenosine monophosphate (cAMP) and enhance protein kinase A (PKA) activity. This activation triggers the phosphorylation of DA and cAMP-regulated phosphoprotein (DARPP)-32, which acts as downstream modulator of signaling pathways. In contrast, stimulation of D2-like family receptors inhibits AC and thus, decreasing PKA activity and DARPP-32 phosphorylation (Islam & Meli et al., 2021; Missale et al., 1998; Tritsch & Sabatini, 2012). In the mPFC, DRD1 and DRD2 are the most abundantly expressed DRDs. They are present in both excitatory pyramidal neurons and inhibitory interneurons, distributed across all cortical layers (Islam & Meli et al., 2021; Santana et al., 2009; Tritsch & Sabatini, 2012). In the rodent mPFC, mRNA *in situ* hybridization and receptor binding studies revealed that Drd1 is most abundant in the deeper layers (5 and highest in layer 6) and only in few cells in layer 2 (Islam & Meli et al., 2021; Santana & Artigas, 2017; Vincent et al., 1993). Around 20% of pyramidal neurons

in layers 2/3 and between 20-40% in layers 5/6 express Drd1, while 30-60% of interneurons across all layers express it (Santana et al., 2009; Tritsch & Sabatini, 2012). Drd2 is also most prominently expressed in the deeper layers (highest in layer 5) with sparse expression in layers 2/3 (Islam & Meli et al., 2021; Santana & Artigas, 2017; Vincent et al., 1993). Around 5% of pyramidal neurons in layers 2/3 and 25% in layers 5/6 expressing Drd2, and in fewer than 20% of the interneurons (Santana et al., 2009; Tritsch & Sabatini, 2012).

In the human PFC, mRNA *in situ* hybridization studies show that both *DRD1* and *DRD2* are also expressed in pyramidal and non-pyramidal cells. *DRD1* is absent in layer 1, is expressed at moderate levels in layers 3 and 4 and is most prominently expressed in layers 2, 5 and 6 (Islam & Meli et al., 2021; Weickert et al., 2007). *DRD2* is absent in layer 1, is expressed at intermediate levels in layer 3 and 4 and shows high expression in layer 2 and even higher expression in layers 5 and 6 (Islam & Meli et al., 2021; Weickert et al., 2007). The expression of these receptors does not only follow specific area and lamination patterns but is also age-dependent, varying throughout development. Different studies report varying timelines for the peak expression of these DRDs, leading to an inconclusive account of the developmental timeline of their expression (Islam & Meli et al., 2021). RNA *in situ* hybridization in rat frontal cortex detected the expression of *Drd1* and *Drd2* already at E14 and E18, respectively, with peak expression levels occurring between P14 and P30 (Islam & Meli et al., 2021; Schambra et al., 1994). qPCR studies in the rat mPFC detected increasing mRNA expression levels of *Drd1* and *Drd2* long isoform (*Drd2l*), but not *Drd2* short isoform (*Drd2s*), from juvenile to adolescence stages (P45) and decreased expression in adulthood (P70) (Islam & Meli et al., 2021; Naneix et al., 2012). Quantitative autoradiography of *Drd1* in the rat mPFC reports the peak receptor binding levels at P14 and P21 followed by a decrease between P21-P42 (Islam & Meli et al., 2021; Leslie et al., 1991). However, another autoradiography study detected a gradual increase of *Drd1* and *Drd2* receptor binding from P7 until it reached peak levels at P60 (Islam & Meli et al., 2021; Tarazi & Baldessarini, 2000).

The DRD expression dynamic in human PFC follows a pattern distinct from that described in rodents (Islam & Meli et al., 2021). mRNA *in situ* hybridization studies in human post-mortem PFC tissue revealed that *DRD1* mRNA is present at neonatal stages, but the

expression levels decrease during the first year of life and then peak in adolescence and early adulthood before gradually declining again in older adults (Islam & Meli et al., 2021; Weickert et al., 2007). In contrast, another study performing qPCR and microarray analysis in the dorsolateral PFC showed that *DRD1* mRNA gradually increase until adolescence, followed by a slight decrease in young and older adults. However, protein analysis by Western blot in the same study indicated that *DRD1* levels increase with age, peaking in young adults and older adults (Islam & Meli et al., 2021; Rothmond et al., 2012). In contrast to *DRD1*, *DRD2* expression is the highest during the neonatal stage and then significantly decreases in infancy and remains lower than neonatal levels through all subsequent developmental stages (Islam & Meli et al., 2021; Weickert et al., 2007). Likewise, qPCR study of 2 *DRD2* isoforms, the short (*DRD2S*) and long (*DRD2L*) form, report that the peak of mRNA expression is reached at the neonatal stage in the dorsolateral PFC, with a consistent decline with progressing age (Islam & Meli et al., 2021; Rothmond et al., 2012).

1.4.1.3. Dopaminergic modulation of local PFC circuitry

The age-dependent DA innervation and expression of DRD1 and DRD2 in the mPFC is crucial for the proper maturation of cortical circuits. As described above, during early postnatal development, the expression of these receptors is relatively low, coinciding with the sparse DA innervation of the mPFC. As the density of DA fibers and varicosities increases through adolescence, so does the expression of DRD1 and DRD2, suggesting a coordinated and parallel development of DA input, receptor availability and functional maturation of the mPFC (Naneix et al., 2012; Reynolds et al., 2018). While it remains speculative, DA's role in local circuit development is supported by studies showing that altered DA innervation disrupts circuit maturation. In a study using DCC knockout mouse mode demonstrated that reduced DCC expression leads to increased and disorganized DA innervation in the mPFC, which in turn disrupts the maturation and organization of layer V pyramidal neurons during adolescence, a key developmental period for establishing proper mPFC connectivity and cognitive functions (Manitt et al., 2013). Another study, involving a conditional knockout mouse model lacking mesoprefrontal DA innervation during development, revealed that the maturation of parvalbumin (PV) and calbindin (CB) interneurons in the mPFC is disrupted during a critical adolescent period,

with alterations extending into adulthood (Islam & Blaess, 2024). These findings highlight adolescence as a sensitive period for DA-driven maturation of mPFC circuitry, though further research is required to elucidate underlying mechanisms.

Beyond development, DA also plays a key role in the mature PFC by modulating the E/I balance influencing both pyramidal neurons and interneurons to ensure proper cognitive function and behavioral control. This effect of DA modulation in PFC circuitry is largely complex and has been extensively reviewed in the PFC (Seamans & Yang, 2004; Tritsch & Sabatini, 2012). Most of the evidence shows that DA acts primarily through D1-like receptors to increase the intrinsic excitability of deep-layer PFC pyramidal neurons by raising the resting membrane potential or inducing a sustained rise in action potential frequency during somatic depolarization (Gao & Goldman-Rakic, 2003; Gulledge & Jaffe, 2001; Lavin & Grace, 2001; Tritsch & Sabatini, 2012; Yang & Seamans, 1996). However, some studies reveal that D1 activation may have an inhibitory effect on pyramidal neuron firing under specific conditions (Moore et al., 2011; Rotaru et al., 2007; Tritsch & Sabatini, 2012). Similarly, D2-like receptors have been suggested to counteract D1-driven excitation by reducing intrinsic excitability (Gulledge & Jaffe, 1998; Tritsch & Sabatini, 2012; Tseng & O'Donnell, 2004). Conversely, other research suggests that D2 receptors can also enhance excitability, particularly in deep-layer pyramidal neurons (Gee et al., 2012; Tritsch & Sabatini, 2012). DA is also affecting the interneurons, mostly PV-expressing fast-spiking (FS) interneurons. Reports from *in vitro* PFC slice studies show that DA acting through D1-like receptors induces membrane depolarization and increases excitability in most FS interneurons (Gao & Goldman-Rakic, 2003; Gorelova et al., 2002; Trantham-Davidson et al., 2008; Tritsch & Sabatini, 2012), however D2-like activation was also observed to increase the firing rate and excitability of FS interneurons in the PFC (Tritsch & Sabatini, 2012; Tseng & O'Donnell, 2004). This variability highlights the complex DA-dependent effects of D1-like and D2-like receptor signaling, suggesting that DA's actions in the PFC rely on an intricate interplay among receptor types and neuron subtypes. Additionally, studies have proposed that the low or high levels DA concentration may elicit different effects in the mPFC: low DA levels stimulate D1 receptors and thus cAMP and PKA and thereby increase IPSCs; high DA levels stimulate D2 receptors and decrease IPSCs in the mPFC (Trantham-Davidson et al., 2004). Consequently, DA

concentration can fine-tune local circuitry by modulating cortical inhibition in the mPFC. Notably, mesoprefrontal-projecting mDA neurons in rodents have been shown to co-release glutamate. This glutamate release increases excitability of fast-spiking interneurons, thus impacting the excitatory-inhibitory balance in the mPFC (Kabanova et al., 2015; Mingote et al., 2015; Pérez-López et al., 2018). All this evidence suggests that DA modulation plays an essential role in the maturation and E/I balance of local mPFC circuits, impacting the development of higher-order cognitive functions.

1.4.2. Noradrenergic inputs

The NA axons projecting to the mPFC originate from the locus coeruleus (LC) located in the brainstem (Jones et al., 1977; Jones & Moore, 1977; Levitt & Moore, 1978; Robertson et al., 2013) **(Fig. 3)**. The development of NA neurons begins early in embryogenesis: NA neurons differentiate between E10-13 in rats and E10.5-15.5 in mice (Lauder & Bloom, 1974; Plummer et al., 2017). Once differentiated the neurons extend their axons towards the cortex reaching the frontal cortex at E17-18 (Levitt & Moore, 1979). NA innervation continues to increase in density postnatally, resembling the adult one by the beginning of the fourth postnatal week. However, the general innervation pattern - with dense horizontal axons present in the molecular layer and numerous horizontal and vertical axons innervating the deeper layers - appears to be already established within the first postnatal week (Levitt & Moore, 1979). In this study, we primarily focus on the effects of DA innervation and receptor expression in our models of interest, whereas for NA, we examine only its innervation. Therefore, the information provided on NA is limited to its innervation in the mPFC, without exploring functional modulation or other aspects.

It is important to note that DA and NA are part of the same biosynthetic pathway in which tyrosine is first converted first into L-DOPA by TH, then into DA and further converted into NA by the enzyme dopamine β-hydroxylase (DBH) (Cooper et al., 2003; Iversen et al., 2009). TH is commonly used as a marker for mDA neurons and axons due to its role as the rate-limiting enzyme in DA synthesis. Since DA is a precursor of NA, TH can label both DA and NA axons. However, since it has been reported that only about 10% of NA axons in the PFC of rats and humans co-express TH, TH is frequently used as a marker that labels predominantly DA axons in this region (Gaspar et al., 1989; Miner et al., 2003).

1.4.3. Serotonergic inputs

The serotonergic (5-HT) innervation in the mPFC originates from neurons in the median and dorsal raphe nuclei in the brainstem (Bang et al., 2012; Lidow & Rakic, 1992; Reader, 1981; Steinbusch, 1981) **(Fig. 3)**. The 5-HT neurons in the raphe nuclei begin to develop early in embryonic life between E10-E12 in mice and E12-E15 in rats (Gaspar et al., 2003; Vitalis et al., 2013; Wallace & Lauder, 1983). These neurons extend their axonal projections rapidly after having differentiated, crossing the telencephalic floor at E15-E16 and finally innervating the frontal cortex by E17 in rats (Wallace & Lauder, 1983). Progressively, the 5-HT innervation increases and distributes evenly in the cortex. Innervation density increases further postnatally until it acquires the mature pattern by in the third postnatal week in rats (Lidov & Molliver, 1982; Vitalis et al., 2013).

In this study, our primary focus is on DA, specifically investigating its innervation and receptor expression within our models of interest. In contrast, for 5-HT, we assess only its innervation in the mPFC. Therefore, the information provided on 5-HT is restricted to its axonal innervation in the mPFC, without exploring functional modulation or other developmental aspects.

1.5. Dysfunctions of the monoaminergic inputs in the PFC and disease implications

Dysfunctions of these monoaminergic systems, particularly of DA, in the PFC are strongly implicated in the pathophysiology of several psychiatric and neurodevelopmental disorders, such as schizophrenia, attention deficit/hyperactivity disorder (ADHD), and autism spectrum disorder (ASD). DA dysregulation is particularly studied in schizophrenia. The DA hypothesis of schizophrenia states that hypodopaminergic activity in the PFC is associated with the cognitive deficits and negative symptoms of the disorder, such as impaired working memory and social withdrawal, whereas hyperactivity of DA in subcortical regions like the striatum is linked to the positive symptoms of psychosis, including hallucinations and delusions (Biol Psychiat, 2017; Islam & Meli et al., 2021). Studies have shown that the PFC in individuals with ADHD exhibits delayed maturation and reduced cortical thickness (Shaw et al., 2007). Poor functioning of the PFC is reflected in ADHD symptoms like hyperactivity, impulsivity and attention deficits which are manifested in mice heterozygous for DA transporter (DAT) and Drd2, Drd4 and Drd5

polymorphisms (Islam & Meli et al., 2021; Wu et al., 2012). Moreover, positron emission tomography (PET) with fluorine-18-fluorodopa (F18-DOPA) studies found reduced ratios of F18 in the PFC of adult ADHD patients compared to healthy controls. This reduction reflects lower DOPA-decarboxylase activity - an enzyme critical for converting L-DOPA to DA - in the PFC of adult ADHD patients, suggesting impaired mesoprefrontal DA neurotransmission (Ernst et al., 1998). Main ADHD treatment like methylphenidate, enhance DA and NA levels in the PFC by blocking their reuptake transporters (del Campo et al., 2011; Islam & Meli et al., 2021). A DA hypothesis is also proposed for ASD. DA dysfunctions in the mesocorticolimbic and nigrostriatal pathways have been proposed to contribute to deficits in social and communication behaviors, as well as stereotypic behaviors in ASD (Islam & Meli et al., 2021; Pavăl, 2017; Pavăl & Micluția, 2021). This is supported also by genetic studies which link ASD to mutations in genes encoding components of the DA system, such as the DAT and DA receptors (DRD3 and DRD4) (Cartier et al., 2015; Gadow et al., 2010; Hamilton et al., 2013; Islam & Meli et al., 2021; Neale et al., 2012; Staal, 2015). Additionally, PET scanning study for F18-DOPA also report reduced F-DOPA in the medial PFC of ASD children, suggesting decreased DA activity in the PFC of ASD (Ernst et al., 1997). Antipsychotic treatments that act as DRD and 5-HT receptor blockers, such as risperidone, can relieve some stereotypic repetitive behaviors, improve social interaction and verbal communication, and reduce aggression and self-injury in children with ASD (Ghaeli et al., 2014; Islam & Meli et al., 2021; McCracken et al., 2002; McDougle et al., 2005). Importantly, studies have also reported that monoaminergic modulation involving DA, 5-HT, NA, play significant roles in modulating seizure activity in epilepsy (Bozzi & Borrelli, 2013; Strac et al., 2016; Tripathi & Bozzi, 2015). However, most research has focused on their signaling effects on network activity in the limbic system and not in the frontal cortical areas. FCD type 2b is frequently occurring in the frontal lobe (Blümcke et al., 2017), thus these modulatory systems can affect the local circuitry and impact seizure susceptibility in the FCD patients. Additionally, any dysregulation in these monoaminergic system may play a role in the depressive and anxiety symptoms commonly seen in patients with FCDs (Khoo et al., 2022). Moreover, a few case studies from FCD patient biopsies have investigated the density of these monoaminergic innervations by staining for TH, DBH and 5-HT and found out that in the

dysplastic epileptogenic tissues the density and distribution of these innervations were altered (Trottier et al., 1994; Trottier et al, 1996).

1.6. Aims

The overall goal of this study is to gain insight whether monoaminergic systems, particularly DA, are altered in FCD type 2. A comprehensive analysis of the role of monoaminergic innervation in FCD type 2 pathogenesis is lacking, particularly in the frontal cortex, a region highly innervated by monoaminergic systems and commonly affected by FCD. Hence, this study aims to explore the following aspects:

1. Investigate if DA innervation density and receptors (*Drd1* and *Drd2*) mRNA expression is affected across upper and deeper layers of the mPFC in an established mouse model of FCD type 2 generated by *IUE* to induce mTOR hyperactivation. Analyses are conducted at two developmental stages, adolescence (P30) and early adulthood (P60), to capture the dynamic maturation of DA signaling in the postnatal mPFC.

2. In addition to DA, the study conducts an initial analysis of NA and 5-HT innervation density in the mPFC at P30 to identify potential changes in these systems.

3. Explore if any alterations of DA innervation density and receptor (*DRD1* and *DRD2*) mRNA expression are also present in upper, middle and deeper layers of human FCD type 2b cortical specimen. Similar to the mouse analysis, the analyses in human specimen are conducted at pediatric (9-16 y.o.) and adult (44-57 y.o.) ages. Specimen from the frontal cortex and parietal cortex patient were analyzed to account for region-specific DA alterations.

By addressing these objectives, this research provides an initial understanding of the role of DA signaling in FCD type 2, offering insights into neurobiological mechanisms underlying cortical malformation development and associated aberrant neuronal network emergence.

2. Material and methods

2.1. Experimental animal models and human biopsy samples

2.1.1. Animals

All the mice used for this project were of CD1 background. Timed-pregnant E14 CD1 females were purchased from Charles River (Strain code: #022CD1) to perform *in utero* electroporation (IUE) experiments on developing embryos. All animals were housed in a controlled environment, with 12 hr light/night cycles and ad libitum availability of food and water. Offspring mice that were not successfully electroporated were not included in the analysis. All experiments from this project were performed according to the welfare animal regulations of Federal German Government, European Union and the University of Bonn Medical Centre Animal Care Committee. The experimental protocols were approved by the Landesamt für Natur, Umwelt und Verbraucherschutz Nordrhein-Westfalen (Animal Permit Number: 81-02.04.2019.A294).

2.1.2. Human biopsy samples

All the human FCD type 2b patients had drug-resistant focal epilepsy and underwent presurgical evaluation at the Department of Epileptology, University Hospital Bonn. The potential epileptogenic zone's location and extent were assessed using seizure semiology, scalp EEG, and often stereotactic intracranial EEG, along with brain MRI. When necessary, fluorodeoxyglucose-PET (FDG-PET) and both ictal and interictal single-photon emission computed tomography (SPECT) were also employed as described by Rácz et al., 2021. Each patient subsequently underwent epilepsy surgery aimed at achieving seizure freedom. All procedures adhered to the guidelines of the Declaration of Helsinki. **Table 1** summarizes information on the patient biopsies used for this study.

Table 1. List of FCD type 2b patients used in this study

Patient nr.	Age group	Age at surgical resection (y.o.)	Age at seizure onset (y.o.)	FCD Localiz-ation	Gender	Total serial sections	Mean Area (µm²) Ctrl	Mean Area (µm²) FCD
1	Pediatric	9	8	Frontal	Female	6	7169040	7733350
2	Pediatric	16	3	Frontal	Female	9	2466100	2752870
3	Pediatric	14	1	Parietal	Female	9	7252430	12303500
4	Adult	57	4	Frontal	Male	10	6532400	8983620
5	Adult	45	6	Frontal	Female	7	2401390	2302600
6	Adult	44	5	Parietal	Male	9	29281900	21231200

2.2. Plasmids

mTOR plasmids were generously provided by Jeong Ho Lee Lab from the Graduate School of Medical Science and Engineering, KAIST, Daejeon, Korea (Lim et al., 2015). The wild type (WT) mTOR plasmid: pCIG-mTOR-WT-IRES-EGFP **(Fig. 4A)** and mTOR mutated plasmid: pCIG-mTOR-Leu2427Pro-IRES-EGFP **(Fig. 4B)** were used for IUE of E14 mouse embryos. A pAAV-U6-mRFP plasmid was co-electroporated only with the WT-mTOR plasmid to discern WT animals from their siblings, that were electroporated with the p.Leu2427Pro mTOR mutated plasmid. pAAV-U6-mRFP plasmid was provided by the Becker/Schoch laboratory, Institute of Neuropathology, University Hospital, Bonn.

2.3. Plasmid preparation

To secure high plasmid yields, plasmids were transformed in competent bacterial cells (E. coli Stbl2^{TM} strain, Ref: 10268-019, Invitrogen). First, 1µg of plasmid DNA was mixed with 50 µl bacteria and incubated on ice for 1 hr. Then, heat shock was induced by incubating

them at 42°C for 45 sec and placed back on ice for 1-2 min. After adding 200 µl of Luria-Bertani (LB) medium, they were placed on shaking platform at 700 rpm for 1 hr at 37°C. The medium was spread on LB agar plates and incubated at 37°C overnight (ON). On the next day, a colony was picked and cultivated in liquid culture with 250 ml LB and 250 µl (1:1000) Ampicilin on a shaker (125-150 rpm) at 37°C ON. Endotoxin-free (EF) plasmid DNA was isolated with NucleoBond® Xtra Maxi Plus EF kit (Ref: 740424.10, Macherey-Nagel). All plasmid preparation steps were executed according to the manufacturer's manual https://www.mn-net.com/media/pdf/18/eb/8f/Instruction-NucleoBond-Xtra-EF.pdf. DNA pellets were reconstituted in sterile water used for injections (Ampuwa®) and the final concentrations were measured via NanoDrop. Every plasmid preparation was sequenced to assess the mTOR-WT sequence and mTOR-Leu2427Pro mutated sequence utilizing the primer s344 (mTOR mid9), sequence (5'-3'): GAGGTGTTTGAGCATGCCGTCA, Invitrogen. Furthermore, GFP expression was assessed by transfecting the plasmids into HEK293T cells by adding 1 µg plasmid DNA, 60 µl Cacl2 and 65 µl HEPES and distributing 60 µl /well. GFP expression was verified with a fluorescent microscope the following day. Only plasmid preps with detectable GFP expression were used for further experiments.

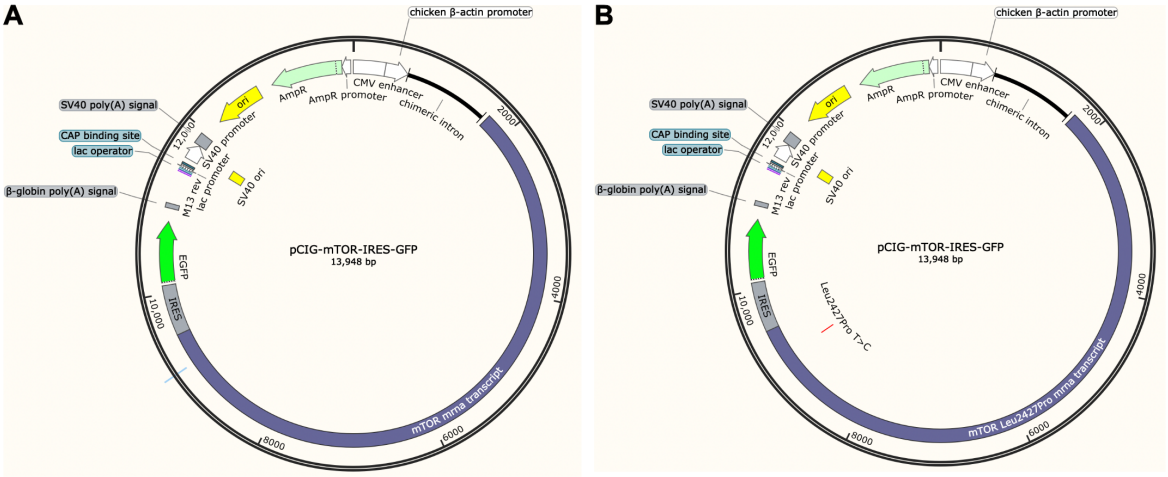

Fig. 4. mTOR plasmid maps. **A)** WT-mTOR plasmid construct. **B)** p.Leu2427Pro mTOR-mutated plasmid with mutation site c.7280T>C encoding p.Leu2427Pro. Plasmids provided from Jeong Ho Lee Lab, Graduate School of Medical Science and Engineering, KAIST, Daejeon, Korea.

2.4. Intraventricular *in utero* electroporation (IUE)

Timed-pregnant (E14) female mice were injected subcutaneously with Buprenovet (0.05 mg/kg) and Ketoprofen (5 mg/kg) 30 min before beginning with the surgical procedure. They were anaesthetized with 1-2% Isoflurane inhalation during the whole surgery. The DNA solution to be injected was prepared at a final concentration of 2 µg/µl for the mTOR plasmids and 1.5 µg/µl for the mRFP plasmid and further mixed with 2 mg/ml Fast Green FCF to visualise the injected solution in the lateral ventricles. For the surgery, an abdominal incision was made along the mildline and the uterine horns were exposed. The prepared DNA solution was injected into the lateral ventricles of each embryo brain via a glass capillary (Glas, Drummond Scientific Company USA) attached to a pressure pulse generator (Picospritzer III, General Valve Corporation) **(Fig. 5A)**. For each surgery, half of the embryos received the p.Leu2427Pro plasmid solution and the other half received the mixed WT-mTOR and mRFP plasmid solution, to distinguish the experimental animals post-birth. Subsequently, a triple electrode was placed onto the head of the embryos and positioned to target the mPFC as described here (Szczurkowska et al., 2016). Briefly, 2 lateral electrodes connected to the negative poles were placed laterally on the embryo's head whereas, the 3^{d} middle electrode connected to the positive pole was placed in front of the embryo's head. Electroporation occurs by discharging a 500 µF capacitor with a voltage of 30 V and a pulse duration of 20 ms (CUY21 SC Square Wave Electroporator, Nepa Gene) **(Fig. 5A)**. After IUE of all the embryonic brains, the uterine horns were carefully placed back inside the abdominal cavity. The abdominal incision was closed with surgical sutures and then the skin was surgically closed with metal wound clips. Postoperative care was provided by daily subcutaneous injections of ketoprofen (5 mg/kg) for 3 consecutive days.

2.5. Tissue collection

2.5.1. Mice

Adult mice were anesthetised by intraperitoneal injection of 0.1 ml/20 g body weight of 100 mg/kg bodyweight (BW) Ketamine & 16 mg/kg BW Xylazine. After absence of foot withdrawal reflexes upon pinching, mice were transcardially perfused first with 1x phosphate-buffered saline (PBS) and then with 4% paraformaldehyde (PFA), followed by

head decapitation and brain extraction **(Fig. 5B)**. The brains were post-fixed in 4% PFA overnight on a shaker at 4°C. For tissue cryopreservation, brains were placed first in 15% sucrose/PBS solution overnight on a shaker at 4°C and after sinking to the bottom, they were similarly incubated in 30% sucrose/PBS. Afterwards, the brains were embedded in cryomolds with Tissue-Tek® O.C.T.™ Compound and kept at -80°C until cryosectioned. Brains were sectioned at 40 μm thickness with a Leica cryostat (CM 3050S, Leica Biosystems) **(Fig. 5C)** and collected in 24-well plates with Walter's antifreeze solution (400 mL Phosphate buffer 100 mM: 1.57 g Na2HPO4 + 5.45 g Na2HPO4 in ~400 mL dH2O, 300 mL Etylene glycol, 300 mL Glycerol) and stored at -20°C.

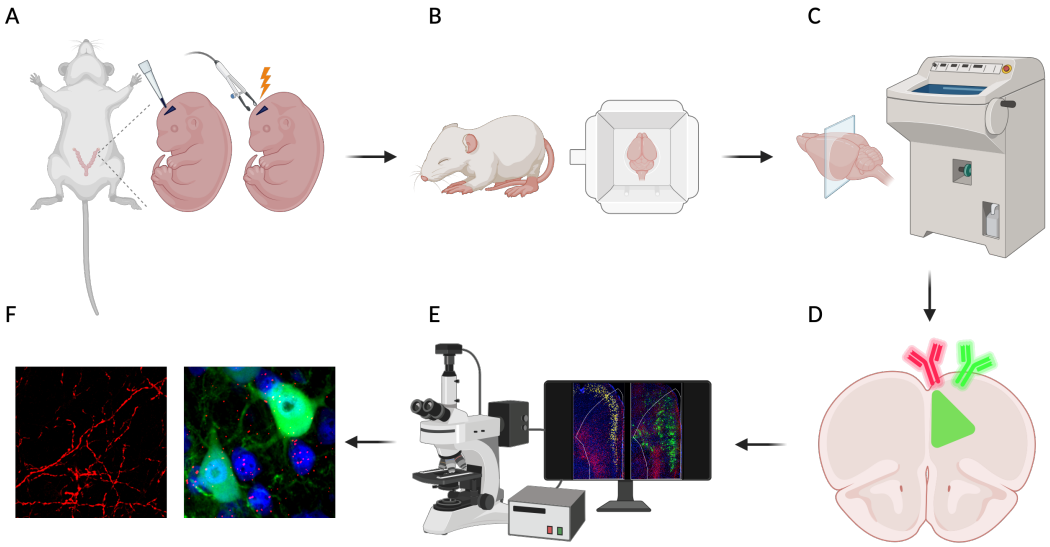

Fig. 5. Schematic workflow of mouse brain analysis. **A)** IUE at E14 of mouse embryonic brains. **B)** Offspring mice were sacrificed and brains extracted at P30 and P60. **C)** Brain cryosectioning. **D)** Immunohistochemistry and RNAscope for target proteins and mRNA expressions in the mPFC. **E)** Imaging with confocal microscope. **F)** Analysis of monoaminergic axonal density and dopaminergic receptor expression. Created with BioRender.com

2.5.2. Human samples

Biopsy samples from human FCD type 2b patients, diagnosed according to the current International League Against Epilepsy (ILAE) classification (Najm et al., 2022), were collected during surgical resections at the University of Bonn Medical Center's Epilepsy-Surgery Program (**Fig. 6A**). These samples were obtained with patient consent and ethical

approval (nr. 308/19). All following steps were done by the Neuropathology Department of the University, Bonn. Resected biopsy samples were processed for formalin-fixation paraffin-embedding (FFPE) **(Fig. 6B)**, according to standard protocols of the Section for Translational Epilepsy Research at the Neuropathology Department. Serial 4 µm sections were collected on slides **(Fig. 6B)** and processed for further analysis **(Fig. 6C)**. 1 section was processed for Haematoxylin and Eosin (H&E) staining for FCD type 2b pathology assessment **(Fig. 6C)**.

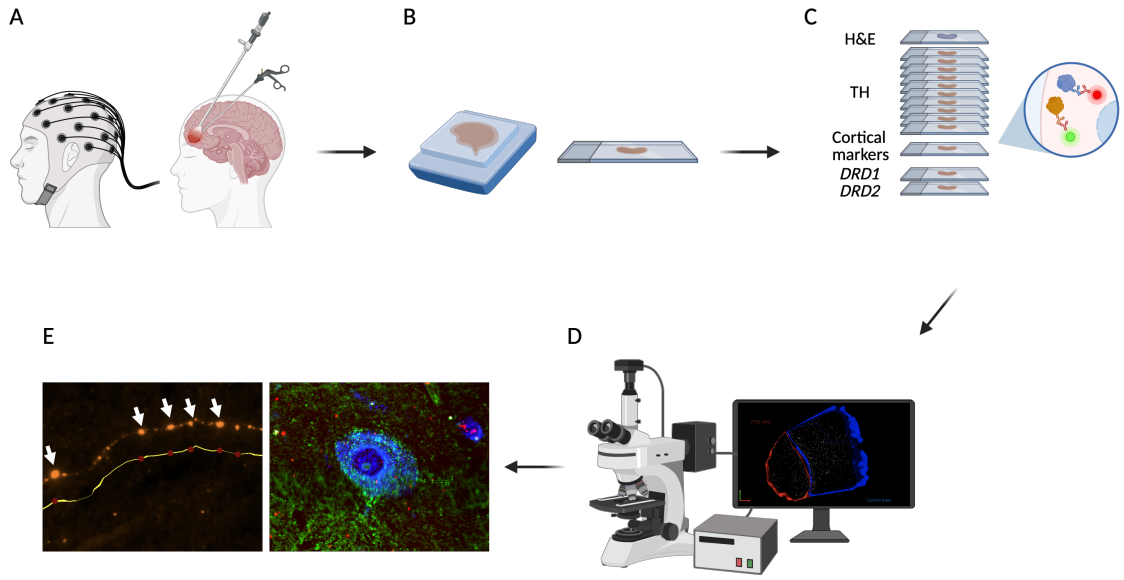

Fig. 6. Schematic workflow of human brain analysis. **A)** FCD type 2b area localization and tissue resection surgery. **B)** Tissue processing embedding (FFPE) and tissue sectioning. **C)** IHC and RNAscope for target proteins and mRNA expression on serial sections. **D)** Tissue imaging with fluorescent microscope. **E)** Manual tracing of dopaminergic axons and dopaminergic receptor expression. Created with BioRender.com

2.6. Immunohistochemistry (IHC)

2.6.1. Mouse sections

Per animal, 1-2 sections from the frontal cortex (Bregma level 1.94 - 1.78) were used for each of the monoaminergic axonal markers (TH/NET/SERT) **(Fig. 5D)**. Free-floating 40 µm sections were washed with PBS for 5 min and then 2 times with 0.3% Triton X-100 in PBS (PBT) for 5 min each. Afterwards, to minimize unspecific antibody binding, sections

were blocked with 10 % normal donkey serum (NDS) in PBT for 1 hr and then incubated with primary antibodies ON at 4°C. Primary antibodies were diluted in 3% NDS/PBT in the concentrations stated in **Table 2**. The following day, the sections were washed 3 times with 0.3% PBT for 5 min and then incubated with secondary antibodies for 2 hr at room temperature (RT) in the dark. All secondary antibodies were raised in donkey and diluted in 3% NDS/PBT in the concentrations stated in **Table 3**. Hoechst 33258 (10mg/mL, used at 1:10000) was added to the secondary antibody solution to counterstain the nuclei. Sections were washed 2 times with 0.3% PBT and 1 time in PBS for 5 min, mounted on slides and cover slipped with Aqua-PolyMount (Polysciences Inc.). The slides were left ON to dry at RT and then stored at 4°C. All washing and incubation steps were carried out in a 24-well plate on a rotating platform.

2.6.2. Human sections

For every human patient, 10 serial sections were stained for TH, while 1 section was stained for cortical layer markers (Calretinin and SMI32) and a global neuronal marker Neuronal Nuclear protein (NeuN) **(Fig. 6C)**. 4 μm human FFPE brain sections were deparaffinised by a series of 3 times Xylol for 3 min each, followed by a decreasing gradient ethanol series of 2 times 100% for 2 min, 2 times 95% for 2 min, 1 time in 70% for 1min and then briefly washed in ddH2O. Afterwards, a permeabilization step in 0.3% PBT for 10 min was done before performing an antigen retrieval step by incubating the sections in 10 mM sodium citrate buffer in a pressure cooker for ~10 min. Then they were washed 2 times in 0.1% PBT for 5 min and then blocked in 10 % NDS/PBT for 1 hr. The sections were incubated in primary antibodies ON at 4°C and washed 3 times in 0.1% PBT for 5 min before incubating in secondary antibodies for 2 hr at RT in the dark. For primary antibodies labelled with biotin, an extra step of Cy3-Streptavidin detection was performed for 1 hr at RT in the dark. Sections were washed again for 3 times in 0.1% PBT for 5 min and cover slipped with Aqua-PolyMount. The slides were left ON to dry at RT and then stored at 4°C. Primary and secondary antibodies were diluted in 3% NDS/PBT in the corresponding concentrations according to **Table 2** and **3**, respectively.

Table 2. List of primary antibodies

Antibody	**Host species**	**Dilution**	**Catalog no.**	**Manufacturer**	**Used tissue**
TH	rabbit	1:500	AB152	Merck	human & mouse
NET (SLC6A2)	mouse	1:500	AMAB91116	Atlas Antibodies	mouse
SERT	rabbit	1:1000	24330	ImmunoStar	mouse
NeuN	rabbit	1:500	ab177487	Abcam	human & mouse
NeuN	guinea pig	1:500	266004	Synaptic Systems	human
Neurofilament H (SMI32)	mouse	1:1000	801702	BioLegend	human
Calretinin	goat	1:1000	CG1	Swant	human
GFP	rat	1:1000	04404-84	Nacalai Tesque, Inc	mouse
RFP	rat	1:1000	5f8-20	ChromoTek	mouse
Phospho-S6 Ribosomal (Ser240/244)	rabbit	1:1000	5364	Cell Signaling Technology	mouse

Table 3. List of secondary antibodies and fluorescent dyes

Antibody/ Fluorophore	**Target**	**Dilution**	**Catalog no.**	**Manufacturer**
Alexa 647	rabbit	1:500	A31573	Invitrogen
Alexa 647	mouse	1:500	A31571	Invitrogen
Alexa 647	guinea pig	1:500	706-605-148	Jackson ImmunoResearch
Alexa 546	rabbit	1:500	A10040	Invitrogen
Alexa 488	mouse	1:500	A21202	Life Technologies
Alexa 488	rat	1:500	A21208	Invitrogen
Alexa 405	rabbit	1:500	ab175649	Abcam
biotin	goat	1:200	705-065-147	Jackson ImmunoResearch
biotin	rabbit	1:200	711-065-152	Jackson ImmunoResearch
Cy3-Streptavidin	biotin	1:1000	016-160-084	Jackson ImmunoResearch
Cy3	rat	1:200	712-165-153	Jackson ImmunoResearch
Cy5	RNAscope® probes	1:3000	FP1171024UG	Perkin Elmer
TSA Vivid 650	RNAscope® probes	1:3000	7527	Tocris

2.7. Multiplex fluorescent *in situ* hybridization (FISH)

RNAscope® Multiplex Fluorescent v2 Assay was utilized to detect the expression of dopaminergic receptors *Drd1/DRD1* and *Drd2/DRD2* mRNA *in situ* in fixed-frozen adult mouse brain sections and FFPE human brain sections. **Table 4** summarizes all the probes used for this study.

Table 4. List of RNAscope probes

Target Probe	**Target species**	**Channel**	**Reference nr.**
Drd1	Mouse	C3	461901-C3
Drd2	Mouse	C2	406501-C2
DRD1	Human	C1	524991
DRD2	Human	C2	553991-C2
(-) control DapB	any species	C1; C2; C3	320871
(+) control: *POLR2A; PPIB; UBC*	Human	C1; C2; C3	320861

2.7.1. Mouse frozen tissue

Fixed-frozen mouse PFC sections were processed for RNAscope according to the manufacturer's manual for frozen tissue (User Manual: 323100-USM) **(Fig. 5D)**. Prior to RNAscope, IHC was performed as described above for NeuN and GFP/RFP **(Table 2)** to visualize the all neurons and the transfected, respectively. All antibodies for IHC were diluted in RNAscope® Co-Detection Antibody Diluent. The following RNAscope protocol was performed afterwards:

Day 1: Tissue pre-treatment and probe hybridisation

1. Mount the sections on HistoBond Adhesive slides.
2. Dry the slides in a dry air oven at 40°C for 30 min.
3. Fix in 4% PFA for 10 min.
4. Wash the slides in sterile Dulbecco's phosphate-buffered saline (DPBS) 3 times for 3 min.
5. Dehydrate sections in 50% ethanol for 3 min.
6. Dehydrate in 70% ethanol for 3 min.
7. Dehydrate in 100% ethanol for 3 min.
8. Dry sections at 40°C for 20 min in the oven.

9. Incubate with RNAscope® Hydrogen Peroxide and cover them for 10 min at RT.
10. Wash 2 times with Ampuwa for 2 min.
11. Heat up the RNAscope® 1X Target Retrieval reagent at 100°C.
12. Submerge the slides in the copling jar containing Ampuwa water in the steamer for 10 seconds.
13. Submerge the slides in the RNAscope® 1X Target Retrieval reagent for 3 min.
14. Wash in Ampuwa water for 2 min.
15. Transfer slides to 100% ethanol for 3 min.
16. Dry the slides for 20 min at 60°C.
17. Create a barrier around the sections with hydrophobic pen.
18. Incubate the samples with RNAscope® Protease III for 15 min at 40°C in the HybEZ Oven.
19. Wash 2 times with Ampuwa for 2 min.
20. Warm probes for 10 min at 40 °C, cool to RT and dilute C2 and C3 probes in probe diluent (1:50).
21. Incubate with probes **(Table 4)** for 2 hr at 40 °C in HybEZ oven.
22. Wash 2 times with RNAscope® 1X wash buffer for 2 min at RT.
23. Incubate the slides in 5x SSC ON.

Day 2: RNAscope® Multiplex Fluorescent v2 Assay

24. Wash 2 times with 1X wash buffer for 2 min at RT.
25. Incubate with RNAScope® Multiplex FL v2 Amp 1 for 30 min at 40°C in HybEZ oven.
26. Wash 3 times with 1X wash buffer for 5 min at RT.
27. Repeat steps 25-26 with RNAScope® Multiplex FL v2 Amp 2.
28. Incubate with RNAScope® Multiplex FL v2 Amp 3 for 15 min at 40°C in HybEZ oven.
29. Wash 3 times with 1X wash buffer for 5 min at RT.
30. For Drd2-C2, incubate with RNAScope® Multiplex FL v2 HRP-C2 for 15 min at 40°C in HybEZ oven.
31. Wash 2 times with 1X wash buffer for 2 min at RT.

32. Incubate with Cy5/TSA Vivid 650 fluorophore **(Table 3)** diluted in TSA buffer for 30 min at 40°C.
33. Wash 3 times with 1X wash buffer for 5 min at RT.
34. Add RNAScope® Multiplex FL v2 HRP blocker for 15 min at 40°C.
35. Wash 2 times with 1X wash buffer for 2 min at RT.
36. Perform the same steps (30-35) for Drd1-C3 signal.
37. Add PolyMount immediately and coverslip the slides. Dry slides ON in the dark and store slides at 4°C in the dark.

2.7.2. Human FFPE tissue

A set of FFPE brain sections were prepared as described in the manufacturer's manual for FFPE tissue (User Manual: 323100-USM) **(Fig. 6C)**. IHC was performed for Neurofilament H (SMI32) and NeuN **(Table 2)** to visualise dysmorphic and in general neurons, respectively. All antibodies for IHC were diluted in RNAscope® Co-Detection Antibody Diluent. The following protocol was used:

Day 1: Tissue pre-treatment and primary antibody IHC

1. Bake slides in a dry air oven for 1 hr at 60°C.
2. Deparaffinize the sections in 2 times Xylol for 5 min.
3. Incubate slides 2 times in 100% ethanol for 1 min.
4. Bake slides in a dry air oven for 30 min at 60°C.
5. Incubate with RNAscope® Hydrogen Peroxide and cover them for 10 min at RT.
6. Wash 2 times with Ampuwa for 2 min.
7. Heat up the RNAscope® 1X Co-Detection Target Retrieval reagent at 100°C.
8. Submerge the slides into the hot the RNAscope® 1X Co-Detection Target Retrieval solution for 20 min.
9. Wash 2 times with Ampuwa for 2 min.
10. Bake slides in a dry air oven for 30 min at 60°C.
11. Incubate in 0,1% Tween-20 in PBS (PBS-T) for 10 min at RT.
12. Create a barrier around the sections with hydrophobic pen.
13. Place slides in the HybEZ™ Slide Rack and add primary antibodies **(Table 2)** diluted in RNAscope® Co-Detection Antibody Diluent and incubate ON at 4°C.

Day 2: Secondary antibody IHC and probe hybridisation

14. Next day, wash 2 times with 0,1% PBS-T for 5 min.
15. Incubate in secondary antibodies **(Table 3)** diluted in RNAscope® Co-Detection Antibody Diluent and incubate for 2 hr at RT in the dark.
16. Wash 2 times with 0,1% PBS-T for 5 min.
17. Post IHC fix in 4% PFA for 10 min at RT.
18. Wash 4 times with PBS-T for 2 min.
19. Incubate with RNAscope® Protease Plus for 30 min at 40°C in HybEZ™ Oven.
20. Wash 2 times with Ampuwa for 2 min.
21. Warm probes for 10 min at 40 °C, cool to RT and dilute C2 in probe diluent (1:50). C1 probe can be used directly.
22. Incubate with probes **(Table 4)** for 2 hr at 40 °C in HybEZ oven.
23. Wash 2 times with RNAscope® 1X wash buffer for 2 min at RT.
24. Incubate the slides in 5x SSC ON.

Day 3: RNAscope® Multiplex Fluorescent v2 Assay

25. Same steps as described above (page) for Drd1-C1 and Drd2-C2 probe detection assay. Exception: Incubated with TSA vivid 650 fluorophore **(Table 3)** diluted in TSA buffer for 30 min at 40°C. All washing steps with 1X wash buffer were done 2 times for 2 min at RT.

2.8. Fluorescent microscopy imaging

2.8.1. Monoaminergic axons

2.8.1.1. IHC on mouse tissue

Mouse PFC sections fluorescently-labelled for monoaminergic axons, GFP and Hoechst were imaged with the Visitron VisiScope Confocal Spinning Disk Microscope (UKB Microscope Core Facility) **(Fig. 5E)**. First, an overview image of the whole brain section was taken with an 5x air objective with laser lines 405 nm, 640 nm and 561 nm or 488 nm for WT or mutated sections, respectively. Afterwards, the region of interest (PFC) was imaged at a higher magnification with a 40x water immersion objective with laser line 640

nm and for WT sections with an additional laser line 561 nm. The 561 nm laser captures the endogenous mRFP expression in the WT sections, which emits a very high-intensity signal that causes a bleed-through signal into the 640 nm channel. This channel was incorporated to distinguish between real signal and background noise and utilized as autofluorescence channel in the axonal quantification pipeline. To obtain full area coverage and maximum focus, tile regions and 11-15 z-stacks with 2 μm step/each were obtained, respectively. Tiled images were stitched with the Visitron Software.

2.8.1.2. IHC on human tissue

Serial human sections fluorescently-labelled for DA axons, NeuN and cortical markers were imaged with Zeiss AxioScan.Z1 Widefield Microscope (UKB Microscope Core Facility) **(Fig. 6D)**. First, a coarse focus map and a fine focus map were acquired with the 633 filter at 10x and 20x objective, respectively. Then, whole-section areas were imaged at 20x objective utilizing 488, 555 and 633 filters.

2.8.2. FISH

Mouse (**Fig. 5E)** and human sections **(Fig. 6D)** fluorescently-labelled for *Drd1*/*Drd2* mRNA and neuronal markers were imaged with the Visitron VisiScope Confocal Spinning Disk Microscope (UKB Microscope Core Facility). First, overview images of the whole section were taken with an 5x air objective magnification, then a 40x water immersion objective was used to image the region of interest with laser lines 405 nm, 488 nm/561 nm and 640 nm for mouse sections and 488 nm, 561 nm and 640 nm for human sections. Whole areas were covered by tile regions and multiple z-stacks with 2 μm step/each were acquired to reach maximum focus. Tiled images were stitched with the Visitron Software.

2.9. Monoaminergic axonal analysis

2.9.1. Quantification of innervation density in mouse tissue

First, the imaged PFC area was overlaid with matching sections from the Allen Mouse Brain Reference Atlas (http://atlas.brain-map.org) in Fiji (https://imagej.net/software/fiji/) based on DAPI signal (**Fig. 7A)**. PFC sub-structures (AC, PL and IL) and upper (Layers I, II/III) and deeper (Layers V & VI) were defined for each section and cropped as regions of

interest (ROIs) **(Fig. 7B & C)**. Then, ROIs were subjected to Digital Enhancement of Fibers with Noise Elimination (DEFiNE) plugin on Fiji (Powell et al., 2019) to quantify the axonal density in the defined ROIs (**Fig. 5F)**. The pipeline analysis follows a 2-step process in which 1) the images are "cleaned" from autofluorescence non-axonal particles and 2) the axonal fibers are quantified. 1) Autofluorescence signal due to bleed-through signal of high-expressing mRFP cells in the WT was defined by a threshold cut-off of 2 standard deviation (SD) above average pixel intensity and removed from the image. Another crucial pre-processing step was the identification and removal of large non-axonal particles due to artefacts. For this reason, 5 classes of particles with customized size and circularity were removed from the images. Then, background noise objects smaller than 5 μm^2 and 6 μm^2 in upper and deeper layer images, respectively and with a circularity range 0,5-1 were also subtracted. 2) Axonal fibre quantification step was performed by first measuring the intensity pixel of 10 50 μm x 50 μm background regions without visible axons and calculating the mean pixel intensity and SD of these selected regions. Then, a threshold of 4 SD above the mean pixel intensity of these background areas was set. Finally, only pixel intensities above this threshold were quantified as axonal fibres (μm^2). Axonal occupation index was defined as the percentage of the ROI area covered by axonal fibres: the quantified axonal output area (μm^2) divided by the respective total ROI area (μm^2) *100.

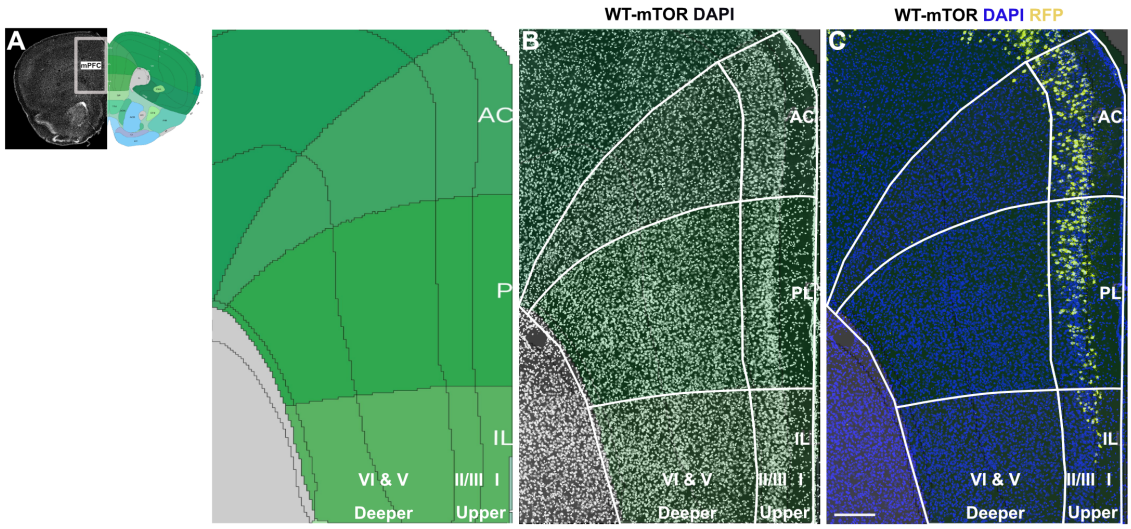

Fig. 7. Dividing the mPFC into layers and sub-regions in the mTOR mouse model. **A)** An overview of a mouse mPFC section was aligned with the corresponding level from the Allen Brain Reference Atlas. (Figure legend continued on next page).

B) The upper layers (I & II/III) and deeper layers (V & VI) and mPFC subregions: AC, PL and IL of the mouse were defined based on DAPI staining and their alignment with the corresponding level from the Allen Brain Reference Atlas. **C)** RFP+ IUE-targeted neurons were primarily located in the upper layers (mainly layer II/III), as defined by the approach described in panels **A** and **B**, thereby validating this method of layer identification. Data shown in this figure contributed to Supplementary Figure 4 in Meli et al., 2025.

2.9.2. DA axonal tracing in human tissue

For each human FCD type 2b sample, the control and FCD type 2b area were pre-defined based on H&E staining and cortical neuronal markers. The control area was defined as a region distinct from the FCD type 2b area showing proper cortical lamination and absence of any cytological abnormalities. Experimental control and FCD type 2b areas were outlined in Neurolucida software, MBF Bioscience (https://www.mbfbioscience.com/products/neurolucida). Cortical layers markers such as Calretinin (mostly expressed in Layer II), SMI32 (expressed in Layer III & V) in combination with the general neuronal markers NeuN were utilized to define cortical layers (Fauser et al., 2014; Nakagawa et al., 2017) **(Fig. 8)**. Layer I & II were categorized and outlined as upper layers, Layer III as middle layer and Layer V & VI as deeper layers inside the control area. Control area outlines were overlaid on the FCD type 2b area and “layers” were marked accordingly. Afterwards, TH-labelled DA axons were manually traced inside the control or FCD type 2b area and the axonal diameter was adjusted accordingly **(Fig. 6E)**. Axonal varicosities were marked along the axons if swellings with a diameter bigger than 0.2 μm were detected. Following TH axonal tracings on 10 serial sections, the outlines were overlaid on the section stained for cortical layer markers and matched to fully 3D reconstruct the tissue. Sections with scarce TH IHC were excluded from the analysis. Final 3D-reconstructed files were exported to Neurolucida Explorer (https://www.mbfbioscience.com/products/neurolucida-explorer) to obtain datasheets containing axonal lengths, axonal varicosities and area size.

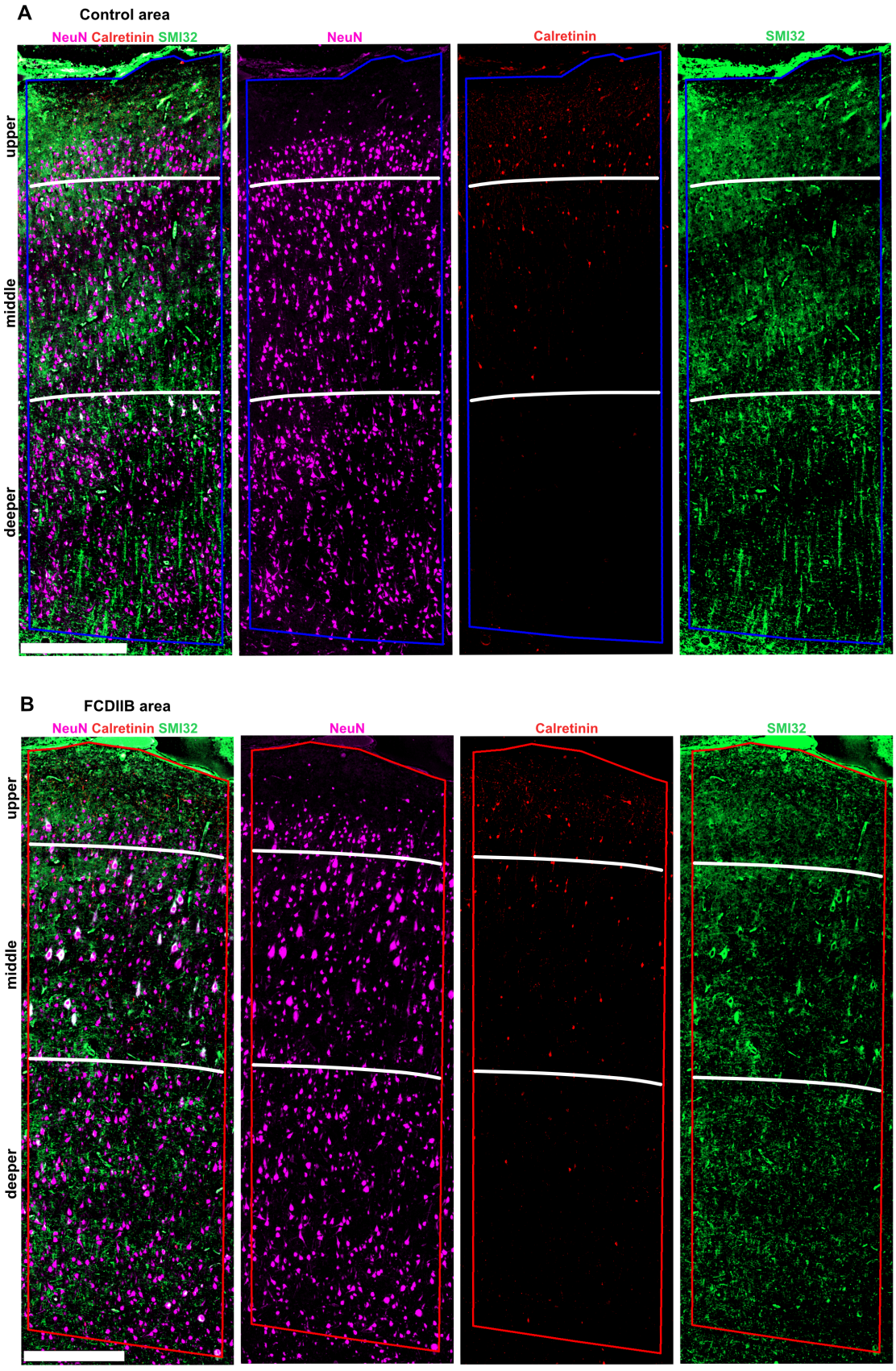

Fig. 8. (Figure legend continued on next page)

Fig. 8. Layer distinction in **A)** Control and **B)** FCD type 2b areas in human specimen. IHC was performed on human tissue samples using NeuN, Calretinin, and SMI32 to delineate cortical layers. NeuN, which labels all neurons, was used to visualize the overall cortical structure. Calretinin is primarily expressed in supragranular interneurons, with strong expression in layer II and more dispersed expression in layer III. When combined with NeuN, Calretinin helps distinguishing the upper layers (Layers I and II) from the middle layers (Layers III and IV). SMI32 is highly expressed in neuronal processes within layers III and V, aiding in the differentiation of middle from deeper layers (Layers V and VI). The example provided is from a pediatric patient. Scale bars: 500 µm. Data shown in this figure contributed to Supplementary Figure 7 in Meli et al., 2025.

2.10. Quantification of *Drd1/DRD1* and *Drd2/DRD2* mRNA expression

The expression of *Drd1/DRD1* and *Drd2/DRD2* mRNA was quantified by counting the fluorescent puncta within individual cell somas, where each punctum represents a single mRNA transcript. For assessing receptor expression in mouse mPFC **(Fig. 5F)** and human FCD type 2b tissue sections **(Fig. 6E)**, regions of interest (ROIs) were defined using the same criteria as for the axonal density quantifications. Several of these ROIs were first utilized to train Cellpose, a machine learning tool for cell segmentation, in 2D (Pachitariu & Stringer, 2022; Stringer et al., 2021). Models trained for specific markers (GFP, RFP, and NeuN for mouse; SMI32 and NeuN for human) were then employed to segment cells in 3D for mouse samples *via* Cellpose-napari plugin (https://cellpose-napari.readthedocs.io/en/latest/) **(Fig. 9)** using a stitch threshold of 0.3 and for human samples in 2D *via* Cellpose (v2.0) **(Fig. 10)**.

Following segmentation, *Drd1/DRD1* and *Drd2/DRD2* puncta were quantified using the Radial Symmetry-FISH (RS-FISH) plugin (Bahry et al., 2022). For this analysis, RANSAC model fitting was applied, with sigma and threshold values set to 0.5 and 0.00595 for mouse mPFC images, and 1.5 and 0.00551 for human specimen images. Puncta quantification was restricted to the segmented NeuN-positive cell somas **(Fig. 9, 10)**. The final quantification of puncta per cell was performed using the “mask filtering option” in the RS-FISH plugin.

To identify the electroporated neurons in mouse mPFC, segmented masks of GFP/RFP cells were used **(Fig. 9)**. In human specimens, segmented masks of SMI32-positive cells were employed to identify dysmorphic neurons **(Fig. 10)**. This was achieved by distinguishing the masks corresponding to GFP, RFP, and SMI32-positive neurons from

the negative ones using the median intensity measurement function (2D/3D) in the MorphoLibJ plugin in Fiji (Legland et al., 2016). Moreover, the same plugin was utilised for cell size measurements as volume parameter (μm^3) for 3D NeuN masks from mouse and as cell size (μm^2) for 2D NeuN masks from human samples.

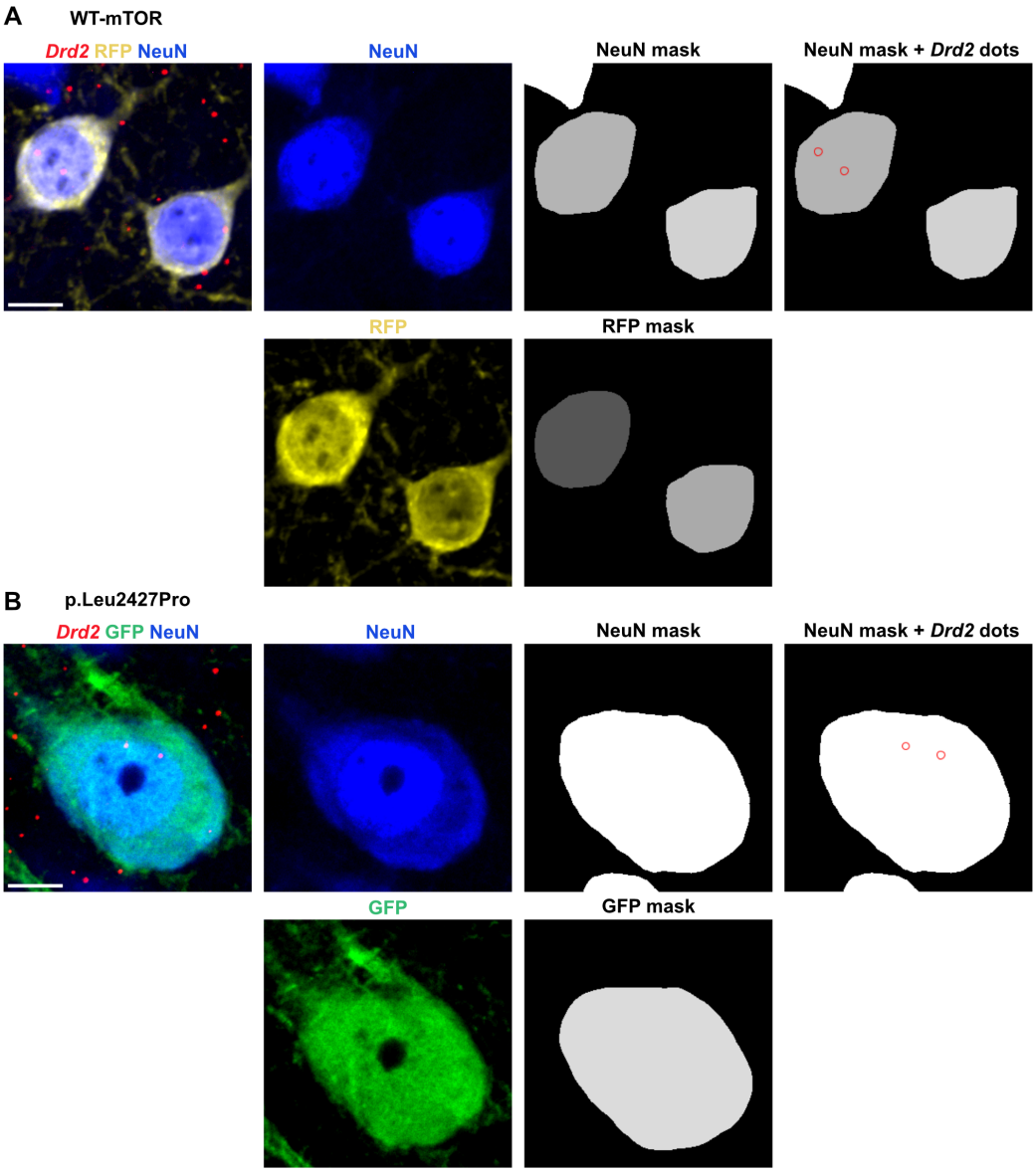

Fig. 9. Analysis pipeline of the *Drd1/Drd2* mRNA puncta quantification in mouse mPFC. **A)** *Drd2* expression in the WT-mTOR mPFC. Separate channels display the RFP signal and NeuN IHC. The neuronal soma (NeuN) identified through the trained model in machine-learning tool Cellpose, and followed by the creation of a binary mask of the thresholded neurons. RFP+ neurons are also separately identified using the same machine-learning tool, allowing for the specific identification of neurons targeted by the WT-mTOR construct. (Figure legend continued on next page)

Drd puncta are identified using RS-FISH software and quantified as the number of puncta within the NeuN mask of each cell. The final image shows *Drd2* mRNA puncta overlaid on the neuronal mask of an RFP+ neuron from the original raq image. **B)** *Drd2* expression in the p.Leu2427Pro mPFC. Separate channels show the GFP signal and NeuN IHC. Similar to panel A, the neuronal soma is identified with NeuN IHC using the Cellpose tool, and a binary mask is created from the thresholded neurons. GFP+ neurons are co-identified using the same tool to specifically distinguish neurons targeted by the p.Leu2427Pro construct. *Drd* puncta are identified using RS-FISH software and quantified as the number of puncta within the NeuN mask of each cell. The final image shows *Drd2* mRNA puncta overlaid on the neuronal mask of a GFP+ neuron. Scale bar: 10 μm.

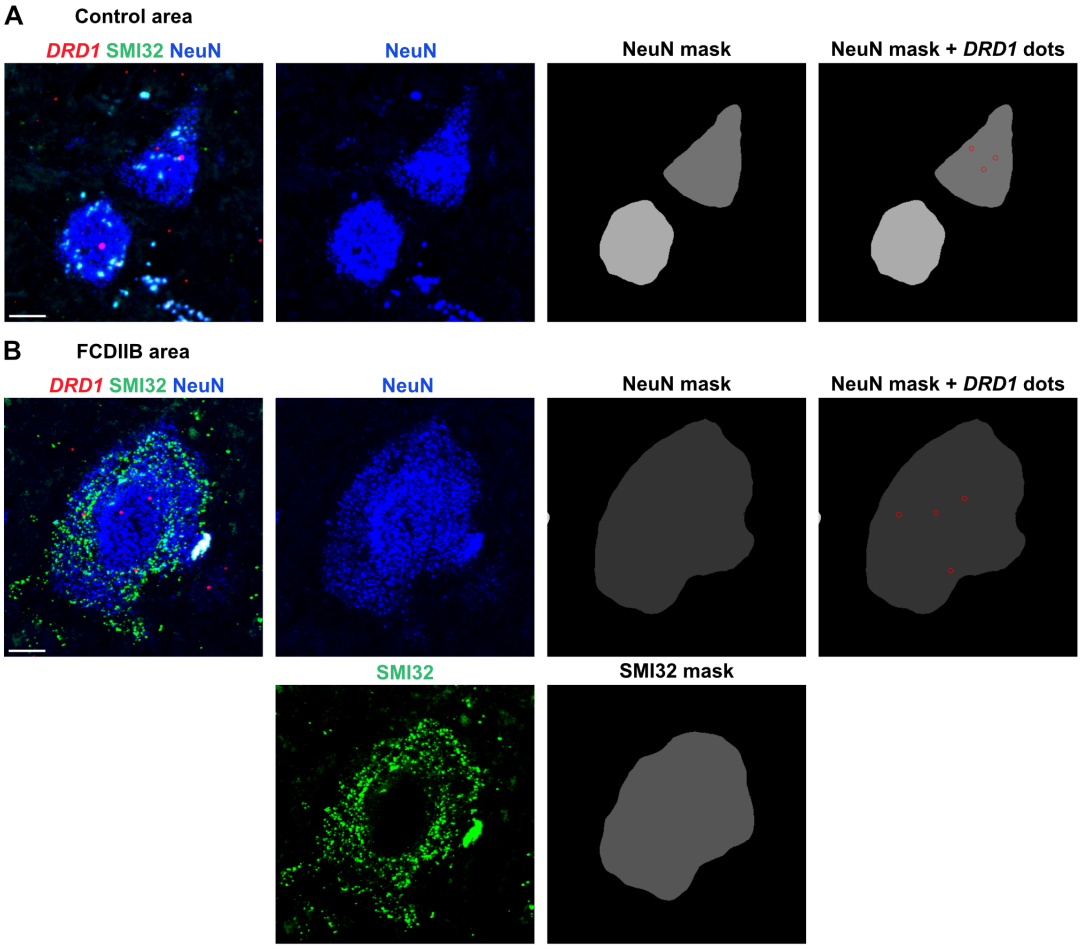

Fig. 10. Analysis pipeline for *DRD1/DRD2* mRNA puncta quantification in human specimen. **A)** *DRD1* expression in the control area of a human FCD type 2b specimen and a separate channel displaying NeuN IHC marking all neurons. The neuronal soma is identified using NeuN IHC, processed through the machine-learning tool Cellpose, followed by the creation of a binary mask of the thresholded neurons. *Drd* puncta are then identified using RS-FISH software and quantified as the number of puncta within each NeuN mask cell. The final image shows *DRD1* mRNA puncta overlaid on the neuronal mask. **B)** The second panel presents an example image of *DRD1* expression in the FCD type 2b area of a human specimen, (Figure legend continued on next page)

with separate channels showing SMI32 and NeuN IHC. Similar to panel A, the neuronal soma is identified with NeuN IHC using the Cellpose tool, and a binary mask is created from the thresholded neurons. Dysmorphic neurons (SMI32+ neurons) are co-identified using the same machine-learning tool, allowing for the specific distinction of these neurons from the surrounding NeuN-only neurons. *Drd* puncta are identified using RS-FISH software and quantified as the number of puncta within each NeuN mask cell. The final image shows *DRD1* mRNA puncta overlaid on the neuronal mask of a dysmorphic neuron. Scale bar: 10 µm.

2.11. Phospho-S6 expression analysis

To assess the overactivation of the mTOR-signaling pathway in electroporated neurons within the WT-mTOR and p.Leu2427Pro mPFC, Phospho-S6 (Ser240/244), a marker of mTORC1 activation, was stained as previously described (Immunohistochemistry - Mouse tissue). The entire mPFC area was imaged using a 20x air objective with the Visitron VisiScope Confocal Spinning Disk Microscope at the UKB Microscope Core Facility. For quantification, RFP+/GFP+ neurons were identified through thresholding in Fiji to create binary masks. To achieve proper segmentation of individual neurons, watershed segmentation was applied, followed by the "analyze particles" function with thresholds set at 80–infinity for RFP+ and 150–infinity for GFP+ neurons. Segmented neurons were then merged using the OR function, overlaid on the pS6 channel, and cleared outside the selection to isolate pS6 expression in RFP+/GFP+ neurons. This process was repeated, clearing areas within the selection to capture pS6 expression in surrounding RFP-/GFP- neurons. Mean grey values were measured and plotted for each neuron group.

2.12. TH-NET colocalization analysis in mouse tissue

To determine whether a subset of TH-expressing axons in the mPFC are NA axons, mPFC tissue was stained for TH and sodium-dependent noradrenaline transporter (NET/SLC6A2) as described previously (Immunohistochemistry - Mouse sections 2.6.1.). Area selection and distinctions between upper and deeper layers of the mPFC were performed similarly as described in Quantification of innervation density in mouse tissue (2.9.1.). For quantification, the TH channel was thresholded in Fiji, converted to a binary image, and the area occupied by axons was measured. The thresholded area was then selected and overlaid on the NET channel, with non-selected areas cleared out to isolate

the colocalizing area with double-labelled axons. The percentage of colocalization was calculated by dividing the colocalized area by the total area occupied by TH axons*100.

2.13. Statistical analysis

All statistical analyses and visualizations were conducted using R Studio (Team, 2020) and GraphPad Prism (Version 10.4.1). To assess data distribution, histograms and Q-Q plots were created, followed by the Shapiro-Wilk test to check for normality. If the normality test was passed, paired or unpaired t-tests (*p*-values were adjusted for multiple comparisons using the Bonferroni-Dunn method), one-way ANOVA with repeated measures followed by Tukey correction for multiple comparisons between groups and two-way ANOVA with repeated measures followed by Bonferroni correction for multiple comparisons were applied. If the normality test was not passed, non-parametric Mann-Whitney-Wilcoxon test or Kruskal-Wallis test followed by post-hoc Dunn's test with Bonferroni correction test for multiple comparisons was applied. The statistical tests applied are indicated in the figure legends. Boxplots and violin plots were used to display value distributions, with mean values represented by data points and median values indicated by horizontal lines within the boxplots. *Drd1/DRD1* and *Drd2/DRD2* mRNA transcript expression values are reported in the text as mean ± standard error of the mean (SEM). Correlation analysis was conducted using the Spearman test, with correlation coefficients and P-values reported in the figures. Statistical significance was denoted as follows: * $p < .05$, ** $p < .01$, *** $p < .001$, **** $p < .0001$.

3. Results

3.1. Establishing a model of FCD type 2 in the murine mPFC

To investigate whether malformations of cortical development influence the development or maintenance of mesocortical DA axons in cortical areas like the mPFC that are highly innervated by DA fibres in mouse, we first needed to establish a mouse model of FCD type 2 in the mPFC. To achieve this, we introduced a somatic hyperactivating mTOR kinase mutation into cortical progenitors in the mPFC. The mTOR mutation was discovered in patients with FCD type 2 and causes delayed migration, cytomegalic neurons, and spontaneous seizures when introduced into the developing murine cortex (see Introduction 1.3.1.) (Lim et al., 2015). However, its effect on frontal cortical brain regions has not been tested so far. We employed IUE to introduce a plasmid harboring the coding sequence for mutated mTOR fused together with EGFP (p.Leu2427Pro-EGFP) into the progenitors of pyramidal neurons at E14, thus targeting the later-born upper layer pyramidal neurons. As a control, we electroporated a plasmid containing the coding sequence for wild-type mTOR also fused with EGFP (WT-mTOR-EGFP) into progenitors of pyramidal neurons at E14. A plasmid containing the coding sequence for RFP under control of the U6 promoter (pAAV-U6-mRFP) was co-electroporated with the WT-mTOR-EGFP plasmid. The RFP expression was used to postnatally distinguish mice electroporated with WT-mTOR (GFP+ and RFP+) from mice electroporated with p.Leu2427Pro-mTOR (GFP+ and RFP-). We adapted the IUE protocol (see Methods 2.4.) to target the mPFC specifically and confirmed the success of this method in postnatal mice at a stage when neuronal migration was completed **(Fig. 11A & B)**. Images of the mPFC at P30 revealed that neurons electroporated with the WT-mTOR construct expressed low GFP signal and thus, were identified in all experiments only by RFP+ expression. These neurons had successfully reached their final position in the upper layers of the cortex **(Fig. 11A & B, upper panel)**. In contrast, neurons electroporated with the p.Leu2427Pro-mTOR construct (GFP+) mostly failed to reach their appropriate location and were dispersed throughout the cortical layers **(Fig. 11A & B, bottom panel)**, recapitulating the migratory defects and cortical dyslamination seen in FCDs and in more posterior cortical areas of the published mouse model (Lim et al., 2015). Hereafter, we will

refer to the mice/neurons electroporated with WT-mTOR as WT-mTOR/RFP+ and those electroporated with p.Leu2427Pro-mTOR as p.Leu2427Pro/GFP+.

Another prominent neuropathological phenotype in FCD type 2 areas is the presence of cytomegalic neurons. p.Leu2427Pro/GFP+ cells appeared to have an increased soma size, based on the expression of the global neuronal marker NeuN that labels nucleus and soma **(Fig. 11B, NeuN panel)**. To assess this in a quantitative manner, the cell soma volumes of NeuN expressing cells in the targeted region of the mPFC were measured at P30 **(Fig. 11C)** and P60 **(Fig. 11D)**. This analysis revealed that p.Leu2427Pro/GFP+ neurons exhibited significantly larger soma volumes compared to surrounding non-electroporated neurons (GFP- in p.Leu2427Pro-mutated mPFC) and WT-mTOR/RFP+ neurons and in the upper layers, and compared to non-electroporated neurons (RFP- in WT-mTOR and GFP- in p.Leu2427Pro-mutated mPFC) in the deeper layers, at P30 **(Fig. 11C)** and P60 **(Fig. 11D)**.

To confirm that the p.Leu2427Pro-mTOR mutation results indeed in hyperactivation of the mTOR pathway, we performed IHC for phospho-S6 (pS6) (Ser240/244), a marker of mTOR kinase activity **(Fig. 12A)**. p.Leu2427Pro/GFP+ cells had significantly elevated expression of pS6 (Ser240/244) in their soma compared to surrounding non-electroporated (GFP-) neurons or WT-mTOR/RFP+ neurons **(Fig. 12B)**. WT-mTOR/RFP+ neurons exhibited a similar expression of pS6 (Ser240/244) to that observed in non-electroporated neurons **(Fig. 12B)**. Thus, p.Leu2427Pro/GFP+ cells exhibited increased mTOR kinase activity due to the hyperactivating mTOR p.Leu2427Pro mutation.

These data demonstrate that IUE of the mTOR p.Leu2427Pro construct in pyramidal neuron progenitors of the mPFC is sufficient to reproduce the neuropathological hallmarks of FCD type 2, such as cortical dyslamination and cytomegalic neurons. This highlights the reproducibility of the model across multiple cortical areas while emphasizing the novelty of this study in establishing its application to more frontal cortical areas, such as the mPFC.

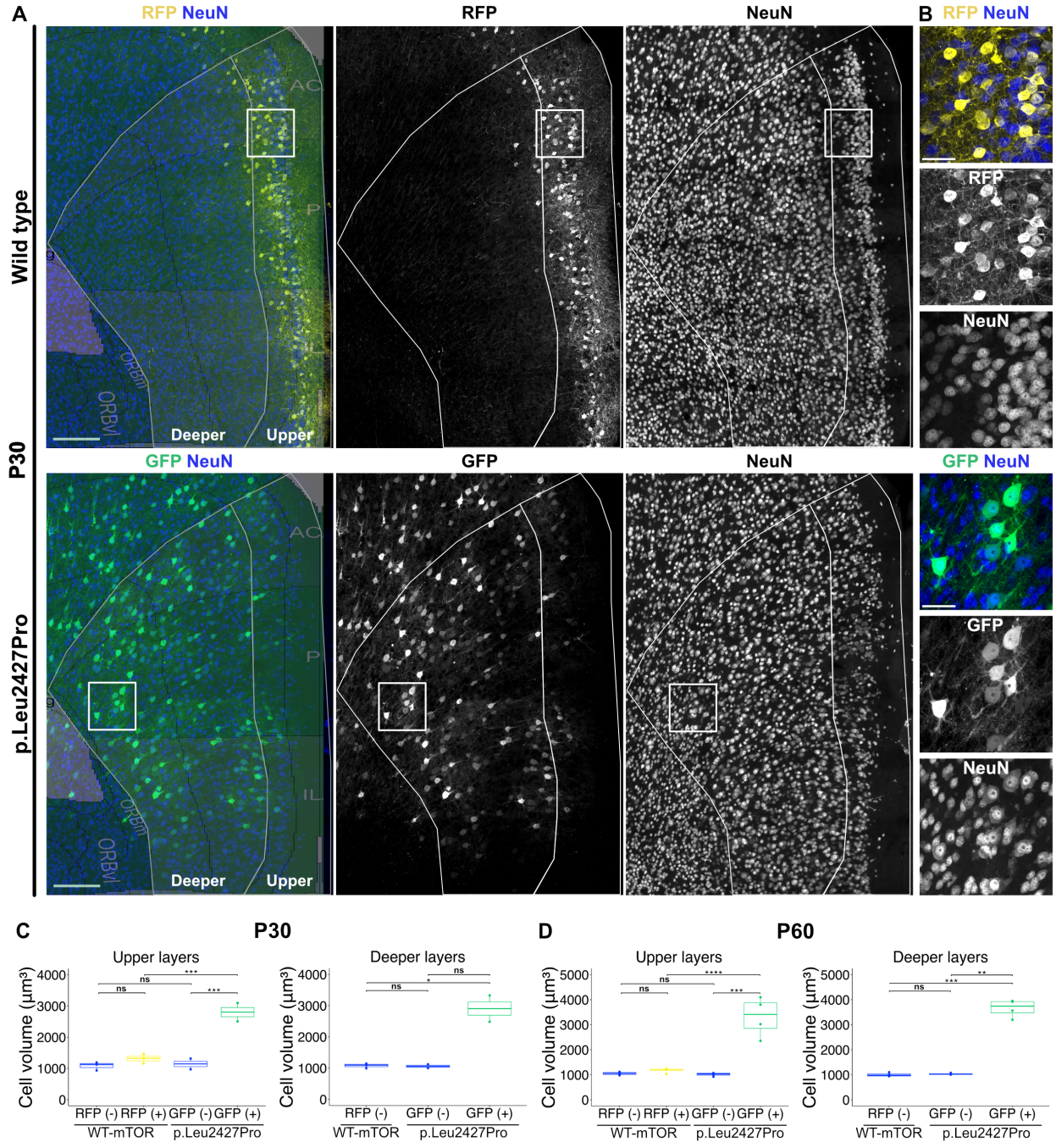

Fig. 11. Establishing a mouse model of FCD type 2 in the mPFC. **A)** Representative images of mTOR-WT (top) and p.Leu2427Pro mTOR mutated (bottom) mPFC at P30 immunostained for NeuN, RFP and GFP. Scale bar 200 µm. **B)** Higher magnifications from the boxed regions in **A** indicating neurons electroporated with WT-mTOR-type construct expressing RFP (top) or with mTOR p.Leu2427Pro mutation expressing GFP (bottom). Scale bar 50 µm. **C, D)** Quantification of soma volume from non-electroporated and electroporated neurons in the upper and deeper layers of the mPFC at **C)** P30 and **D)** P60. Upper layers: 2-way ANOVA with repeated measures to compare within-experimental groups followed by Bonferroni test to correct for multiple comparisons between the indicated groups. (Figure legend continued on next page)

Deeper layers: paired t-test to compare GFP (-) vs. GFP (+) groups within the p.Leu2427Pro experimental group and unpaired t-test to compare between other groups. P-values were adjusted for multiple comparisons using the Bonferroni-Dunn method to control Type I error rate for the family of comparisons. P30: *n* = 3 WT-mTOR vs. 2 p.Leu2427Pro mice, P60: *n* = 4 mice . Groups in WT-mTOR mPFC: RFP (-): non-electroporated, NeuN+ neurons; RFP (+): neurons electroporated with WT-mTOR plasmid, NeuN+. Groups in p.Leu2427Pro mPFC: GFP (-): non-electroporated, NeuN+ neurons; GFP (+): neurons electroporated with mTOR-p.Leu2427Pro plasmid, NeuN+. Data shown in this figure contributed to Supplementary Figure 1 in Meli et al., 2025.

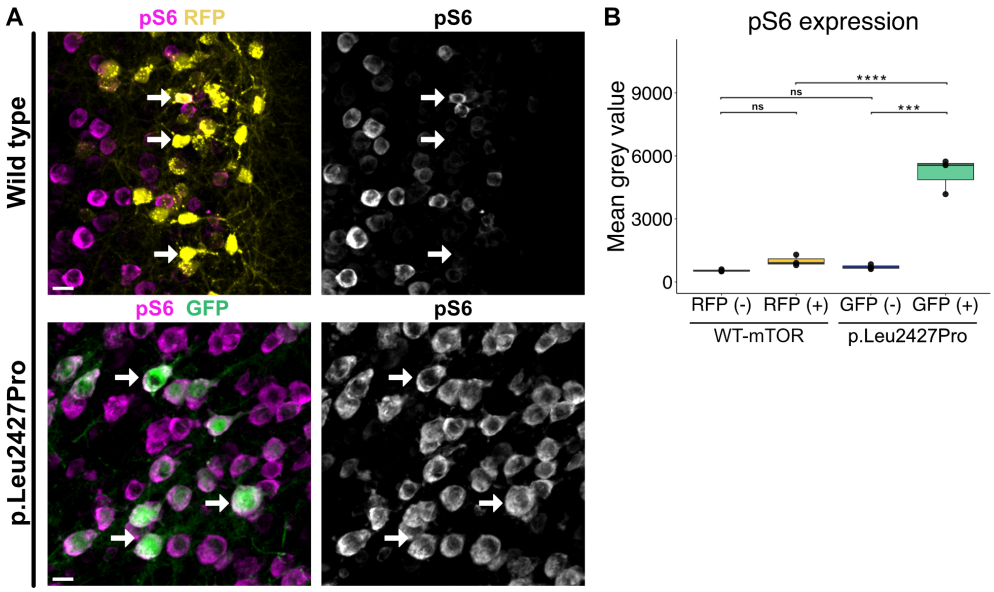

Fig. 12. Phospho-S6 (Ser240/244) expression in mouse mPFC at P30. **A)** Representative images of pS6 (Ser240/244) expression in the WT-mTOR (top) and p.Leu2427Pro (bottom) mPFCs (white arrows indicate electroporated neurons). Scale bar 20 μm. **B)** Quantification of pS6 (Ser240/244) mean grey value intensity expression within RFP+/GFP+ neurons and non-electroporated (RFP-/GFP-) neurons in WT-mTOR and p.Leu2427Pro mPFCs. *n* = 3, 2-way ANOVA with repeated measures to compare within-experimental groups followed by Bonferroni test to correct for multiple comparisons between the indicated groups. Data shown in this figure contributed to Supplementary Figure 2 in Meli et al., 2025.

3.2. Altered DA axonal density and maturation in the mPFC of the FCD type 2 mouse model

After establishing an FCD type 2 model in the murine mPFC, we analyzed the DA axonal density within this region in WT-mTOR **(Fig. 13A)** and p.Leu2427Pro **(Fig. 13B)** mice. We performed IHC against TH to label DA axons in the mPFC at two timepoints: early adolescence (P30) and early adulthood (P60). Since DA innervation density is higher in

the deeper than in the upper layers of the mPFC, we analyzed the innervation density separately in upper and deeper layers. At early adolescence (P30), DA density quantification did not reveal any significant differences between the WT-mTOR and p.Leu2427Pro mPFC in either upper or deeper layers **(Fig. 13C)**. However, at early adulthood (P60), the quantification showed a trend towards decreased DA innervation density in the upper layers of the p.Leu2427Pro mPFC compared to the WT-mTOR mPFC **(Fig. 13D)**. This trend was less pronounced in the deeper layers. As described in the introduction, DA innervation continues to mature during adolescence until adulthood (Naneix et al., 2012), thus we compared the DA innervation density between P30 and P60. This comparison revealed that DA density significantly increases from P30 to P60 in the upper layers of WT-mTOR mPFC, but not in the p.Leu2427Pro mPFC **(Fig. 13E)**. No significant temporal changes in DA innervation density were observed in the deeper layers of the mPFC in either the WT-mTOR mPFC or the p.Leu2427Pro mice **(Fig. 13E)**.

These results suggest that cortical malformations in the mPFC caused by hyperactivating the mTOR kinase impact the maturation of DA axonal innervation density.

TH is a predominant marker for DA axons, but is also expressed in NA neurons and axons. Literature suggests that only 10% of NA axons are co-labelled with TH in human and rat mPFC (See Introduction 1.4.2.), but there are no data from mouse mPFC. Therefore, we first wanted to assess the percentage of NA axons that express TH by performing a double IHC for TH and NET (specific marker for NA axons) **(Fig. 13F)**. We measured the colocalization between these 2 markers in the mPFC and found out that 26% of NA axons in the upper layers and 13% in the deeper layers are co-labelled with TH **(Fig. 13G)**.

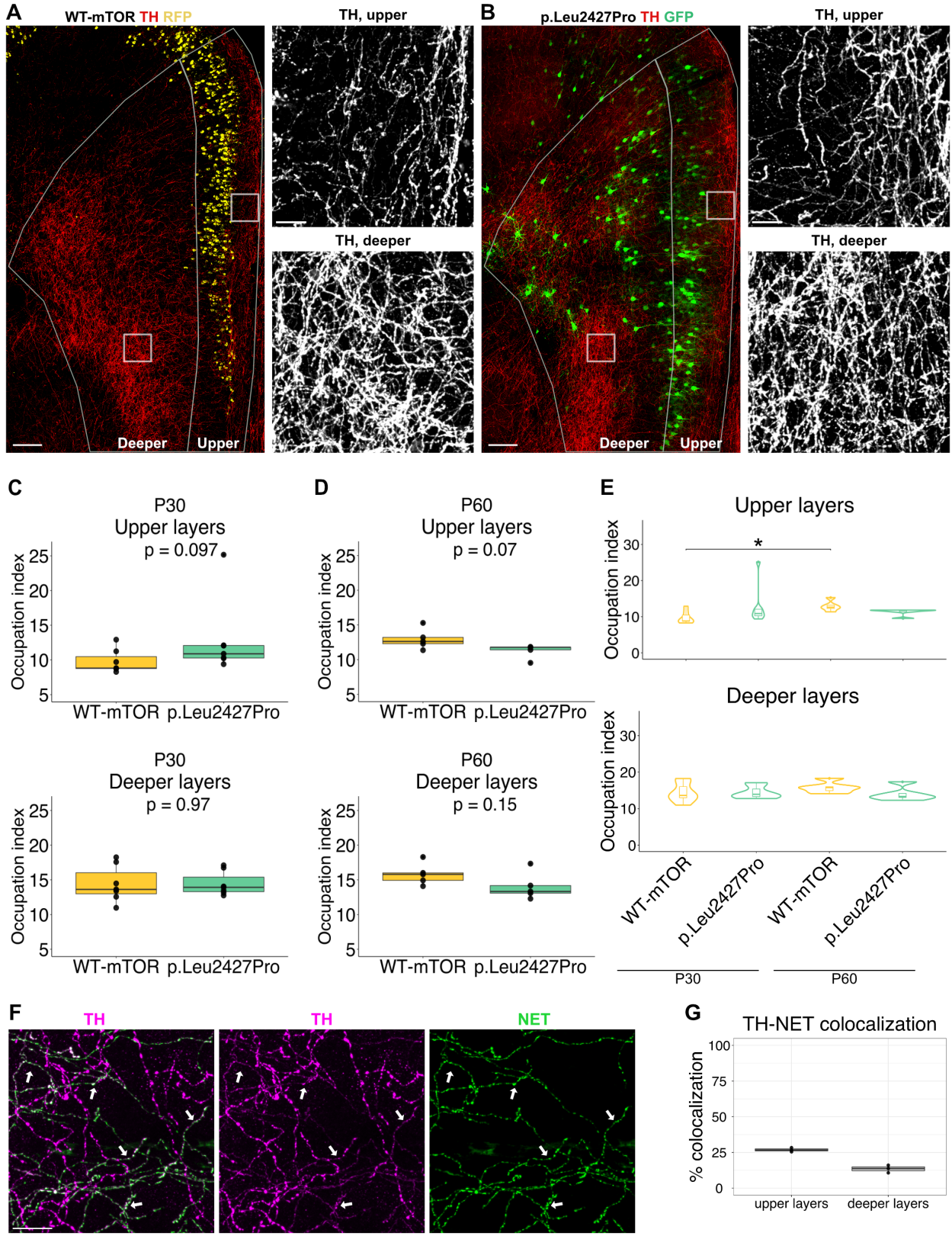

Fig. 13. (Figure legend continued on next page)

Fig. 13. Altered DA innervation density and maturation in the mPFC of FCD type 2 mouse model. **A, B)** Representative images of DA axonal analysis in the mPFC of **A)** WT-mTOR and **B)** p.Leu2427Pro mice at P30 immunostained with TH. Scale bar 200 μm. Right panels: Higher magnifications of TH-expressing DA axons in the upper (top) and deeper layers (bottom) from the indicated regions. Scale bar 30 μm. **C)** Quantification of DA innervation density at P30 (*n* = 7). Tested with Mann-Whitney-Wilcoxon for upper layers and unpaired t-test for deeper layer for statistical difference between the groups. **D)** Quantification of DA innervation density at P60 (*n* = 5). Tested with unpaired t-test for statistical difference between the groups. **E)** Analysis of DA innervation maturation between P30 and P60 in the upper (top) and deeper (bottom) mPFC layers of WT-mTOR and p.Leu2427Pro mice. Tested with Kruskal-Wallis test followed by post-hoc Dunn's test with Bonferroni adjustments for multiple comparisons. Occupation index indicates the percentage of the area occupied by DA axons in each layer divided by the measured area*100. **F)** Representative images of axons stained with TH and NET in the upper layer of the mPFC. Arrows highlight fibers where these markers are colocalized. Scale bar: 20 μm. **(G)** Analysis of TH and NET colocalization in axons across both the upper and deeper layers of the mPFC. The percentage of colocalization represents the proportion of the overlap (TH+ & NET+ area) relative to the total TH+ area. *n* = 3, P45. Data shown in this figure contributed to Figure 1 and Supplementary Figure 3 in Meli et al., 2025.

3.3. Alterations of DA axonal density are most pronounced in the infralimbic cortex of FCD type 2 mPFC mouse model

The mPFC consists of distinct sub-regions identified as AC, PL and IL (See Introduction 1.4.). Given that the DA axonal innervation density varies between these sub-regions of the mPFC (Naneix et al., 2012), we further divided the mPFC into AC, PL and IL for further analysis **(Fig. 14A & B)**. This detailed comparison revealed a significant increase of DA innervation density specifically in the deeper layers of the p.Leu2427Pro AC at P30 **(Fig. 14C)**. This difference between WT-mTOR and p.Leu2427Pro AC was however not maintained at P60 **(Fig. 14D)**. In the PL there was no significant change in DA innervation density at the two analyzed stages. In contrast, DA innervation in the P60 IL was altered by the mTOR p.Leu2427Pro mutation. DA innervation in both the upper and deeper layers of p.Leu2427Pro IL was significantly reduced compared to the WT-mTOR mPFC **(Fig. 14D)**.

These results indicate that DA innervation is potentially reduced throughout in the cortically malformed mTOR mutated adult mPFC, with the IL sub-region being the most affected.

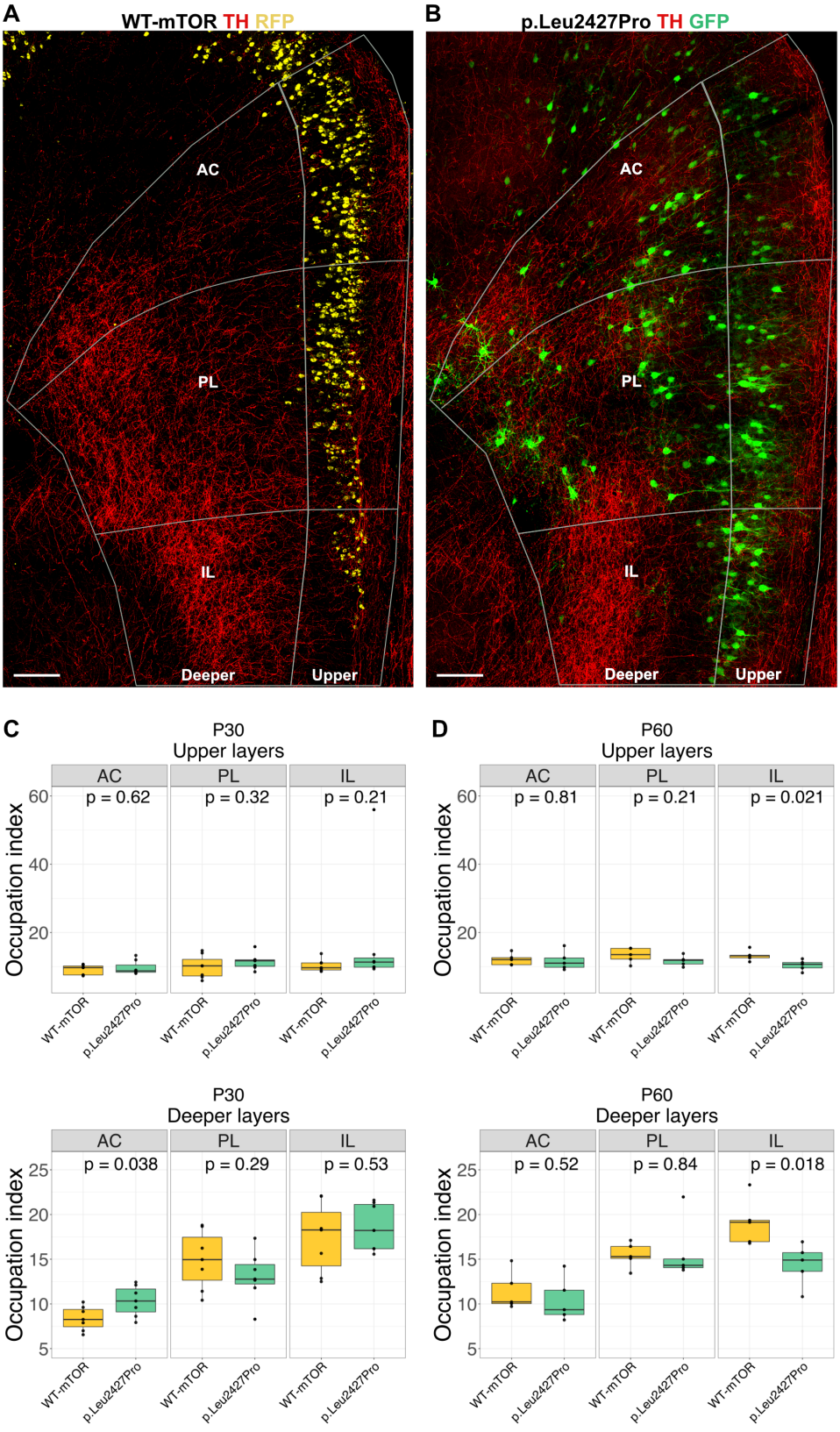

Fig. 14. (Figure legend continued on next page)

Fig. 14. Alterations of DA innervation density in the sub-regions of the FCD type 2 mouse model mPFC. **A, B)** Representative images of DA axonal analysis in the sub-regions of **A)** WT-mTOR and **B)** p.Leu2427Pro mPFC immunostained with TH. Scale bar 200 μm. **C)** Quantification of DA innervation density across the sub-regions of mPFC at P30 (*n* = 7). Tested with Mann-Whitney-Wilcoxon for upper layers and unpaired t-test for deeper layer for statistical difference between the groups. **D)** Quantification of DA innervation density across the sub-regions of mPFC at P60 (*n* = 5). Tested with unpaired t-test for statistical difference between the groups. Occupation index indicates the percentage of the area occupied by DA axons in each sub-region divided by the total area of that sub-region*100. Data shown in this figure contributed to Supplementary Figure 4 in Meli et al., 2025.

3.4. NET and SERT axonal density are not altered in the mPFC of the FCD type 2 mouse model

The mPFC also receives substantial NA and 5-HT axonal innervation, each mediating important neural functions (See Introduction 1.4.2. and 1.4.3.). Therefore, we next investigated if the axonal density of these neuromodulatory systems is also altered in the mPFC of the FCD type 2 mouse model. For this, we performed IHC for NET and 5-HT transporter (SERT) and quantified innervation density in the sub-structures of the mPFC for upper and deeper layers at P30 **(Fig. 15)**.

We observed no changes in NA axonal density in either the upper **(Fig. 15A)** or in the deeper layers **(Fig. 15B)** between WT-mTOR and p.Leu2427Pro mouse mPFC. Similarly, analysis of the density of SERT positive axons did not reveal any changes in density in the upper layers between WT-mTOR and p.Leu2427Pro mPFC **(Fig. 15C).** In the deeper layers, a trend towards increased 5-HT innervation was detected in the PL of the p.Leu2427Pro mouse mPFC compared to WT-mTOR mPFC **(Fig. 15D)**. Overall, this analysis did not reveal any significant changes in the NA or 5-HT innervation in the mouse mPFC at P30. Given that, unlike DA, these monoaminergic systems have been reported to be fully mature at early postnatal stages (See Introduction 1.4.2. and 1.4.3.), we did not perform any quantitative analysis at adult stages.

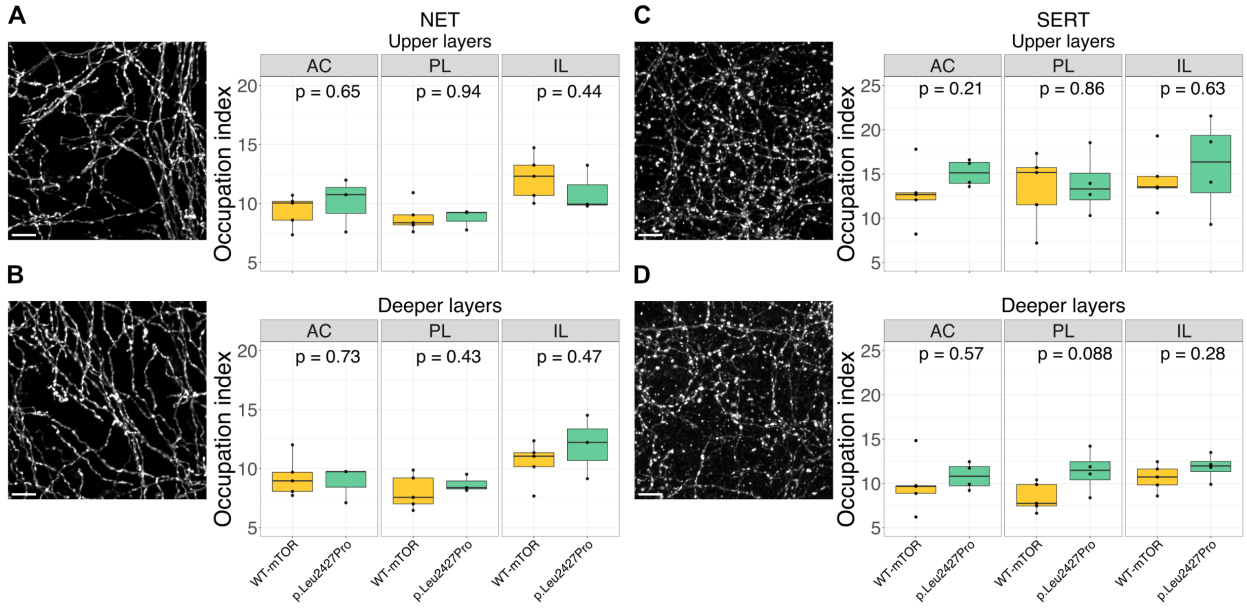

Fig. 15. Unaltered NET and SERT axonal innervation density in the mPFC of the FCD type 2 mouse model. **A, B)** Examples of NET IHC and quantification analysis in the **A)** upper and **B)** deeper layers of the sub-regions of mouse mPFC. *n* = 5 WT-mTOR vs. 3 p.Leu2427Pro P30 mice. **C, D)** Examples of SERT IHC and quantification analysis in the **C)** upper and **D)** deeper layers of the sub-regions of mouse mPFC. *n* = 5 WT-mTOR vs. 4 p.Leu2427Pro P30 mice. Scale bar 10 μm. Tested with unpaired t-test for statistical difference between the groups. Occupation index indicates the percentage of the area occupied by the axons in each sub-region divided by the total area of that sub-region*100. Data shown in this figure contributed to Supplementary Figure 3 in Meli et al., 2025

3.5. Increased expression of *Drd1* and *Drd2* mRNA in p.Leu2427Pro-mTOR mutated neurons in the mouse mPFC

The observed changes in DA axonal innervation in adult mPFC of p.Leu2427Pro mice could result in changes in DA neurotransmission and DA availability in the extracellular space. Additionally, the effectiveness of DA neurotransmission and its subsequent impact on DA-receiving neurons is heavily influenced by the type and level of DA receptor expression (See Introduction 1.4.1.) (Tritsch & Sabatini, 2012). As described in the introduction, *Drd1* and *Drd2* are the most abundantly expressed DA receptors in the mPFC. Thus, we performed FISH for either *Drd1* and *Drd2* in the mPFC of WT-mTOR and p.Leu2427Pro mice at P30 **(Fig. 16)** and P60 **(Fig. 17)** in combination with IHC for NeuN to label all the neurons in the mPFC and RFP or GFP to label the electroporated neurons **(Fig. 16A)**. In this manner we were able to quantify the expression of *Drd1* and

Drd2 mRNA transcripts as single punctae inside the cell somas of our labelled neurons **(Fig.9)**.

The expression levels of *Drd1* and *Drd2* differ in different layers of the mPFC (See Introduction 1.4.1). Thus, we analyzed upper and deeper layers separately **(Fig. 16A)**. Our quantitative analysis confirmed the difference in expression levels between upper and deeper layers of the mPFC: in the WT-mTOR mPFC *Drd1* expression was higher in the deeper layers (mean ± SEM P30: 3.58 ± 0.615 puncta per cell (ppc), P60: 2.93 ± 0.091 ppc) than in upper layers (P30: 1.30 ± 0.233, P60: 1.40 ± 0.140 ppc), while *Drd2* expression was a little higher in the upper layers (P30: 3.65 ± 1, P60: 2.06 ± 0.106 ppc) than in the deeper layers (P30: 2.81 ± 0.463, P60: 1.67 ± 0.125 ppc).

When comparing *Drd1* expression levels in upper layers of the mPFC between targeted and non-targeted neurons at P30 we found that the p.Leu2427Pro-mTOR/GFP+ expressed significantly more *Drd1* mRNA transcript (3.71 ± 0.804 ppc) compared to surrounding non-electroporated neurons (GFP-) (1.60 ± 0.116 ppc) and to WT-mTOR/RFP+ neurons (1.27 ± 0.490 ppc) in the upper layers of the WT-mTOR mPFC **(Fig. 16B)**. In the deeper layers, no significant change in *Drd1* mRNA transcript expression was observed among the groups: GFP+ neurons (3 ± 1.145 ppc), GFP- neurons (3.60 ± 0.543 ppc) in the p.Leu2427Pro mPFC or RFP- neurons (3.57 ± 0.614 ppc) in the WT-mTOR mPFC **(Fig. 16B)**.

Analysis of *Drd2* mRNA transcript expression at P30 in the upper layers showed that GFP+ neurons (8.59 ± 0.197 ppc) in the p.Leu2427Pro mPFC expressed significantly more *Drd2* mRNA transcript than non-targeted surrounding neurons (GFP-) (3.37 ± 0.135 ppc) or RFP+ neurons (4.70 ± 0.910 ppc) in the WT-mTOR mPFC **(Fig. 16C)**. An increase in *Drd2* mRNA transcript expression was also observed in GFP+ neurons (7.01 ± 1.284 ppc) in the deeper layers of the p.Leu2427Pro mPFC compared to surrounding non-targeted GFP- neurons (3.11 ± 0.370 ppc) or RFP- neurons (2.81 ± 0.462 ppc) in the WT-mTOR mPFC, however this did not reach a statistical significance **(Fig. 16C)**. Since GFP+ neurons in the deeper layers are destined to migrate to the upper layers, we examined whether their final location in the cortex affects *Drd* expression. There was no significant

difference in *Drd1* expression between upper (3.71 ± 0.804 ppc) and deeper (3 ± 1.145 ppc) layer GFP+ neurons in the p.Leu2427Pro mPFC **(Fig. 16D)**. Given that GFP+ neurons in the deeper layers are destined for the upper layers, where *Drd1* expression is typically lower, their similar *Drd1* expression levels to WT-mTOR deeper layer neurons may suggest an upregulation of *Drd1* in p.Leu2427Pro neurons ectopically located in the deeper layers. Similarly, there was no significant difference in *Drd2* expression between upper (8.59 ± 0.197 ppc) and deeper (7.01 ± 1.284 ppc) layer GFP+ neurons in the p.Leu2427Pro mPFC **(Fig. 16E)**, supporting a cell-autonomous effect of the mutation that is independent of the local environment.

At P60, similar trends were observed. In the upper layers, GFP+ neurons expressing the p.Leu2427Pro mTOR mutation had elevated *Drd1* mRNA levels (3.60 ± 0.432 ppc) compared to surrounding non-electroporated neurons (GFP-) (1.44 ± 0.062 ppc) and to RFP+ neurons (1.17 ± 0.148 ppc) in the WT-mTOR mPFC **(Fig. 17A)**. In the deeper layers, GFP+ neurons (2.81 ± 0.710 ppc) did not show significant differences in *Drd1* expression when compared to non-electroporated GFP- neurons (2.51 ± 0.270 ppc) in the p.Leu2427Pro mPFC or to RFP- neurons (2.93 ± 0.091 ppc) in the WT-mTOR mPFC **(Fig. 17A).**

Analysis of *Drd2* mRNA transcript expression at P60 also revealed that GFP+ cells in the upper layers express more *Drd2* mRNA (4.82 ± 0.596 ppc) than surrounding non-electroporated GFP- neurons (1.45 ± 0.136 ppc) and RFP+ neurons (2.86 ± 0.382 ppc) in the WT-mTOR mPFC **(Fig. 17B)**. Additionally, in the deeper layers, GFP+ cells (5.96 ± 0.475 ppc) displayed significantly higher *Drd2* expression compared to non-electroporated GFP- neurons (1.65 ± 0.2 ppc) in the p.Leu2427Pro mPFC and RFP- neurons (1.67 ± 0.125 ppc) in the WT-mTOR mPFC **(Fig. 17B)**.

Again, *Drd1* expression did not differ significantly between upper (3.60 ± 0.432 ppc) and deeper (2.81 ± 0.710 ppc) layer GFP+ neurons in the p.Leu2427Pro mPFC **(Fig. 17C)**. Similarly, *Drd2* expression remained similar between upper (4.82 ± 0.596 ppc) and deeper (5.96 ± 0.475 ppc) layer GFP+ neurons in the p.Leu2427Pro mPFC **(Fig. 17D)**, reinforcing the cell-autonomous effect of the mutation regardless of layer-specific conditions.

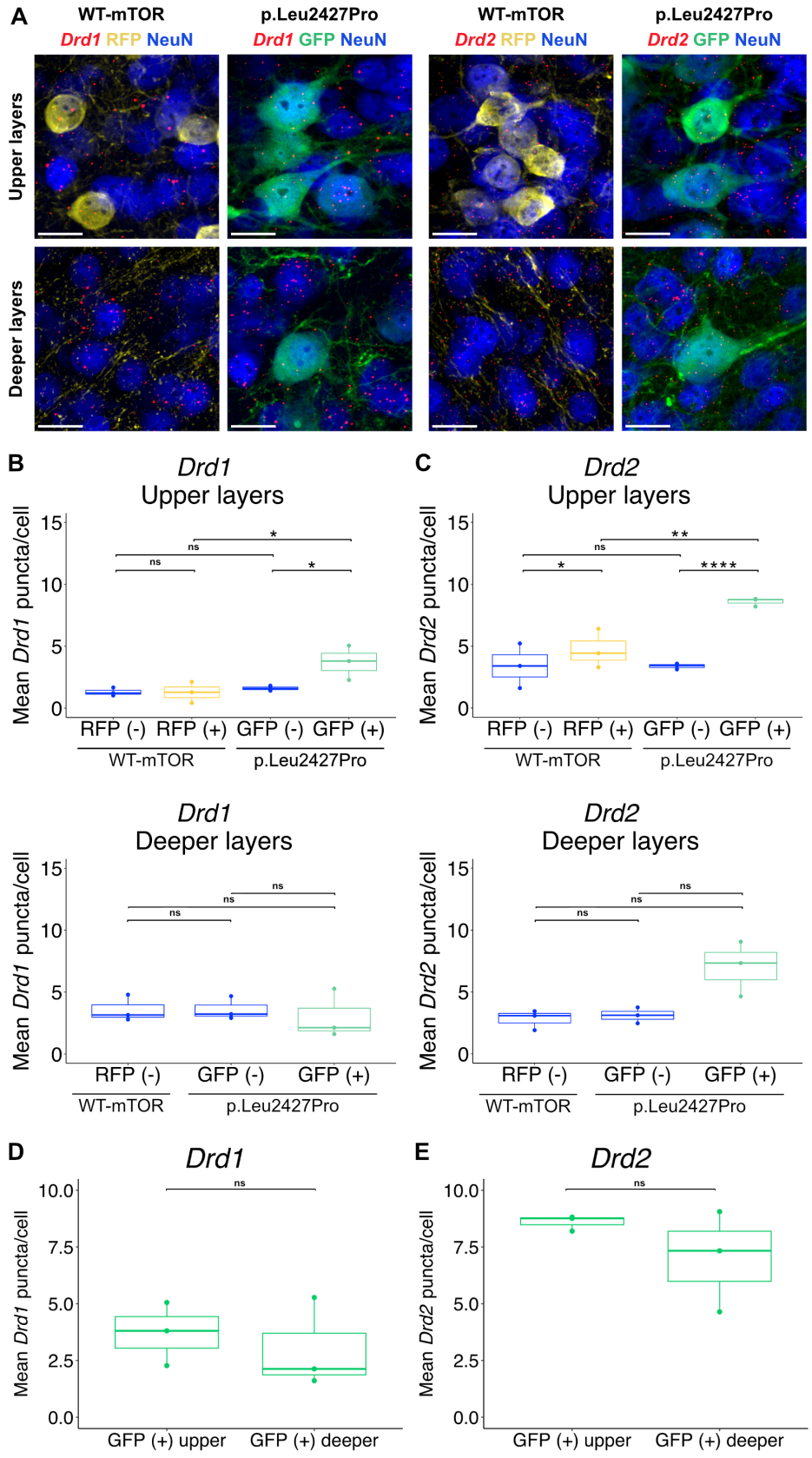

Fig. 16. (Figure legend continued on next page)

Fig. 16. Increased expression of *Drd1* and *Drd2* mRNA transcripts in p.Leu2427Pro mTOR mutated neurons at P30. **A)** Representative images of FISH for *Drd1* (left) and *Drd2* (right) combined with IHC for NeuN and GFP or RFP in the upper and deeper layers of WT-mTOR and p.Leu2427Pro mPFC. Scale bar 20 μm. **B, C)** mRNA puncta quantification of **B**) *Drd1* and **C**) *Drd2* transcript levels in different groups of neurons in WT-mTOR and p.Leu2427Pro mPFC. Groups in WT mPFC: RFP (-): non-electroporated, NeuN+ neurons; RFP (+): neurons electroporated with mTOR-WT plasmid, NeuN+. Groups in p.Leu2427Pro mPFC: GFP (-): non-electroporated, NeuN+ neurons; GFP (+): neurons electroporated with mTOR-p.Leu2427Pro plasmid, NeuN+. Number of neurons quantified for *Drd1* analysis: upper layers: 508 RFP (-), 125 RFP (+), 578 GFP (-), 60 GFP (+), deeper layers: 1069 RFP (-), 571 GFP (-), 83 GFP (+). Number of neurons quantified for *Drd2* analysis: upper layers: 572 RFP (-), 124 RFP (+), 527 GFP (-), 69 GFP (+), deeper layers: 1073 RFP (-), 607 GFP (-), 66 GFP (+). *n* = 3 mice per group. Upper layers: Two-way ANOVA with repeated measures to compare within-experimental groups followed by Bonferroni test to correct for multiple comparisons between the indicated groups. Deeper layers: paired t-test to compare GFP (-) vs. GFP (+) groups within the p.Leu2427Pro experimental group and unpaired t-test to compare between other groups. P-values were adjusted for multiple comparisons using the Bonferroni-Dunn method to control Type I error rate for the family of comparisons. **D, E)** Mean expression of **D)** *Drd1* and **E)** *Drd2* mRNA transcripts shown only for the GFP (+) groups from both upper and deeper layers of WT-mTOR and p.Leu2427Pro mPFC. *n* = 3 mice per group, unpaired t-test. Data shown in this figure contributed to Figure 2 and Supplementary Figure 5 in Meli et al., 2025.

The elevated expression of *Drd* may be a result of the generally larger cell size of mTOR mutated/dysmorphic neurons (Ransdell, Faust, & Schulz, 2010). To determine if the increased mRNA transcript expression of *Drd1* and *Drd2* was correlated with the enlarged soma volume of p.Leu2427Pro/GFP+ neurons, we performed a Spearman correlation analysis between neuron volume and *Drd1* or *Drd2* mRNA transcript expression at P30 **(Fig. 18A, B)** and P60 **(Fig. 18C, D)**. This analysis did not reveal any strong correlation between neuron volume and *Drd1* or *Drd2* mRNA transcript expression at either P30 or P60.

In summary, we demonstrate that p.Leu2427Pro GFP+ neurons express significantly higher levels of *Drd1* and *Drd2* mRNA transcripts than the surrounding non-targeted neurons or neurons in the WT-mTOR mPFC at both P30 and P60. These data indicate a cell-autonomous effect of the p.Leu2427Pro mTOR hyperactivating mutation on *Drd* expression that appears to be independent of the increased soma size of the affected neurons or their positioning across the cortical layers.

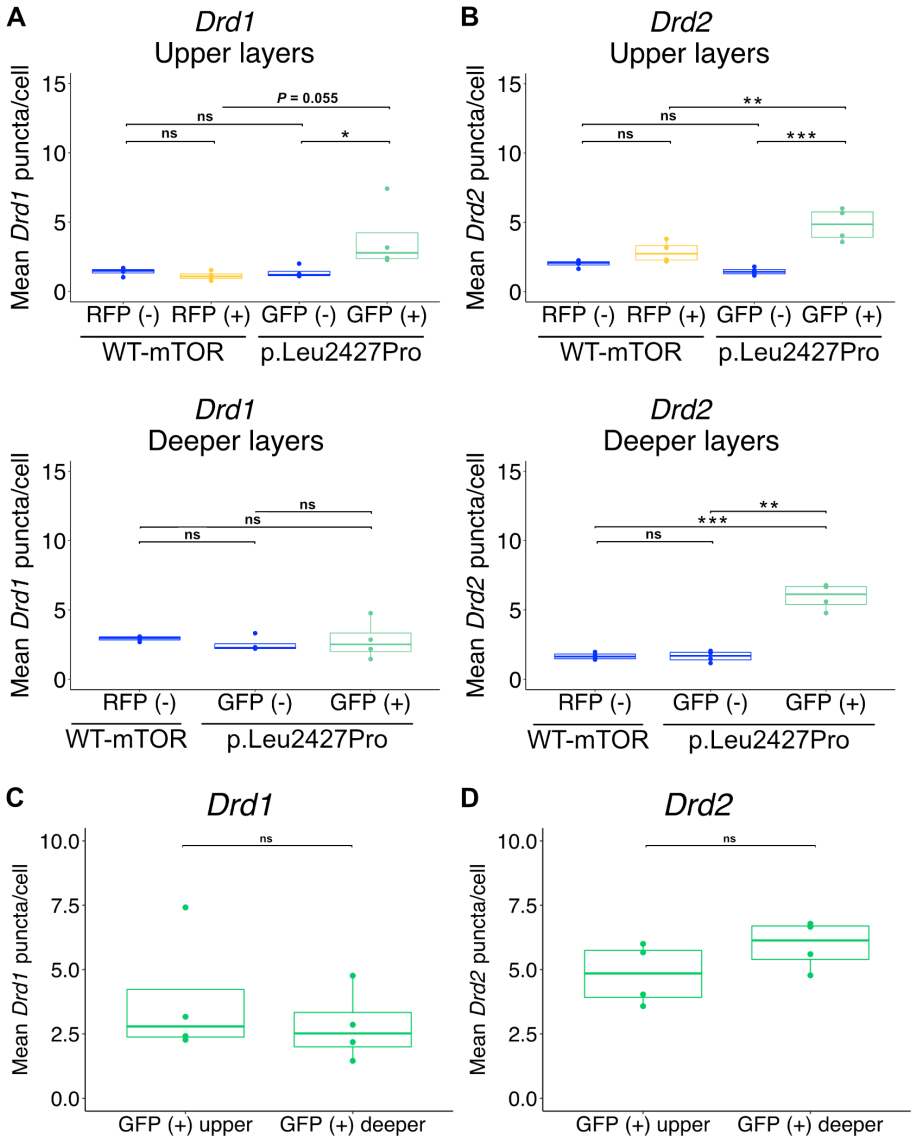

Fig. 17. Increased expression of *Drd1* and *Drd2* mRNA transcripts in p.Leu2427Pro mTOR mutated neurons at P60. **A, B)** mRNA puncta quantification of **A**) *Drd1* and **B**) *Drd2* transcript levels in different groups of neurons in WT-mTOR and p.Leu2427Pro mPFC. Groups same as explained above. Number of neurons quantified for *Drd1*: upper layers: 1123 RFP (-), 88 RFP (+), 1081 GFP (-), 53 GFP (+), deeper layers: 1912 RFP (-), 1231 GFP (-), 60 GFP (+). Number of neurons quantified for *Drd2*: upper layers: 1303 RFP (-), 98 RFP (+), 1069 GFP (-), 72 GFP (+), deeper layers: 1805 RFP (-), 971 GFP (-), 72 GFP (+). *n* = 4 mice per group. Tested same as explained above. **C, D)** Mean expression of **C)** *Drd1* and **D)** *Drd2* mRNA transcripts shown only for the GFP (+) groups from both upper and deeper layers of WT-mTOR and p.Leu2427Pro mPFC. *n* = 4 mice per group, unpaired t-test. Data shown in this figure contributed to Figure 2 and Supplementary Figure 6 in Meli et al., 2025.

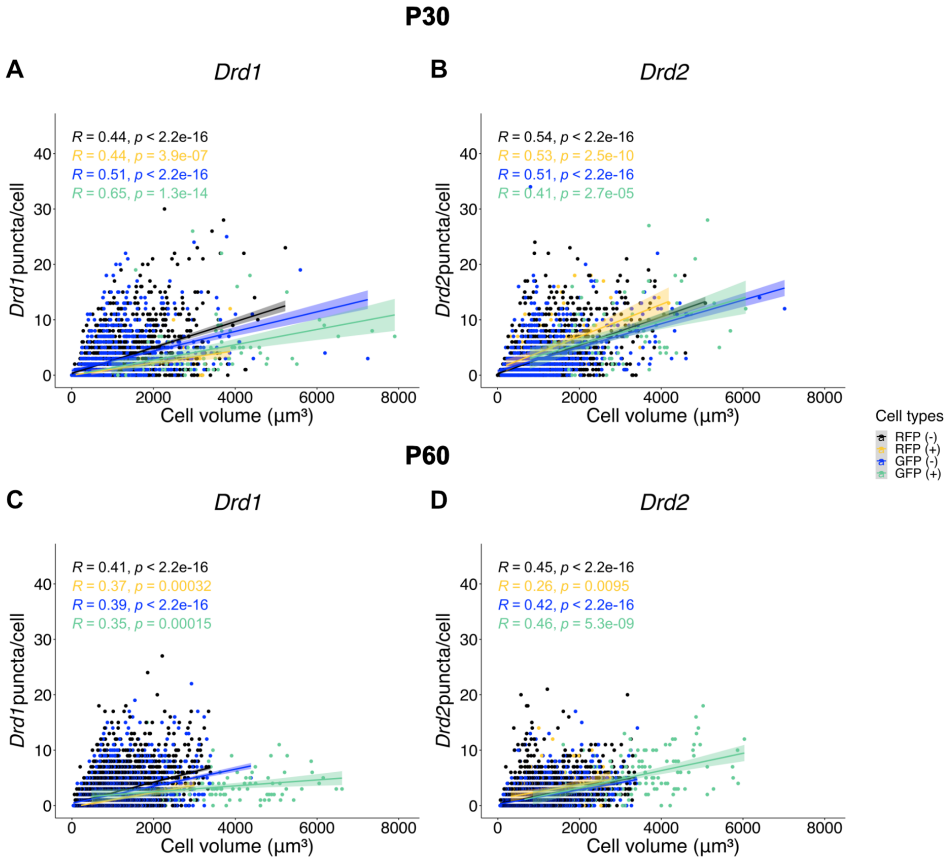

Fig. 18. No strong correlation between neuron volume and *Drd1* or *Drd2* mRNA transcript expression in the mouse mPFC. **A, B)** Correlation analysis between cell volume and **A)** *Drd1* or **B)** *Drd2* mRNA receptor expression in the mouse mPFC at P30. *n* = 3 WT-mTOR vs. 2 p.Leu2427Pro mice. **C, D)** Correlation analysis between cell volume and **C)** *Drd1* or **D)** *Drd2* mRNA receptor expression in the mouse mPFC at P60. *n* = 4 mice per group. Spearman correlation coefficients and *p* values calculated for each cell type. Data shown in this figure contributed to Supplementary Figure 5 and 6 in Meli et al., 2025.

3.6. Characterizing human FCD type 2b specimen and defining lesion and control areas for analysis

Due to the observed changes in DA innervation and *Drd* expression in the mTOR cortical malformation mouse model, our next step was to investigate whether similar alterations are present in patients with FCD type 2b. Previous studies have established that DA innervation matures during postnatal development in both rodents and humans and the mature innervation pattern is only reached in early adulthood (Islam & Meli et al., 2021). To align our human studies with the stages analyzed in our mouse model, we divided our patient cohort into two age groups: pediatric (9-16 y.o.) and adult (44-57 y.o.), based on

the timing of the surgical resections **(Table 1)**. Cortical area selection criteria were focused primarily on specimens from the frontal cortex to be consistent with the analysis in mouse, although parietal cortex specimens were also included to account for potential region-dependent changes. Human FCD type 2b biopsies were obtained from pharmacoresistant patients during surgical resection and processed for FFPE. An initial assessment of the tissue was performed to characterize the FCD type 2b pathology. Cytological abnormalities, a key neuropathological features of type 2b, were detected by H&E and NF (clone 2F11) staining. Dysmorphic neurons were identified by their enlarged cell somas and nuclei observed in H&E staining and by the accumulation of NF in the cell cytoplasm **(Fig. 1B)**. Balloon cells were characterized by enlarged cell somas, glassy eosinophilic cytoplasm and laterally displaced nuclei **(Fig. 1C)** (Blümcke et al., 2011). Further tissue characterization for each patient was performed with NeuN staining and cortical markers **(Fig. 8)** to determine FCD type 2b areas with cortical dyslamination **(Fig. 19A & B, red rectangle)** and cytological abnormalities, such as dysmorphic neurons labelled fluorescently with SMI32 accumulation in the somas **(Fig. 19A, lower panel, arrows)**. For each patient, a control area defined as a region with normal cortical lamination and no presence of dysmorphic neurons or balloon cells **(Fig. 19A & B, blue rectangle)** and an FCD type 2b area with presence of cytological and dyslamination was selected. These regions were then used for the analysis of DA axonal density and DA receptor expression.

Lastly, given the bi-laminar pattern of DA innervation in human frontal and parietal cortex, with upper and deeper layers being highly innervated compared to sparser innervation in the middle layers (See Introduction 1.4.1.), we divided the selected areas in upper, middle and deeper layers **(Fig. 19B)**. Defining these layers in the control area using cortical markers and NeuN staining was straightforward as the layer were easily distinguishable **(Fig. 19B, blue rectangle)**. However, in FCD type 2b regions, this was more challenging due to cortical dyslamination. Thus, we used the layers defined in the control area as a reference and superimposed them on the FCD type 2b area to delineate “layers” and define a layer-to-area ratio **(Fig. 19B, red rectangle)** that was comparable between control and FCD type 2b area. These defined layers were consistently used for subsequent quantitative analysis of DA innervation density and *DRD1/DRD2* transcript expression.

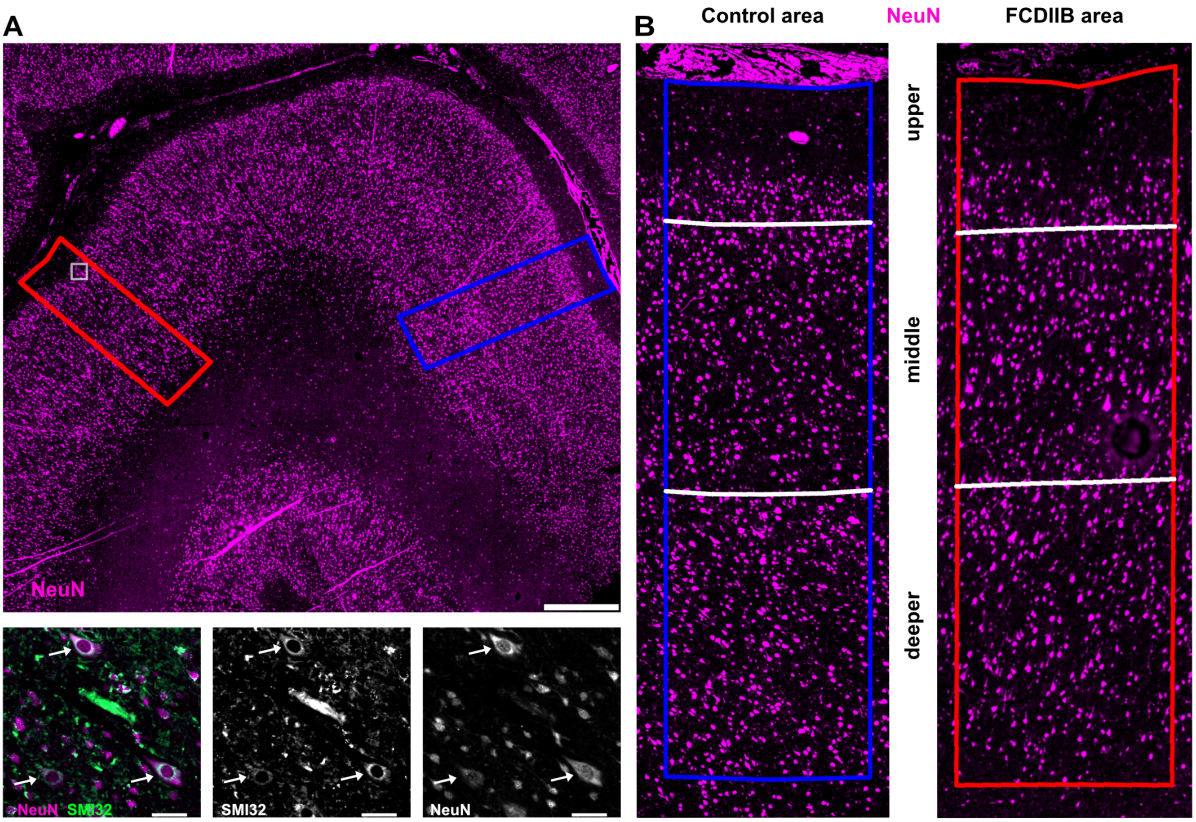

Fig. 19. Characterization of FCD type 2b human specimen and selection of control and FCD type 2b areas for analysis. **A)** Example image from a frontal cortex patient biopsy. Control (blue rectangle) and FCD type 2b (red rectangle) areas were determined based on NeuN expression for each patient biopsy. Scale bar 1000 μm. Right panels: higher magnification of the boxed region in the FCD type 2b area immunostained for SMI32 and NeuN indicating dysmorphic neurons (arrows). Scale bar 50 μm. **B)** Higher magnification of the control and FCD type 2b areas in **A** showing the separation in upper, middle and deeper layers. Data shown in this figure contributed to Figure 3 in Meli et al., 2025.

3.7. Altered density of and distribution of DA innervation in FCD type 2b area in human specimen

After defining the control and FCD type 2b areas for each patient, we analyzed the DA axonal distribution and density within these regions using a reconstruction of serial sections. For this, we performed IHC against TH to label DA axons and performed manual tracings of the TH+ axons on all serial sections for each patient from both pediatric and adult ages **(Fig. 20A & B)**. DA axons were defined as TH+ fibres and their lengths and diameters were adjusted accordingly while manually tracing **(Fig. 20C)**. After performing manual tracing of DA axons in both control and FCD type 2b areas, all analyzed serial

sections were combined and reconstructed in 3D **(Fig. 20A & B)**. The DA innervation density was calculated as the percentage of area occupied by the traced axons within the defined region, normalised to the total area of that region.

The overall quantification of DA density did not reveal any significant differences between FCD type 2b and control areas in biopsies from pediatric patients **(Fig. 20D)**. However, in adult patient derived biopsies, a significant decrease in DA innervation density was observed in the FCD type 2b area compared to control area **(Fig. 20D)**.

Layer quantification did not show any difference between control and FCD type 2b areas in the pediatric patients **(Fig. 20E)**. In adult patients, an altered innervation density was particularly evident in the upper and deeper layers, with FCD type 2b areas showing decreased innervation density compared to control areas **(Fig. 20E)**. This DA density reduction disrupts the typical bi-lamination pattern of DA innervation observed in frontal and parietal cortex **(Fig. 20B)**. Notably, the decreased DA innervation density and disrupted bi-laminar pattern were more pronounced in frontal cortex specimens. However, it should be noted that only one parietal cortex sample was available for each age group.

Overall, these results suggest a decreased DA innervation density in the FCD type 2b areas compared to control areas in adult, but not pediatric patient biopsies. This decrease was most evident in upper and deeper layers of the cortex resulting in a disrupted lamination pattern of DA innervation.

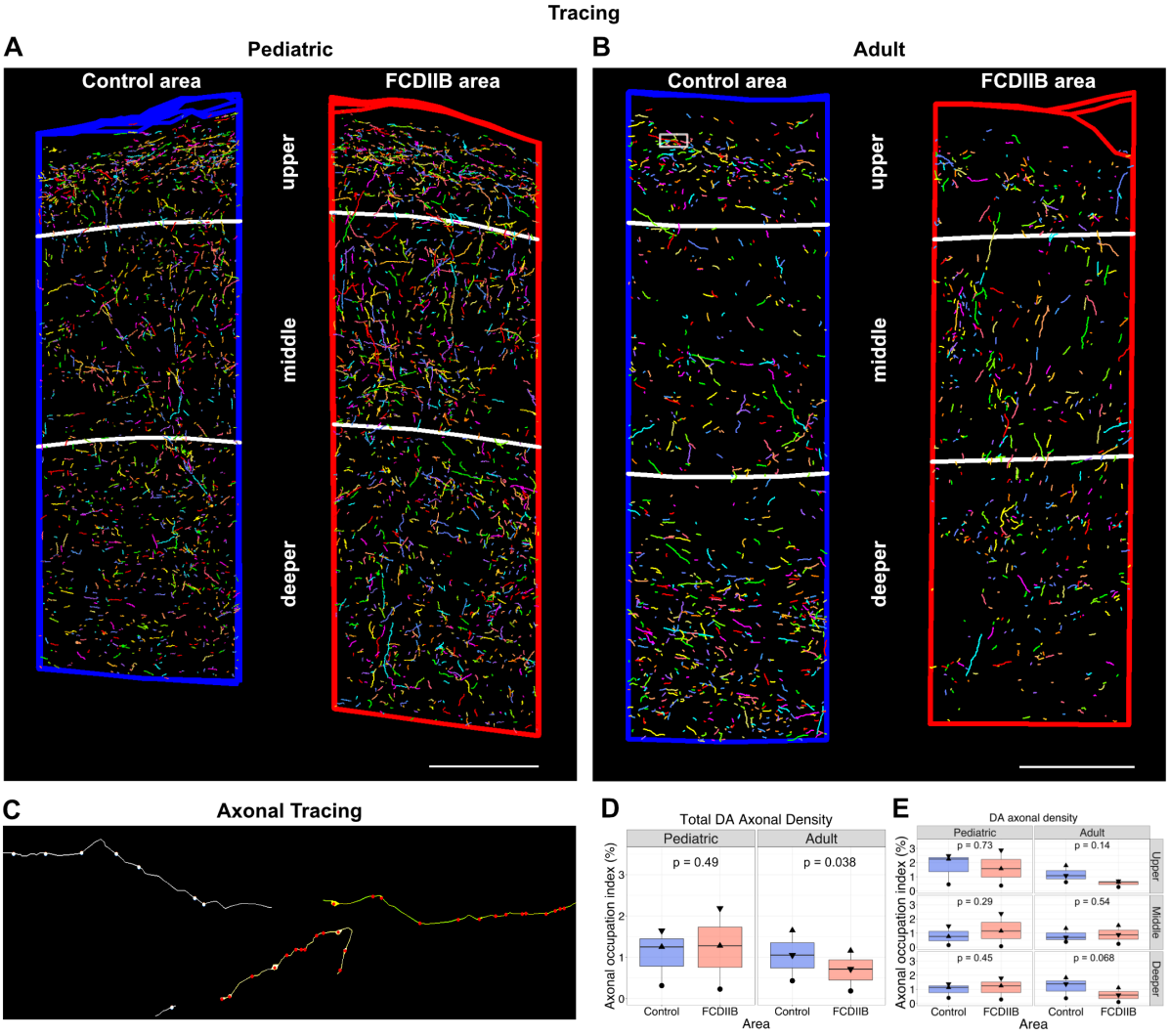

Fig. 20. Altered density and lamination pattern of DA innervation in human FCD type 2b specimen. Manual tracing of TH axons in 3D reconstructions of sectioned tissue. Examples from one **A)** pediatric and one **B)** adult specimen. Scale bar 500 μm. **C)** Higher magnification from the boxed area in **B)** depicting an example of manually traced axons throughout serial sections. Yellow and green-colored axons were traced on the same section, while the white axon was traced in the adjacent sections. **D)** DA axonal density quantification from the entire control and FCD type 2b areas in pediatric and adult patients. **E)** Quantification of DA axonal density in upper, middle and deeper layers from control and FCD type 2b areas in pediatric and adult patients. *n* = 3 patients per age group. Tested with paired t-test for statistical difference between the areas. Occupation index is calculated as percentage of total axonal length for each analyzed area normalized for the total area. Symbols: ▼▲ frontal cortex, ● parietal cortex. Data shown in this figure contributed to Figure 4 in Meli et al., 2025.

3.8. Altered quantity of DA axonal varicosities in FCD type 2b human specimen

The manual DA axonal tracings allowed us to also monitor the presence and distribution of axonal varicosities in control and FCD type 2b area of both pediatric and adult patients' biopsies **(Fig. 21A and B)**. These varicosities may represent DA release sites (See Introduction 1.4.1). Axonal varicosities were defined as visible swellings along the axon with a diameter larger than 0.2 μm **(Fig. 21C)**. The number of these varicosities per analyzed regions was normalized to the total axonal length quantified in the region. This analysis was repeated for each section and then overall quantified for each tissue from pediatric and adult specimen **(Fig. 21A and B)**. This analysis revealed a trend towards a decrease in the overall varicosity density in FCD type 2b areas compared to control areas in pediatric, but not adult specimen **(Fig. 21D)**.

Layer-specific quantification revealed that the decrease in the relative number of varicosities in pediatric patients was apparent in all layers of the FCD type 2b specimen but reached statistical significance only in the middle layers **(Fig. 21E)**. In adult specimen, the relative number of varicosities were not altered between control and FCD type 2b area.

In summary, this analysis showed a change in the relative number of DA axonal varicosities in the FCD type 2b area in pediatric, but not adult specimen. The trend towards a decreased number of varicosities was observed in all analyzed layers.

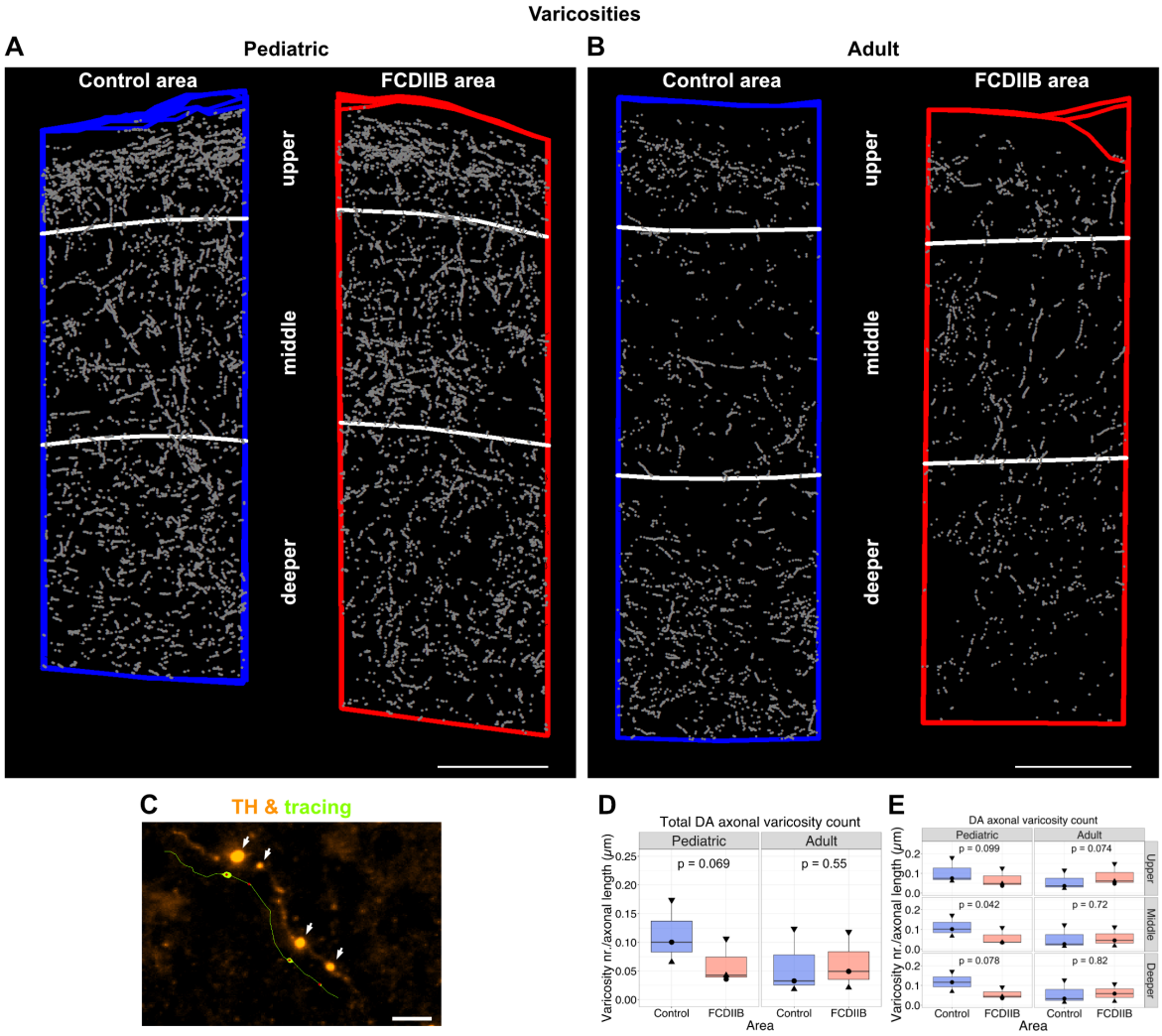

Fig. 21. Altered density of DA axonal varicosities in human FCD type 2b specimen. Manually labeled TH axonal varicosities in 3D reconstructed tissue from frontal cortex of one **A)** pediatric and one **B)** adult specimen. Scale bar 500 μm. **C)** Example of varicosity labelling along the TH positive, traced axons (arrows). Scale bar 10 μm. **D)** Quantification of the relative number of DA axonal varicosities in the control and FCD type 2b area in pediatric and adult patients. **E)** Quantification of the relative number of DA axonal varicosities in upper, middle and deeper layers from control and FCD type 2b areas in pediatric and adult patients. *n* = 3 patients per age group. Tested with paired t-test for statistical difference between the areas. Symbols: ▼▲ frontal cortex, ● parietal cortex. Data shown in this figure contributed to Figure 4 in Meli et al., 2025.

3.9. Increased expression of *DRD1* and *DRD2* transcripts in dysmorphic neurons in FCD type 2b areas

Based on our findings showing altered *Drd1* and *Drd2* mRNA expression in the mPFC of the FCD type 2 mouse model, we next analyzed the expression of DA receptor mRNA in human FCD type 2b specimen. We performed quantitative FISH for *DRD1* and *DRD2* in human specimen combined with IHC for NeuN to mark neurons in the regions previously defined for the DA axonal analysis. Additionally, we performed IHC for SMI32 to distinguish the dysmorphic neurons (NeuN+ SMI32+) from the surrounding non-dysmorphic neurons in FCD type 2b area (NeuN+ SMI32- designated as “NeuN only”) **(Fig. 22A)**. Neurons in the control area were designated as “NeuN”. We trained a machine-learning tool to identify the two groups of neurons and then quantified the *DRD1/DRD2* mRNA transcripts with each dot representing a single mRNA transcript **(Fig. 10)**.

The quantitative analysis in pediatric specimens revealed a significantly higher *DRD1* mRNA transcript expression in dysmorphic neurons (13.89 ± 1.651 ppc) compared to surrounding NeuN-only neurons in the FCD type 2b area (4.61 ± 0.804 ppc) or NeuN neurons in the control area (4.41 ± 1.213 ppc) **(Fig. 22B)**. Likewise, *DRD2* mRNA transcript levels were also significantly upregulated in dysmorphic neurons (4.51 ± 0.568 ppc) compared to NeuN-only (1.94 ± 0.237 ppc) or NeuN (2.28 ± 0.8 ppc) in pediatric patients **(Fig. 22B)**.

In adult patients, dysmorphic neurons expressed higher levels of *DRD1* mRNA transcripts (13.2 ± 2.04 ppc) than either NeuN-only (4.41 ± 0.672 ppc) or NeuN (4.65 ± 0.358 ppc) neurons and showed increased *DRD2* mRNA transcript levels (3.79 ± 0.646 ppc) compared to NeuN-only (1.8 ± 0.207 ppc) or NeuN (1.6 ± 0.087 ppc) neurons, though these differences were not statistically significant **(Fig. 22C)**. This may reflect specific upregulation of *DRD1* and *DRD2* in dysmorphic neurons in the frontal cortex, with no similar increase observed in the parietal cortex **(Fig. 22C)**.

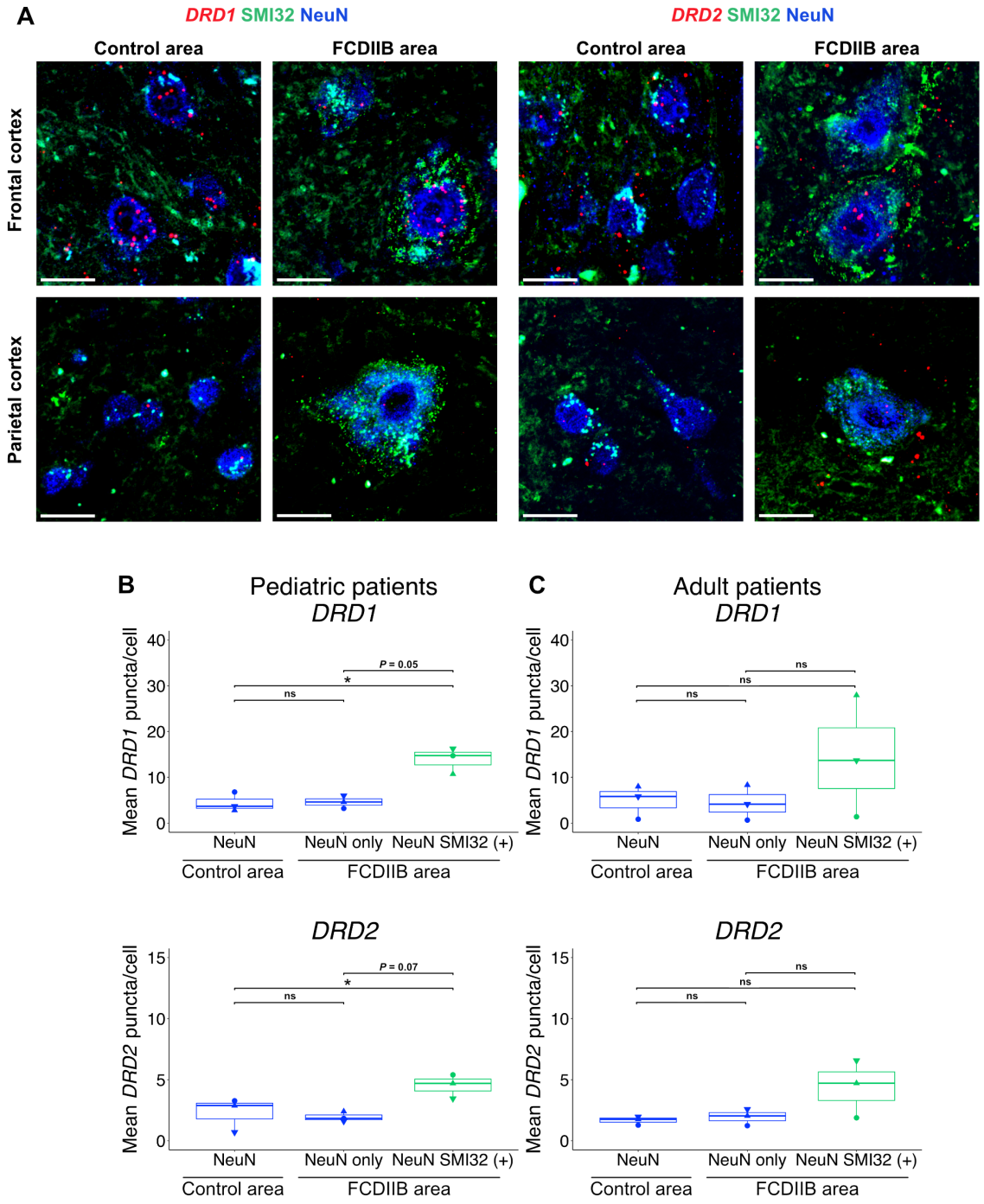

Fig. 22. Increased expression of *DRD1* and *DRD2* mRNA in dysmorphic neurons in FCD type 2b areas in human specimen. **A)** Example images of FISH for *DRD1* and *DRD2* in control and FCD type 2b areas of adult frontal and parietal cortex. Co-IHC with NeuN was performed to label all neurons in both areas. Co-IHC with SMI32 allows to distinguish dysmorphic neurons due to accumulations of SMI32 in the cell soma of dysmorphic neurons. Scale bar 20 μm. **B)** Quantification of *DRD1* and *DRD2* mRNA transcript expression in pediatric human FCD type 2b specimen. Quantified neurons for *DRD1*: 105 NeuN, 39 NeuN only, 26 NeuN SMI32 (+). *DRD2*: 110 NeuN, 37 NeuN only, 31 NeuN SMI32 (+). (Figure legend continued on next page)

C) Quantification of *DRD1* and DRD2 mRNA transcript expression in adult human FCD type 2b specimen. Quantified neurons for *DRD1*: 213 NeuN, 101 NeuN only, 42 NeuN SMI32 (+). *DRD2*: 289 NeuN, 100 NeuN only, 38 NeuN SMI32 (+). *n* = 3 patient specimen for age group. Tested with one-way ANOVA with repeated measures followed by Tukey's test for multiple comparisons between groups. Symbols: ▼▲frontal cortex, ● parietal cortex. Data shown in this figure contributed to Figure 5 in Meli et al., 2025.

Given the distinct expression levels of *DRD1* and *DRD2* mRNA transcripts in different cortical layers in human (See Introduction 1.4.1.) (Islam & Meli et al., 2021), we attempted to analyze *DRD1* and *DRD2* mRNA expression in different cortical layers in more detail **(Fig. 23, Table 5 & 6)**. Since the number of dysmorphic neurons that could be analyzed was low, especially in the upper layers, it was difficult to draw valid conclusions for all the layers. Generally, dysmorphic neurons in the middle and deeper layers of both pediatric **(Fig. 23A)** and adult **(Fig. 23B)** patient biopsies showed increased expression of both *DRD1* **(Table 5)** and *DRD2* **(Table 6)** mRNA transcripts compared to NeuN-only and NeuN neurons.

In conclusion, these results demonstrate that dysmorphic neurons exhibit increased expression of *DRD1* and *DRD2* mRNA transcripts across cortical layers. This effect is intrinsic to these neurons and might be independent of their cortical position.

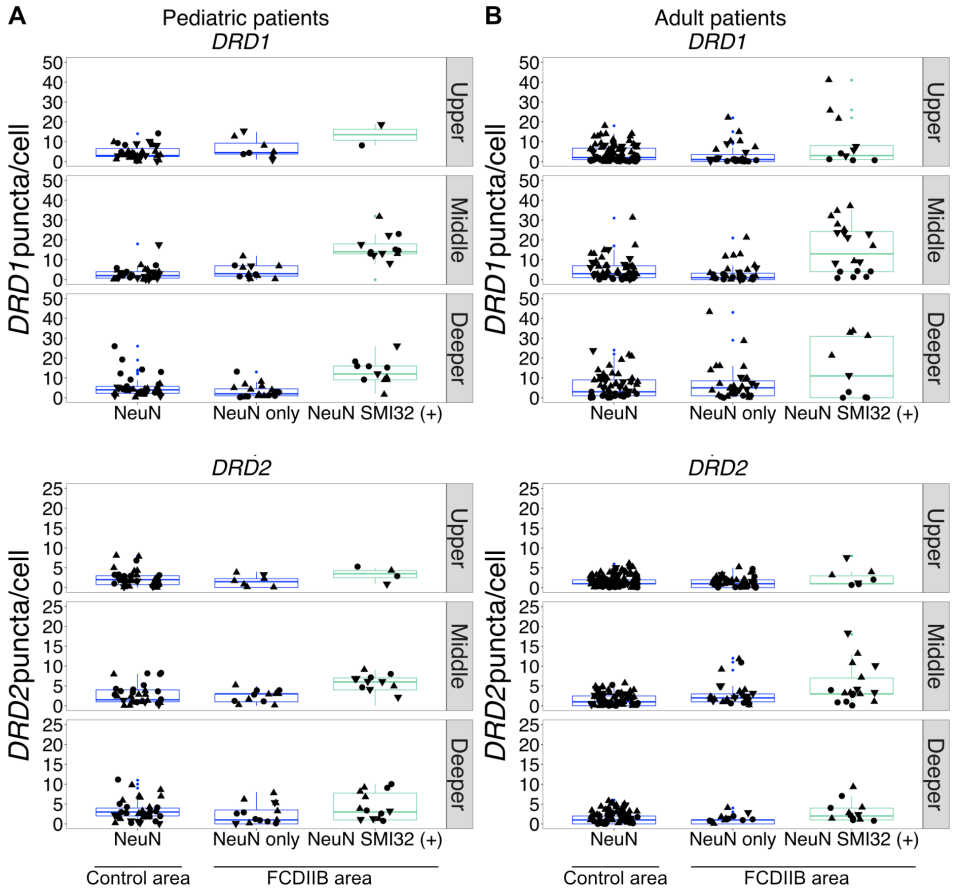

Fig. 23. Expression of *DRD1* and *DRD2* mRNA in the upper, middle and deeper cortical layers of FCD type 2b specimen. **A)** Distribution of *DRD1* and *DRD2* mRNA transcripts (puncta per cell) in pediatric human FCD type 2b specimen separated for upper, middle and deeper layers. Quantified neurons for *DRD1*: upper layers: 31 NeuN, 8 NeuN only, 2 NeuN SMI32 (+), middle layers: 40 NeuN, 12 NeuN only, 13 NeuN SMI32(+), deeper layers: 34 NeuN, 19 NeuN only, 11 NeuN SMI32 (+). Quantified neurons for *DRD2*: upper layers: 40 NeuN, 8 NeuN only, 4 NeuN SMI32 (+), middle layers: 34 NeuN, 13 NeuN only, 13 NeuN SMI32(+), deeper layers: 36 NeuN, 16 NeuN only, 14 NeuN SMI32 (+). **B)** Distribution of *DRD1* and *DRD2* mRNA transcripts (puncta per cell) in adult human FCD type 2b specimen separated for upper, middle and deeper layers. Quantified neurons for *DRD1*: upper layers: 82 NeuN, 31 NeuN only, 13 NeuN SMI32 (+), middle layers: 59 NeuN, 36 NeuN only, 20 NeuN SMI32(+), deeper layers: 72 NeuN, 34 NeuN only, 9 NeuN SMI32 (+). Quantified neurons for *DRD2*: upper layers: 126 NeuN, 50 NeuN only, 9 NeuN SMI32 (+), middle layers: 75 NeuN, 33 NeuN only, 17 NeuN SMI32(+), deeper layers: 88 NeuN, 17 NeuN only, 12 NeuN SMI32 (+). *n* = 3 patient specimen for age group. Symbols: ▼▲frontal cortex, ● parietal cortex. Data shown in this figure contributed to Supplementary Figure 8 in Meli et al., 2025.

Table 5. *DRD1* expression across layers in human FCD type 2b specimen

Age group	Area	Cell type	Layer	Mean	± SEM
Pediatric	Control	NeuN	Upper	4.45	0.627
			Middle	2.62	0.507
			Deeper	5.59	0.941
	FCD type 2B	NeuN only	Upper	6.62	1.76
			Middle	4.17	1.05
			Deeper	3.32	0.761
	FCD type 2B	SMI32 (+)	Upper	13.5	5.50
			Middle	15.2	2.13
			Deeper	12.9	1.89
Adult	Control	NeuN	Upper	4.07	0.485
			Middle	4.68	0.732
			Deeper	5.29	0.678
	FCD type 2B	NeuN only	Upper	3.13	0.935
			Middle	3.08	0.779
			Deeper	6.97	1.54
	FCD type 2B	SMI32 (+)	Upper	8.69	3.57
			Middle	15.4	2.81
			Deeper	14.8	5.02

Table 6. *DRD2* expression across layers in human FCD type 2b specimen

Age group	Area	Cell type	Layer	Mean	± SEM
Pediatric	Control	NeuN	Upper	2.1	0.328
			Middle	2.5	0.429
			Deeper	3.33	0.463
	FCD type 2B	NeuN only	Upper	1.5	0.535
			Middle	2.23	0.469
			Deeper	2.31	0.631
	FCD type 2B	SMI32 (+)	Upper	3.25	0.854
			Middle	5.08	0.796
			Deeper	4.29	0.952
Adult	Control	NeuN	Upper	1.61	0.121
			Middle	1.56	0.185
			Deeper	1.60	0.167
	FCD type 2B	NeuN only	Upper	1.52	0.194
			Middle	2.61	0.511
			Deeper	1.06	0.277
	FCD type 2B	SMI32 (+)	Upper	2.22	0.846
			Middle	5.18	1.21
			Deeper	3	0.759

As with the analysis in mouse, we investigated the correlation between enlarged neuronal soma size and higher mRNA transcript expression. Spearman correlation analysis revealed no correlation effect between the larger soma sizes of dysmorphic neurons and increased *DRD1* or *DRD2* mRNA transcript expression in either pediatric **(Fig. 24A)** or adult **(Fig. 24B)** FCD type 2b patients, indicating that the increase in DA receptor mRNA expression in dysmorphic neurons is independent of cell soma sizes.

In summary, this analysis demonstrates that *DRD1* and *DRD2* mRNA transcripts are upregulated in dysmorphic neurons in FCD type 2 areas of pediatric and adult patients. This upregulation is intrinsic to dysmorphic neurons, as no changes in expression were evident in non-dysmorphic surrounding neurons or neurons from control areas. Importantly, the elevated expression did not correlate with the increased soma size.

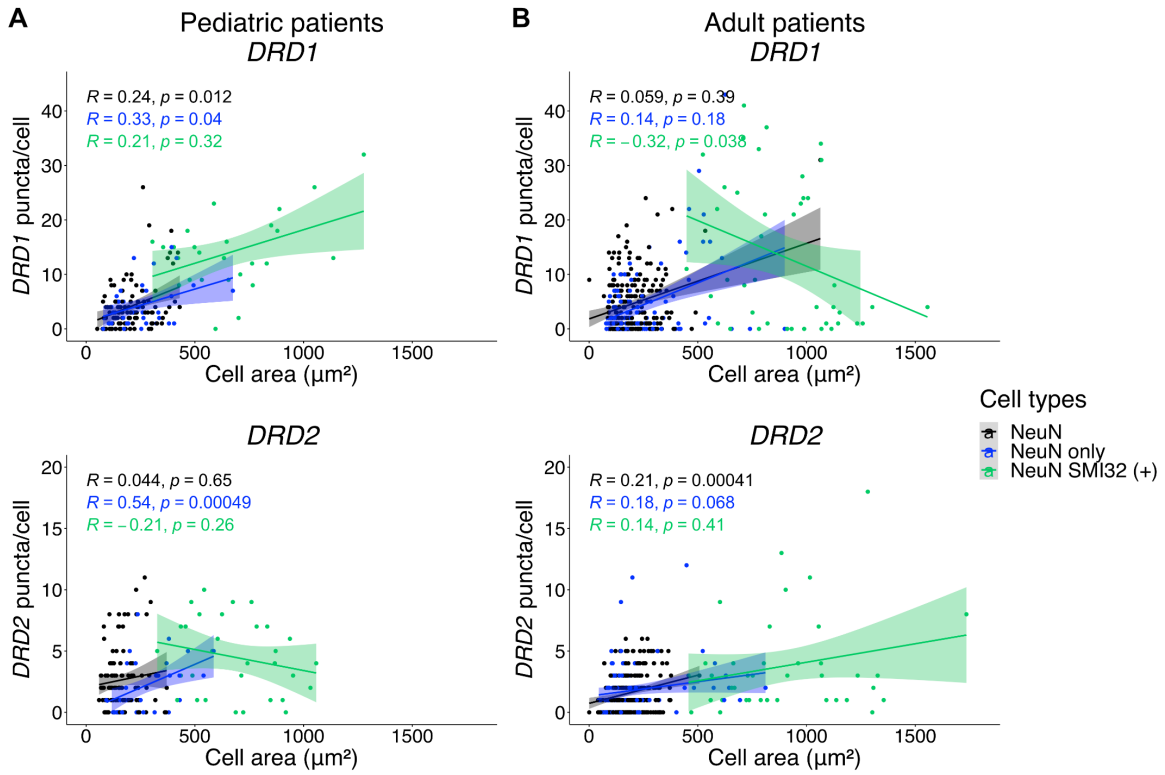

Fig. 24. No strong correlation between cell soma size and *DRD1* or *DRD2* mRNA transcript expression in **A)** pediatric and **B)** adult human specimen. Spearman correlation coefficients and *p* values calculated for each cell type. Data shown in this figure contributed to Supplementary Figure 9 in Meli et al., 2025.

4. Discussion

FCD type 2 is a leading cause of pharmacoresistant epilepsy, marked by disrupted cortical layering and cellular abnormalities. Abnormal activity recorded in the area stems from malformed networks both within the lesion and in the surrounding perilesional microenvironment. DA input to cortical areas plays a crucial role in regulating the signal-to-noise ratio and maintaining the E/I balance in local networks. Therefore, changes in this monoaminergic input may contribute to the heightened excitability observed in FCD lesions. In this study, we investigated DA inputs and receptors in human FCD type 2b tissue and a mouse model of FCD type 2. Our findings reveal alterations in DA innervation patterns, varicosity density, and abnormal *Drd/DRD* expression in dysplastic neurons in FCD type 2 areas **(Fig. 25)**. These results highlight that variations in DA innervation and receptor dynamics in FCD type 2 may play a role in the abnormal network activity associated with the condition.

4.1. The significance of murine models to study mTORopathies

To assess whether malformations during cortical development impact DA input in the mouse mPFC, we employed an established mouse model of FCD type 2 and adapted it specifically for the mPFC. Lim and colleagues established this model by introducing a mutated mTOR (p.Leu2427Pro), initially identified as a somatic mutation in FCD type 2 patients, into the developing murine neocortex, which led to disrupted cortical migration, the presence of cytomegalic neurons, and spontaneous seizures postnatally (Lim et al., 2015). The same plasmid constructs were used in this study; however, the delivery technique was modified to specifically target more frontal cortical areas, as opposed to more posterior ones like the motor or somatosensory cortices, which are typically the focus in similar models. Examination of the postnatal mPFC revealed that WT-mTOR neurons migrated correctly to the upper layers, whereas neurons expressing the mutated mTOR were distributed across cortical layers and exhibited larger somas compared to WT-mTOR neurons **(Fig. 11)**. Additionally, mutated mTOR neurons displayed elevated pS6 (Ser240/244) expression **(Fig. 12)**, a marker of mTOR pathway activation. This experiment successfully replicated previously observed phenotypes of mTOR mutation in posterior cortical regions, demonstrating that targeting the p.Leu2427Pro-mTOR mutation

to late-born pyramidal neurons in the mPFC produces developmental abnormalities similar to the ones observed in FCD type 2 patients. These results highlight the robustness of the model and technique, regardless of the targeted cortical area. Furthermore, the successful rescue of the enlarged neuron phenotype and seizure activity using rapamycin, an mTOR inhibitor, demonstrates the potential of these *in vivo* rodent models for pre-clinical therapy development. Although seizure activity was not recorded in our mouse model — since it was not the primary focus of the study — the established and widespread use of this model supports its validity and relevance for investigating seizure-related cortical malformations.

The efficacy of murine models in investigating cortical development malformations has been explored in multiple studies. The laboratory of Jeong Ho Lee has been studying several brain somatic mutation in MTOR in FCD patients such as the one used in this study, p.Leu2427Pro, and also p.Cys1483Y. They have characterised these mutations in IUE mice in detail with translational ribosome profiling and have found new targets of mTOR activation and tested therapeutic potentials in alleviating epileptic activity (Kim et al., 2019). Moreover, reports have revealed defective mechanisms of autophagy and ciliogenesis and associating it to cortical dyslamination phenotypes present in FCD patients (Park et al., 2018).

Other mTORopathies have also been the focus of additional studies. TSC1/TSC2 inactivation leads to hyperactivation of mTORC1 and developmental malformations. Meikle and colleagues have studied this effect by using a conditional knockout model of *Tsc1* allele with Synapsin I promoter-driven Cre recombination during early embryogenesis. This model has aided in investigating the neuropathological hallmarks of the disease like dysplastic neurons, spontaneous seizure activity characterisation and hypomyelination mechanisms in TSC and thus, shedding light on the crucial *in vivo* functions of the TSC genes in neuronal development (Meikle et al., 2007). Germline loss-of-function mutations in DEPDC5 have been associated with FCD in patients. Ribierre and colleagues have utilized this mechanism and replicated it in mouse models by inactivating the *Depdc5* gene *via* CRISPR-Cas9 editing and have successfully recapitulated FCDs. Moreover, this model has provided key insights into the two-hit mechanism of germline and somatic mutations of the disease and has further elucidated

on the role of DEPDC5 in dendritic and spine modelling, linking it to increased excitatory transmission and epileptogenesis (Ribierre et al., 2018).

These studies emphasize the crucial role of *in vivo* murine models in exploring mechanisms underlying cortical malformations and therapeutic approaches in epilepsy. This is particularly relevant given the limitations of human studies and the challenges associated with fully investigating these mechanisms using *in vitro* approaches.

4.2. Alterations of dopaminergic neurotransmission modulation in FCD type 2

4.2.1. Dopaminergic innervation

The mesoprefrontal DA system undergoes continued postnatal development in both rodents and human PFC, reaching full maturation in early adulthood (Islam & Meli et al., 2021). This protracted development coincides with PFC circuitry maturation and influences local circuit establishment.

In our experimental mouse model, we observed a significant increase in DA innervation density, evident only in the upper layers, from adolescence to adulthood in mPFC of WT-mTOR mice **(Fig. 13E)**, which aligns with the reported developmental patterns (Naneix et al., 2012). However, this increase was absent in the upper layers of the p.Leu2427Pro mPFC **(Fig. 13E)**, indicating that the developmental maturation of DA innervation is impaired in these layers. These results imply that alterations in early cortical development, resulting in structural malformations, begin to impact DA innervation during adolescence, but the full extent of these changes only becomes apparent in adulthood. This delayed manifestation suggests a complex interplay between early developmental disruptions in the mPFC and later-stage maturation processes that may affect local circuits as well as long-range inputs.

Our findings reveal a reduction in DA innervation density in adult p.Leu2427Pro mice **(Fig. 13D)** and in FCD type 2b areas **(Fig. 20D)** when compared to WT-mTOR animals and control areas, respectively **(Fig. 25)**. Notably, at adolescent/pediatric stages, we did not observe any significant differences in DA innervation density between WT-mTOR and p.Leu2427Pro mice **(Fig. 13C)**, or between control and FCD type 2b areas **(Fig. 20D)**. This suggests again that during the adolescence, when DA axons in the cortex undergo

significant remodeling and innervation density increases towards early adulthood in both rodents and humans, the expected developmental trajectory is disrupted in p.Leu2427Pro mice and FCD type 2b lesion areas. Furthermore, in human FCD type 2b lesions, the reduction in axonal density is most pronounced in highly innervated layers, such as the upper and deeper cortical layers **(Fig. 20E)**. The alteration in DA axonal distribution resulted in disruption of the bi-lamination pattern, which is typical of human prefrontal and parietal cortical areas (Gaspar et al., 1989). This suggests that these layers, which are crucial for local circuit integration due to their high DA innervation, are particularly susceptible to disruption. Early studies on DA innervation in FCD patients reported similar findings, noting a decrease in TH fibers across the entire FCD lesion and disrupted layer-specific innervation, though these studies were done on the medial primary motor cortex, where the FCD area from one patient coincided with the seizure onset area (Trottier et al., 1994).

DA axons typically innervate the cortex only after the establishment of cortical layers, indicating that early disturbances in cortical layer architecture may lead to abnormal DA axonal distribution in later stages, affecting the adult lamination pattern of DA axons (Kolk et al., 2009). However, further investigation is necessary to understand the mechanisms by which early cortical malformations impact DA innervation. Our analysis also revealed that reductions in DA innervation are more prominent in the frontal cortex compared to the parietal cortex, suggesting a greater sensitivity of the frontal regions to altered DA modulation and cortical malformations. However, given that our study included parietal cortex from only one patient compared to two frontal patient cortices, definitive conclusions about regional susceptibility cannot be drawn at this stage. Future research should focus on expanding these observations to better understand the differential impact of cortical malformations on DA innervation across various cortical regions.

The mechanisms underlying the maturation of DA innervation in cortical areas are not well understood, particularly in the context of cortical malformations. Several factors could contribute to the observed disruptions in DA innervation. One possibility is the alteration of molecular guidance cues, such as Netrin-1 and its receptor DCC, which are known to play a role in mesocortical DA axon guidance, where high Netrin-1 levels in the PFC attract DA neurons that have low DCC expression during adolescence (Manitt et al., 2011;

Reynolds et al., 2018; Reynolds & Flores, 2021). Disruptions in Netrin-1 levels in the PFC could lead to improper targeting or reduced axonal growth in affected areas. Moreover, alterations of Netrin-1/DCC pathway in the PFC have been associated with psychiatric patients exhibiting suicidal behavior and depression (Manitt et al., 2013; Reynolds & Flores, 2021; Torres-Berrío et al., 2020). So far, there is no evidence for a connection between Netrin-1/DCC signaling and the mTOR pathway. It could be the focus of further research to explore whether such an interaction exists and how it might influence the DA mesocortical system in the PFC. Investigating this interaction could provide new insights into the regulation of DA innervation in the PFC and its implications for neurodevelopmental disorders. Another potential factor could be altered synaptic pruning, which could result from changes in local microglial activity. Microglia are thought to play a crucial role in shaping mesocortical DA circuitry during adolescence, and abnormal microglial function have been associated with DA-related disorders like ADHD and schizophrenia (Rey et al., 2020; Reynolds & Flores, 2021; Yokokura et al., 2021). Several studies have reported microglia activation in FCD type 2 brain specimens and mTOR hyperactivation mouse models (Boer et al., 2006; Iyer et al., 2010; Nguyen et al., 2019). Thus, potential enhanced microglial activation in our mouse model and FCD type 2 tissue could lead to altered pruning, affecting the integration and density of DA fibers.

Additionally, functional alterations within the local neural networks of FCD type 2b areas could directly impact DA innervation. These networks may provide less supportive environments for the maintenance or growth of DA axons due to altered synaptic activity or connectivity.

Overall, our study suggests that cortical malformations in p.Leu2427Pro mTOR mutated mice and FCD type 2b lesions disrupt the normal increase in DA innervation density during postnatal development, with the full impact only becoming evident in adulthood. Future studies should focus on elucidating the specific pathways and cellular interactions that underlie the impaired maturation of DA innervation in FCD type 2b and other MCD models.

4.2.2. Dopaminergic varicosities

Our findings indicate that while the density of DA axonal varicosities is comparable between FCD type 2b and control areas at adult stages, there is a noticeable trend

towards a decreased density of varicosities in FCD type 2b areas in pediatric patients **(Fig. 21D)**. This observation is particularly significant given that varicosities on DA fibres are potential DA release sites, making them crucial indicators of functional DA fibre maturation. The presence and density of these varicosities on DA axons, adjacent to both pyramidal and non-pyramidal somata in the PFC, are indicative of the degree of DA modulation exerted on local circuits. Studies have shown that the number of DA appositions onto GABA-positive neuronal cell bodies in the PFC increases steadily from neonatal stages to adulthood, signifying progressive maturation of the DA system (Benes et al., 1996; Reynolds & Flores, 2021). The observed pattern of DA fibre and varicosity density development corresponds to an increase in DA tissue content during key developmental periods. In rodent models, there is a consistent increase in DA content from early (P25) to late adolescence (P45), followed by a further marked increase as animals transition into adulthood (Naneix et al., 2012). Similarly, in non-human primates, there is a notable increase in DA innervation density in the PFC during adolescence, peaking in 2-3-year-old animals (Rosenberg & Lewis, 1994, 1995). This developmental trajectory is accompanied by a higher concentration of DA in the PFC compared to younger ages (Goldman-Rakic & Brown, 1982).

The disruption of this developmental trajectory in FCD type 2b areas, as evidenced by the reduced density of DA varicosities during adolescence, may have profound implications for the local environment. This observed reduction in DA axonal density and varicosity in adulthood across both models may reflect an overall decrease in DA content within the affected areas. However, due to the absence of *in vivo* measurements of DA release or DA tissue content in our study, this conclusion remains speculative. Investigating DA neurotransmission more comprehensively, including release dynamics and synaptic activity modulation, would be an important direction for future research to elucidate the full extent of DA involvement in FCDs **(Fig. 25)**. A range of advanced tools can be utilized to investigate DA dynamics in mouse models and FCD patients. In mouse models, *in vivo* techniques like fast-scan cyclic voltammetry, optogenetics, fiber photometry with genetically encoded sensors (e.g., dLight1), and microdialysis provide detailed insights into DA release and reuptake. In FCD patients, PET imaging using DA-specific radioligands is a key tool for studying DA receptor binding and synthesis, complemented

by functional MRI to assess DA-related network activity and magnetoencephalography to examine cortical oscillations. Additional approaches, such as high-performance liquid chromatography (HPLC) to measure levels of DA and its metabolites can further elucidate changes in DA signaling. For example, a study measuring levels of DA and its metabolites, 3,4-dihydroxyphenylacetic acid (DOPAC) and homo-vanillic acid (HVA), with HLPC found significantly reduced DA, DOPAC and HVA content in the temporal neocortex of patients with mesial temporal lobe epilepsy (MTLE) and temporal lobe epilepsy (TLE) secondary to brain tumors, compared to controls (Rocha et al., 2012). These findings indicate potential alterations in DA metabolism or release in mechanisms underlying epilepsy. However, data specifically from localized cortical epilepsy models are lacking, and investigating this aspect would be an important direction for future research in FCDs.

The potential mechanisms underlying the observed reduction in DA varicosity density and innervation are not yet understood. DA axonal varicosities exhibit plasticity influenced by their proximity to cholinergic fibers and local neuronal activity, as demonstrated by their greater density in microproximity to cholinergic axons in rat mPFC compared to more distant segments, suggesting activity-dependent adaptations (Zhang et al., 2010). This phenomenon emphasizes how axonal varicosity density can act as an indicator of local neuronal interactions, with areas of high density reflecting enhanced functional connectivity (Zhang et al., 2011). Furthermore, cholinergic depletion in the nucleus accumbens impairs mesocortical DA activation and cognitive function in rats, indicating that disruptions in cholinergic input lead to impaired DA transmission, with significant implications for cognitive deficits in related disorders (Laplante et al., 2012).

It is possible that early disruptions in local network activity due to cortical malformations could impact the maturation of DA signaling during critical periods of brain development. DA release and synaptic plasticity are known to be activity-dependent processes. If an environment where normal patterns of neuronal activity are disrupted, as is the case with FCDs, the typical patterns of DA release and synaptic connectivity might be altered. This could lead to a reduction in the formation of DA varicosities and an overall decrease in DA signaling.

In conclusion, our findings highlight the critical role of DA system maturation in the context of cortical development and its disruption in FCD type 2. Future studies should focus on investigating the specific mechanisms that link cortical malformations like FCD type 2 and other MCDs to disrupted DA neurotransmission. This includes investigating the potential role of altered molecular guidance cues, changes in local synaptic activity, and the impact of cellular abnormalities within these cortical lesions on the growth and stabilization of DA axons.

4.2.3. Dopaminergic receptors

The impact of DA on local networks is not only determined by its release but also by the cell-type-specific expression of DA receptors, which dictate how individual neurons respond to DA input. We utilize the FISH approach for the quantification of *Drd1/DRD1* and *Drd2/DRD2* transcript expressions in the mouse mPFC and human FCD specimens. We demonstrate that both DA receptor transcripts are selectively upregulated in the p.Leu2427Pro mTOR mutated neurons in the mouse model during both adolescence **(Fig. 16)** and adulthood **(Fig. 17)**. Similarly, human FCD type 2b dysmorphic neurons demonstrate higher expression of both DA receptors in pediatric cases and in the frontal cortex of adult cases compared to surrounding neurons and neurons from control areas **(Fig. 22)**. From this observation, several interesting questions arise about how and what functional changes may result from this altered expression.

A possible interpretation of increased DA receptor expression in both p.Leu2427Pro and dysmorphic neurons, is that it is a direct reflection of the enlarged soma size typical of these populations. Larger cell bodies may express higher levels of receptor transcripts innately (Ransdell et al., 2010). However, we found no significant correlation between the expression of either *Drd1/DRD1* and *Drd2/DRD2* with soma size, indicating that this might be due to other mechanisms.

Another possibility is that the upregulation of the *Drd1/DRD1* and *Drd2/DRD2* transcripts is an intrinsic feature of mutated neurons independent of the level of DA signaling. mTOR regulates transcription processes and local protein synthesis critical for synaptic activity and neural circuitry. Antidepressant administrations have shown to facilitate mTOR activation which then increases the expression of synaptic proteins, such as GluR1, PSD-

95 and Synapsin I, supporting the impact of mTOR signaling in spine formation and synaptic plasticity (Dwyer & Duman, 2013; Dwyer et al., 2012; Li et al., 2010, 2011). Thus, dysregulations of the mTOR pathway can alter transcriptional programs and synaptic functions that may lead to aberrant DA receptor expression. Increased DA receptor expression in such a context may not be an adaptive but rather a pathological alteration.

Alternatively, an increase in DA receptors can be a part of an adaptive plasticity mechanism intrinsic to mutant neurons. Similar to the *Tsc1*-inactivated neurons during embryonic development (Wu et al., 2022), the mTOR mutated/dysmorphic neurons may have enhanced plasticity that enables them to compensate for the presumably low levels or decreased signaling of DA in the mTOR mutated mouse mPFC and FCD type 2b lesion area in human specimen. Such a compensatory response could occur by increased sensitivity of p.Leu2427Pro/dysmorphic neurons to reduced DA content, as a possible result of decreased DA innervation density. This could be mediated by the upregulation of receptor expression thereby amplifying the available DA input. However, upregulated receptor expression is not a general feature of neurons in affected areas, as other types of neurons do not show any difference in *Drd1/DRD1* or *Drd2/DRD2* transcript expression. Thus, this compensatory mechanism might be specific to p.Leu2427Pro/dysmorphic neurons and might contribute to the maintenance of network activity under conditions of disrupted DA innervation. Further testing of this hypothesis may be achieved in further studies using *in vivo* DA release measurements combined with pharmacological manipulation using agonists or antagonist of the *Drd* receptors to activate/inhibit signaling.

In adult FCD type 2b patients, the analysis of mean *DRD1* and *DRD2* mRNA transcript expression per patient did not show statistical significance across any neuronal group **(Fig. 22C)**, unlike observations in pediatric patients **(Fig. 22B)**. This may be explained by the evidently higher expression of *DRD1* and *DRD2* mRNA transcripts in dysmorphic neurons in the adult frontal cortex tissue, but not in the parietal cortex. Moreover, across the cortical layers, the expression profile also supports this observation since the dysmorphic neurons that most highly expressed both *DRD1* and *DRD2* were located in the frontal cortex **(Fig. 23B)**. These findings along with the reductions in DA innervation being more prominent in the frontal cortex, emphasize the critical role of DA signaling in the frontal cortex and may suggest a region-specific susceptibility to DA dysfunctions in

FCDs. However, due to our study's limited sample size (only two frontal and one parietal cortex FCD type 2b cases) we cannot draw any final conclusions. Future studies with larger cohorts and addition of other cortical regions are essential to clarify whether DA dysfunctions exhibit a region-specific pattern in FCDs.

In humans, a study measuring the D1 and D2 receptor protein content in the temporal neocortex of patients aged 24-60 years with MTLE and TLE secondary to brain tumors showed some notable differences: western blot assays found increased expression of the D1 receptor protein in both groups of patients, while D2 receptor levels were reduced, but only in MTLE patients. Moreover, autoradiography receptor binding analysis further revealed an increase in D1 receptor binding in MTLE patients, especially in upper (layers I-II) and deep cortical layers (layers V-VI), indicating a higher density of D1 receptors in these regions, but with no significant change in TLE. The D2 receptor binding remained unchanged in both, suggesting that the density of D2 receptors did not differ. However, in TLE, there was significant D2-like G protein activation in all cortical layers, indicating increased functional activity of D2-like receptors despite no change in their density (Rocha et al., 2012). Overall, these findings support the idea that DA signaling through D1 and D2 receptors is altered in epilepsy-related pathologies.

In mice, hyperactivation of mTORC1 signaling has been shown to significantly alter DA receptor expression and signaling in the striatum. In a transgenic mouse model in which a hyperactive $mTOR^{SL1+IT}$ mutation was introduced into medium spiny neurons (MSNs), an upregulation of the number and soma sizes of *Drd1*-positive MSNs and reduced number of *Drd2*-positive MSNs was observed in the olfactory tubercle of the ventral striatum (Chen et al., 2024). Similarly, in another transgenic model expressing the Rheb(S16H) mutation, resulting in persistently elevated mTORC1 signaling canonical D1 receptor signaling is disrupted because of specific impairment of the DARPP-32-dependent pathway in the striatum (Lin et al., 2021). Even though these findings emphasize a distinct impact of mTORC1 hyperactivity on striatal DA pathways, no such mechanism has been reported in the PFC or the cortex in general, to date.

Altered levels of *Drd1/DRD1* and *Drd2/DRD2* receptors might impair DA signaling mechanisms and disrupt the E/I balance in the affected cortical area and lead to

epileptogenic activity. Most of the reports on human and mouse models of limbic epilepsy suggest that DA signaling impacts excitability in a biphasic manner: activation of D1-like receptors primarily enhances excitatory activity and has pro-epileptogenic effects, while D2-like receptor activation predominantly exerts anti-epileptogenic effects (reviewed by Bozzi & Borrelli, 2013; Strac et al., 2016).

In conclusion, the selective upregulation of *Drd1/DRD1* and *Drd2/DRD2* mRNA transcripts in p.Leu2427Pro mTOR mutated neurons and dysmorphic neurons points toward a critical interaction between DA signaling and cortical network dynamics in FCD type 2. However, based on our study we cannot yet determine the overall impact of overexpressed *Drd1/DRD1* and *Drd2/DRD2* mRNA transcripts on local cortical activity and their ultimate influence on epileptic activity in FCD Type 2. Because our analysis is restricted to mRNA levels, we cannot directly infer whether protein expression of these receptors or their activation is altered. Therefore, the net effect on the E/I balance and epileptogenic activity remains to be established **(Fig. 25)**. Furthermore, the combined impact of both receptor types being upregulated and potentially active within the same neurons is uncertain and would require further investigation. Moreover, the expression of other DA receptor subtypes, such as *Drd3*, *Drd4*, and *Drd5*, in mTOR mutated and dysmorphic neurons requires future studies.

4.3. Dopaminergic alterations impact psychiatric symptoms and comorbidities in mTORopathies

The alterations described so far in the DA axonal density, varicosity and *Drd1/DRD1* and *Drd2/DRD2* receptor transcript expression point to an impaired DA modulatory state in the p.Leu2427Pro mPFC and FCD type 2b lesions area. These disruptions in DA signaling could contribute to the cognitive deficits observed in patients with FCD type 2b. Impaired cognition has been reported in approximately 51% of children with FCD (Veersema et al., 2019). In another study, approximately 37% of FCD patients exhibited psychiatric symptoms, with anxiety-related symptoms being the most common, affecting 60% of patients and reported symptoms included irritability (40%), impulsivity (33%), depression (27%), and psychosis (13%) (Ho et al., 2019). These affects are not restricted to FCD types as other MCDs like periventricular nodular heterotopia and polymicrogyria were also

part of the study. Additionally, TSC patients exhibit intellectual disability, autism, anxiety, depression, ADHD, and aggressive/disruptive behaviors (Crino et al., 2006; Curatolo et al., 2015; Muzykewicz et al., 2007). Several of these psychiatric symptoms and neurodevelopmental disorders are strongly associated with impaired monoaminergic systems, particularly of impaired DA, mostly in the PFC areas (discussed in Introduction 1.5.). However, a direct link between the impaired DA signaling in the PFC and psychiatric symptoms or additional neurodevelopmental comorbidities in mTORopathies, particularly in FCDs, is missing. Hyperactivation of the mTORC1 pathway in the striatum of the two different transgenic mouse models mentioned above has been shown to lead to deficits in motor learning and odor preference behavior (Chen et al., 2024) and to sociability impairments (Lin et al., 2021). Interestingly, in the latter study, post-mortem human brain samples from Brodmann area 46 (a region in the DLPFC) from TSC patients exhibited significantly upregulation of S6(pS240/244) and DARPP-32(pT34) levels. The authors suggest a pathogenetic concept where elevated mTORC1 leads to disruptions in DARPP-32-dependent D1 receptor signaling, a deficit that could contribute to the cognitive and behavioral deficits associated with TSC (Lin et al., 2021). Together, these findings highlight the broad impact of mTORC1 dysregulation on motor, sociability, and cognitive functions. However, the analysis of these mouse models was entirely focused on the impact of the mutations on the striatum. Studies that generated a mouse model with downregulated mTORC2/Akt signaling by generating KO of the mTORC2 regulatory subunit Rictor report deficits in prepulse inhibition, schizophrenia-associated behaviors, along with reduced DA content in the mPFC (Siuta et al., 2010).

A potential implication of the mTOR pathway in schizophrenia and the rapid antidepressant effects of ketamine have been reported. mTOR dysregulation is linked to disrupted-in-schizophrenia 1 (*DISC1*) gene, a genetic risk factor in schizophrenia, bipolar disorder, major depression and ASD (Chubb et al., 2008). Knocking out DISC1 results in increased mTOR signaling, excitability and altered dendritic morphology in the neurons of the dentate gyrus in the hippocampus. Moreover, behavioral deficits like cognitive and memory impairment and depressive behavior were observed. Finally, treatment with rapamycin lead to rescue effects for some the behavioral changes (Zhou et al., 2013). Ketamine is a N-methyl-D-aspartate receptor antagonist which is used as a rapid

antidepressant and enhances DA release in the PFC as well as other brain regions (Pham & Gardier, 2019). Administration of ketamine has been reported to activate mTOR pathway in the rat PFC, enhancing synaptic proteins and dendritic spine synapse formation, while treatment with mTOR inhibitor, rapamycin, prevented both its synaptogenesis and antidepressant behaviors (Li et al., 2010, 2011). These findings might provide evidence of the link between mTOR signaling, DA modulation, and the associated cognitive dysfunctions and psychiatric comorbidities.

During adolescence, the PFC undergoes significant structural and functional maturation and the DA mesoprefrontal contributes to establishing stable E/I balance and the proper development of executive functions during this period (Caballero et al., 2016; Larsen & Luna, 2018; O'Donnell, 2010; Peters & Naneix, 2022). The reduction in DA varicosities and the upregulation of *Drd1/DRD1* and *Drd2/DRD2* receptors during this early developmental critical window, observed in our human and mouse models, may hinder the maturation of DA mesoprefrontal circuitry. This disruption could lead to impairments in executive functions and manifest in psychiatric comorbidities often seen in patients with FCD, such as anxiety, depression, and impulsive behavior. The developmental timeline of the DA system is intricately linked with the emergence of these behaviors, as disruptions in the mesoprefrontal system establishment during critical periods of adolescence has been associated with psychiatric disorders (Manitt et al., 2013; Vosberg et al., 2020). In a study of a mutant mouse model targeting an essential gene for synaptic functions, Arc (activity-regulated cytoskeleton-associated protein), a hypofunctional mesofrontal DA system was observed, marked by reduced DA bouton density, impaired mesofrontal connectivity, and deficits in memory-guided decision-making (Mastwal et al., 2023). Furthermore, adolescent chemogenetic and optogenetic stimulation of DA neurons and axons targeting the frontal cortex effectively restored mesofrontal DA signaling and reversed cognitive impairments into adulthood in *Arc* and also *Disc1* mutant models (Mastwal et al., 2023), highlighting adolescence as a critical period for DA-related circuit deficits and cognitive dysfunction.

Thus, exploring therapeutic strategies that could enhance DA signaling during early adolescence may offer new avenues for mitigating the cognitive and behavioral deficits associated with FCD type 2.

4.4. The impact of noradrenaline and serotonin in epilepsy: insights and future directions

We additionally analyzed the innervation pattern of NA and 5-HT axons by staining for NET and SERT in the WT-mTOR and p.Leu2427Pro mPFC. The results of our analysis showed no significant alterations in NET **(Fig. 15A & B)** or SERT **(Fig. 15C & D)** innervation densities between WT-mTOR and p.Leu2427Pro mPFC at P30, however a trend toward increased 5-HT innervation in the deeper layers of the PL in the p.Leu2427Pro mouse suggests potential subtle changes that could influence local circuitry. Unlike DA innervation, which continues to develop until early adulthood, NA and 5-HT innervation appear to be fully established by early postnatal stages (Levitt & Moore, 1979; Lidov & Molliver, 1982; Vitalis et al., 2013). Consequently, we did not analyze later timepoints in the mouse model, such as P60. However, examining innervation at additional timepoints is crucial to determine whether innervation density changes occur in adulthood as shown for DA in our study. Additionally, it is worth exploring potential compensatory mechanisms for the reduced DA innervation observed in our models during adulthood. This compensation is likely since NA and DA share the same biosynthetic pathway and in the frontal cortex, NET has been shown to also uptake DA (Morón et al., 2002). One study discussed above investigating mTORC2/Akt signaling downregulation in Rictor KO mice revealed a hypodopaminergic state in the PFC, characterized by reduced DA levels, unaltered 5-HT levels, elevated NA levels, and increased NET expression (Siuta et al., 2010). The authors hypothesized that enhanced NET function in Rictor KO mice facilitates DA conversion to NA, explaining the observed rise in NA and concurrent DA reduction. Furthermore, NET blockade in these mice restored cortical DA levels and alleviated cognitive deficits (Siuta et al., 2010). These findings emphasize the potential compensatory relationship between DA and NA systems in maintaining cortical neurotransmitter balance.

Like DA, NA and 5-HT neurotransmission are critically involved in modulating cortical circuits and both systems are implicated in epilepsy mechanisms (reviewed by Strac et al., 2016). The greater variety of NA and 5-HT receptors, along with their modulatory roles compared to the five DA receptor subtypes, makes their involvement in epileptic activity very complex to address. For instance, α_1-adrenergic receptors (a subtype of NA

receptors) have been shown to mediate anticonvulsant effects in pentylenetetrazole (PTZ)-induced seizure animal models (Weinshenker et al., 2001), while α_2-adrenergic receptors may contribute to pro- or anticonvulsant activity depending on their localization of the receptor as pre- or postsynaptic, respectively (Szot et al., 2004). On the other hand, 5-HT_{1A} receptors are typically associated with anticonvulsant effects in generalized seizure animal models (López-Meraz et al., 2005), whereas 5-HT_{2A} receptors can exhibit pro and anticonvulsant roles subjective to the type of model or ligand dose (Guiard & Giovanni, 2015). Therefore, examining the expression and activity of these and additional NA and 5-HT receptor subtypes in the mPFC of FCD type 2 models could reveal insights into how NA and 5-HT signaling influences epileptogenesis and seizure modulation. Moreover, extending these analyses to human FCD type 2b tissue is critical for translational relevance. Few case studies from FCD patient biopsies reported altered innervation of NA axons, marked with DBH, and 5-HT axons in the dysplastic epileptogenic tissues compared to control patient tissue (Trottier et al., 1994, 1996).

Further studies are needed to determine if and how these systems are involved in the modulation of FCD type 2 and their potential role in local cortical regulation and seizure activity. A comprehensive investigation could clarify the contribution of monoaminergic modulators to the pathology of FCD and epilepsy, enabling future research for novel therapeutic strategies to address cognitive deficits, psychiatric comorbidities, and seizures in FCD patients.

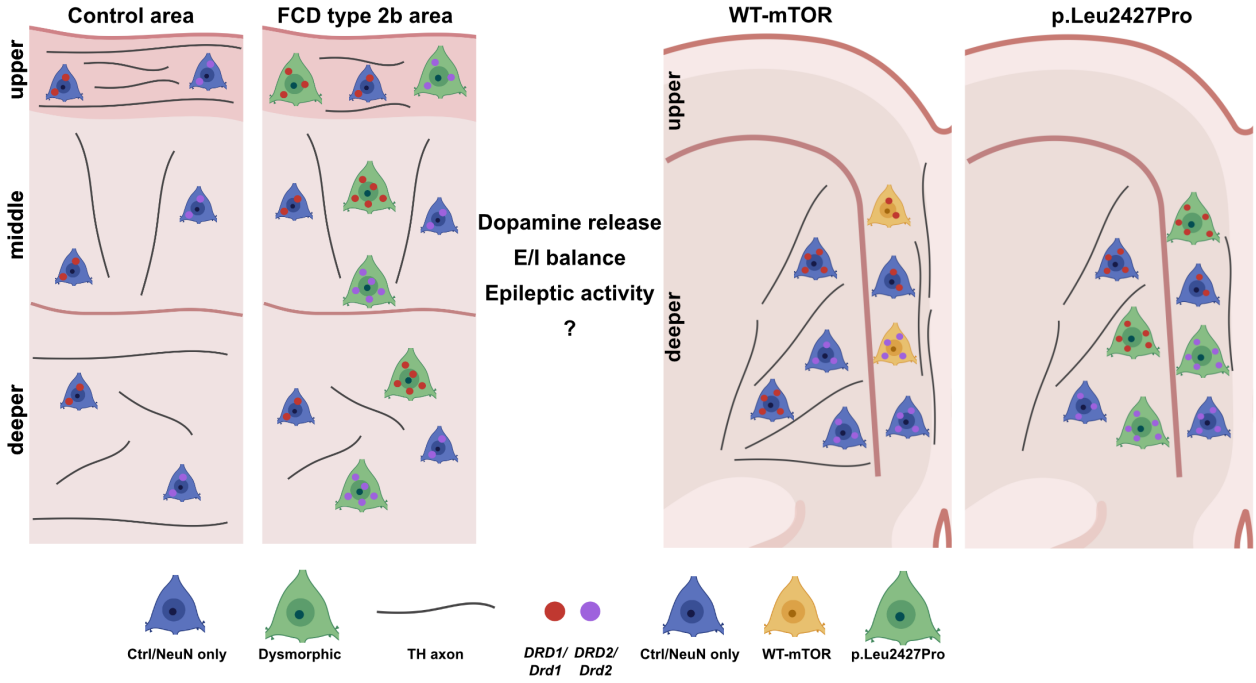

Fig. 25. Summarized findings of DA innervation density and *Drd*/*DRD* receptor mRNA expression in the adult human FCD type 2b biopsies (left) and mouse mTOR hyperactivation model (right) and remaining open questions for future research. Created with BioRender.com

4.5. Conclusions

This study presents findings that suggest significant alterations in both DA innervation and receptor expression in FCD type 2 and paves the way to examine the contribution of DA signaling in the pathophysiology of FCD type 2 **(Fig. 25)**. The mTOR hyperactivation mouse model demonstrated transient changes in DA innervation density in the mPFC during adolescence and a trend toward reduced innervation density in adulthood compared to WT-mTOR mPFC, uncovering the developmental trajectory of DA-related disruptions in FCD type 2. This alteration was mostly evident in the infralimbic cortex of the mPFC. Other monoaminergic systems projecting to the cortex, like NA and 5-HT, did not show any significant alteration in innervation density in the mPFC during adolescence. In pediatric human FCD type 2 biopsies, while no changes were found in the DA innervation density, a reduced DA axonal varicosity density was observed in the FCD type 2b area compared to control areas. In adult human FCD type 2 biopsies, a reduction in overall DA innervation density was observed alongside altered laminar distribution patterns in the FCD type 2b compared to control area.

Additionally, differential expression of *Drd1/DRD1* and *Drd2/DRD2* was identified in mTOR-mutated neurons and dysmorphic neurons. An upregulation of the receptor mRNA in abnormally-developed neurons compared to normal neurons might suggest a compensation for generally decreased DA input manifested in adulthood and/or exacerbate local cortical network dysregulation.

Overall, these findings highlight that DA signaling, which is thought to have an important influence on cortical network activity, could contribute to network disruptions in cortical dysplasia, since DA neurotransmission may be altered in the FCD type 2 area. Future research should focus on exploring the mechanistic pathways underlying DA dysregulation. This knowledge could aid the research for targeted therapeutic interventions aimed at restoring neurotransmitter balance with a potential impact on cognitive deficits, psychiatric comorbidities, and epileptogenesis in FCD type 2 patients.

5. Abstract

Focal Cortical Dysplasia (FCD) type 2 is the most prevalent malformation of cortical development (MCD) associated with pharmacoresistant focal epilepsy, frequently located in the frontal cortex. Neuropathological features include abnormal cortical layering and enlarged dysmorphic neurons and balloon cells. Profoundly altered local neuronal activity has been observed in epilepsy-surgical biopsies from patients with FCD type 2. Notably, FCD type 2 emerges during brain development and integrates into complex connectivity architectures with surrounding neuronal networks. Local cortical microcircuits, especially in the frontal cortex, are extensively modulated by monoaminergic axonal projections from the brainstem. Prior studies of human FCD type 2 biopsies suggested altered density and distribution of monoaminergic axons; however, a systematic investigation remains lacking.

In this study, we provide a comprehensive analysis of dopaminergic (DA) innervation in human FCD type 2b biopsies and in the medial prefrontal cortex (mPFC) of a mouse model with mTOR hyperactivation (FCD type 2 model) during adolescence and adulthood. We also investigate DA receptor transcript expression using multiplex fluorescent RNA *in situ* hybridization in human specimens and the mPFC of this mouse model. Our findings in the mouse model reveal transient alterations in DA innervation density during adolescence and a trend toward decreased innervation in adulthood. Similarly, in human FCD type 2b biopsies, DA innervation density is reduced in the affected cortical areas compared to control regions from the same patients, with an altered lamination pattern of DA axons in the FCD type 2b regions. Additionally, DA receptor 1 (DRD1/*Drd1*) and receptor 2 (DRD2/*Drd2*) mRNA transcripts are upregulated in dysmorphic neurons in human samples and mTOR-mutated neurons in mice, compared to normally-developed neurons from control tissue or surrounding ones.

These findings suggest complex molecular and structural cortical changes impacting DA neurotransmission within FCD type 2 and putatively affecting local cortical activity, manifestation of seizures and psychiatric comorbidities. This impaired DA signaling may have significant implications for understanding the pathology of FCD type 2 and developing targeted therapeutic strategies.

6. List of figures

7. List of tables

8. References

Agirman, G., Broix, L., & Nguyen, L. (2017). Cerebral cortex development: an outside-in perspective. *FEBS Letters*, *591*, 3978–3992.

Alexandre, V., Walz, R., Bianchin, M. M., Velasco, T. R., Terra-Bustamante, V. C., Wichert-Ana, L., … Sakamoto, A. C. (2006). Seizure outcome after surgery for epilepsy due to focal cortical dysplastic lesions. *Seizure*, *15*, 420–427.

ANGEVINE, J. B., & SIDMAN, R. L. (1961). Autoradiographic Study of Cell Migration during Histogenesis of Cerebral Cortex in the Mouse. *Nature*, *192*, 766–768.

Bahry, E., Breimann, L., Zouinkhi, M., Epstein, L., Kolyvanov, K., Mamrak, N., … Preibisch, S. (2022). RS-FISH: precise, interactive, fast, and scalable FISH spot detection. *Nature Methods*, *19*, 1563–1567.

Baldassari, S., Picard, F., Verbeek, N. E., van Kempen, M., Brilstra, E. H., Lesca, G., … Baulac, S. (2019a). The landscape of epilepsy-related GATOR1 variants. *Genetics in Medicine*, *21*, 398–408.

Baldassari, S., Ribierre, T., Marsan, E., Adle-Biassette, H., Ferrand-Sorbets, S., Bulteau, C., … Baulac, S. (2019b). Dissecting the genetic basis of focal cortical dysplasia: a large cohort study. *Acta Neuropathologica*, *138*, 885–900.

Bang, S. J., Jensen, P., Dymecki, S. M., & Commons, K. G. (2012). Projections and interconnections of genetically defined serotonin neurons in mice. *European Journal of Neuroscience*, *35*, 85–96.

Bar-Peled, L., Chantranupong, L., Cherniack, A. D., Chen, W. W., Ottina, K. A., Grabiner, B. C., … Sabatini, D. M. (2013). A Tumor Suppressor Complex with GAP Activity for the Rag GTPases That Signal Amino Acid Sufficiency to mTORC1. *Science*, *340*, 1100–1106.

Barkovich, A. J., Kuzniecky, R. I., Dobyns, W. B., Jackson, G. D., Becker, L. E., & Evrard, P. (1996). A classification scheme for malformations of cortical development. *Neuropediatrics*, *27*, 59–63.

Benes, F. M., Vincent, S. L., & Molloy, R. (1993). Dopamnine-Immunoreactive axon varicosities form nonrandom contacts with GABA-immunoreactive neurons of rat medial prefrontal cortex. *Synapse*, *15*, 285–295.

Benes, F. M., Vincent, S. L., Molloy, R., & Khan, Y. (1996). Increased interaction of dopamine-immunoreactive varicosities with GABA neurons of rat medial prefrontal cortex occurs during the postweanling period. *Synapse*, *23*, 237–245.

Biol Psychiat. (2017). Special Issue: The Dopamine Hypothesis of Schizophrenia. *Biological Psychiatry*, *81*, 1.

Björklund, A., & Dunnett, S. B. (2007). Dopamine neuron systems in the brain: an update. *Trends in Neurosciences*, *30*, 194–202.

Blaess, S., Bodea, G. O., Kabanova, A., Chanet, S., Mugniery, E., Derouiche, A., … Joyner, A. L. (2011). Temporal-spatial changes in Sonic Hedgehog expression and signaling reveal different potentials of ventral mesencephalic progenitors to populate distinct ventral midbrain nuclei. *Neural Development*, *6*, 29.

Blümcke, I., Spreafico, R., Haaker, G., Coras, R., Kobow, K., Bien, C. G., … Avanzini, G. (2017). Histopathological Findings in Brain Tissue Obtained during Epilepsy Surgery. *New England Journal of Medicine*, *377*, 1648–1656.

Blümcke, I., Thom, M., Aronica, E., Armstrong, D. D., Harry, V., Palmini, A., … Vezzani, A. (2011). The clinico-pathological spectrum of Focal Cortical Dysplasias: a consensus classification. *Epilepsia*, *52*, 158–174.

Boer, K., Spliet, W. G. M., van Rijen, P. C., Redeker, S., Troost, D., & Aronica, E. (2006). Evidence of activated microglia in focal cortical dysplasia. *Journal of Neuroimmunology*, *173*, 188–195.

Boyle, N., Betts, S., & Lu, H. (2024). Monoaminergic Modulation of Learning and Cognitive Function in the Prefrontal Cortex. *Brain Sciences*, Vol. 14. https://doi.org/10.3390/brainsci14090902

Bozzi, Y., & Borrelli, E. (2013). The role of dopamine signaling in epileptogenesis.

Frontiers in Cellular Neuroscience, *7*, 1–12.

Bystron, I., Blakemore, C., & Rakic, P. (2008). Development of the human cerebral cortex: Boulder Committee revisited. *Nature Reviews Neuroscience*, *9*, 110–122.

Caballero, A., Granberg, R., & Tseng, K. Y. (2016). Neuroscience and Biobehavioral Reviews Mechanisms contributing to prefrontal cortex maturation during adolescence ☪. *Neuroscience and Biobehavioral Reviews*, *70*, 4–12.

Cadwell, C. R., Bhaduri, A., Mostajo-Radji, M. A., Keefe, M. G., & Nowakowski, T. J. (2019). Development and Arealization of the Cerebral Cortex. *Neuron*, *103*, 980–1004.

Carlén, M. (2017). What constitutes the prefrontal cortex? *Science*, *358*, 478–482.

Cartier, E., Hamilton, P. J., Belovich, A. N., Shekar, A., Campbell, N. G., Saunders, C., … Galli, A. (2015). Rare Autism-Associated Variants Implicate Syntaxin 1 (STX1 R26Q) Phosphorylation and the Dopamine Transporter (hDAT R51W) in Dopamine Neurotransmission and Behaviors. *EBioMedicine*, *2*, 135–146.

Caviness, V. S., Takahashi, T., & Nowakowski, R. S. (1995). Numbers, time and neocortical neuronogenesis: a general developmental and evolutionary model. *Trends in Neurosciences*, *18*, 379–383.

Cepeda, C., André, V. M., Flores-Hernández, J., Nguyen, O. K., Wu, N., Klapstein, G. J., … Mathern, G. W. (2005). Pediatric cortical dysplasia: correlations between neuroimaging, electrophysiology and location of cytomegalic neurons and balloon cells and glutamate/GABA synaptic circuits. *Developmental Neuroscience*, *27*, 59–76.

Cepeda, C., André, V. M., Levine, M. S., Salamon, N., Miyata, H., Vinters, H. V., & Mathern, G. W. (2006). Epileptogenesis in pediatric cortical dysplasia: The dysmature cerebral developmental hypothesis. *Epilepsy and Behavior*, *9*, 219–235.

Cepeda, C., Hurst, R. S., Flores-Hernández, J., Hernández-Echeagaray, E., Klapstein, G. J., Boylan, M. K., … Mathern, G. W. (2003). Morphological and electrophysiological

characterization of abnormal cell types in pediatric cortical dysplasia. *Journal of Neuroscience Research*, *72*, 472–486.

Chen, L., Saito, R., Noda-Narita, S., Kassai, H., & Aiba, A. (2024). Hyperactive mTORC1 in striatum dysregulates dopamine receptor expression and odor preference behavior. *Frontiers in Neuroscience*, *18*. Retrieved from https://www.frontiersin.org/journals/neuroscience/articles/10.3389/fnins.2024.1461178

Chubb, J. E., Bradshaw, N. J., Soares, D. C., Porteous, D. J., & Millar, J. K. (2008). The DISC locus in psychiatric illness. *Molecular Psychiatry*, *13*, 36–64.

Cools, R., & Arnsten, A. F. T. (2022). *Neuromodulation of prefrontal cortex cognitive function in primates : the powerful roles of monoamines and acetylcholine*. https://doi.org/10.1038/s41386-021-01100-8

Cooper, J. R., Bloom, F. E., & Roth, R. H. (2003). The biochemical basis of neuropharmacology, 8th ed. In *The biochemical basis of neuropharmacology, 8th ed.* New York, NY, US: Oxford University Press.

Crino, P. B. (2011). mTOR: A pathogenic signaling pathway in developmental brain malformations. *Trends in Molecular Medicine*, *17*, 734–742.

Crino, P. B. (2015). mTOR signaling in epilepsy: Insights from malformations of cortical development. *Cold Spring Harbor Perspectives in Medicine*, *5*, 1–18.

Crino, P. B., Nathanson, K. L., & Henske, E. P. (2006). The Tuberous Sclerosis Complex. *New England Journal of Medicine*, *355*, 1345–1356.

Curatolo, P., Moavero, R., Roberto, D., & Graziola, F. (2015). Genotype/Phenotype Correlations in Tuberous Sclerosis Complex. *Seminars in Pediatric Neurology*, *22*, 259–273.

D'Gama, A. M., Geng, Y., Couto, J. A., Martin, B., Boyle, E. A., LaCoursiere, C. M., … Poduri, A. (2015). Mammalian target of rapamycin pathway mutations cause hemimegalencephaly and focal cortical dysplasia. *Annals of Neurology*, *77*, 720–725.

D'Gama, A. M., Woodworth, M. B., Hossain, A. A., Bizzotto, S., Hatem, N. E., LaCoursiere, C. M., … Walsh, C. A. (2017). Somatic Mutations Activating the mTOR Pathway in Dorsal Telencephalic Progenitors Cause a Continuum of Cortical Dysplasias. *Cell Reports*, *21*, 3754–3766.

del Campo, N., Chamberlain, S. R., Sahakian, B. J., & Robbins, T. W. (2011). The Roles of Dopamine and Noradrenaline in the Pathophysiology and Treatment of Attention-Deficit/Hyperactivity Disorder. *Biological Psychiatry*, *69*, e145–e157.

Desikan, R. S., & Barkovich, A. J. (2016). Malformations of cortical development. *Annals of Neurology*, *80*, 797–810.

Dobashi, Y., Watanabe, Y., Miwa, C., Suzuki, S., & Koyama, S. (2011). Mammalian target of rapamycin: a central node of complex signaling cascades. *International Journal of Clinical and Experimental Pathology*, *4*, 476–495.

Dumas, S., & Wallén-Mackenzie, Å. (2019). Developmental Co-expression of Vglut2 and Nurr1 in a Mes-Di-Encephalic Continuum Preceeds Dopamine and Glutamate Neuron Specification. *Frontiers in Cell and Developmental Biology*, *7*. Retrieved from https://www.frontiersin.org/journals/cell-and-developmental-biology/articles/10.3389/fcell.2019.00307

Dwyer, J. M., & Duman, R. S. (2013). Activation of mammalian target of rapamycin and synaptogenesis: role in the actions of rapid-acting antidepressants. *Biological Psychiatry*, *73*, 1189–1198.

Dwyer, J. M., Lepack, A. E., & Duman, R. S. (2012). mTOR activation is required for the antidepressant effects of $mGluR_{2/3}$ blockade. *The International Journal of Neuropsychopharmacology*, *15*, 429–434.

Ernst, M, Zametkin, A. J., Matochik, J. A., Pascualvaca, D., & Cohen, R. M. (1997, August). Low medial prefrontal dopaminergic activity in autistic children. *Lancet (London, England)*, Vol. 350, p. 638. England.

Ernst, Monique, Zametkin, A. J., Matochik, J. A., Jons, P. H., & Cohen, R. M. (1998).

DOPA Decarboxylase Activity in Attention Deficit Hyperactivity Disorder Adults. A [Fluorine-18]Fluorodopa Positron Emission Tomographic Study. *The Journal of Neuroscience*, *18*, 5901 LP – 5907.

Falco-Walter, J., Owen, C., Sharma, M., Reggi, C., Yu, M., Stoub, T. R., & Stein, M. A. (2017). Magnetoencephalography and New Imaging Modalities in Epilepsy. *Neurotherapeutics*, *14*, 4–10.

Fauser, S., Häussler, U., Donkels, C., Huber, S., Nakagawa, J., Prinz, M., … Haas, C. A. (2014). Disorganization of neocortical lamination in focal cortical dysplasia is brain-region dependent: Evidence from layer-specific marker expression. *Acta Neuropathologica Communications*, *2*, 1–13.

Gadow, K. D., DeVincent, C. J., Olvet, D. M., Pisarevskaya, V., & Hatchwell, E. (2010). Association of DRD4 polymorphism with severity of oppositional defiant disorder, separation anxiety disorder and repetitive behaviors in children with autism spectrum disorder. *European Journal of Neuroscience*, *32*, 1058–1065.

Gao, W.-J., & Goldman-Rakic, P. S. (2003). Selective modulation of excitatory and inhibitory microcircuits by dopamine. *Proceedings of the National Academy of Sciences*, *100*, 2836–2841.

Gaspar, P., Berger, B., Febvret, A., Vigny, A., & Henry, J. P. (1989). Catecholamine innervation of the human cerebral cortex as revealed by comparative immunohistochemistry of tyrosine hydroxylase and dopamine-beta-hydroxylase. *Journal of Comparative Neurology*, *279*, 249–271.

Gaspar, P., Cases, O., & Maroteaux, L. (2003). The developmental role of serotonin: news from mouse molecular genetics. *Nature Reviews Neuroscience*, *4*, 1002–1012.

Gee, S., Ellwood, I., Patel, T., Luongo, F., Deisseroth, K., & Sohal, V. S. (2012). Synaptic activity unmasks dopamine D2 receptor modulation of a specific class of layer V pyramidal neurons in prefrontal cortex. *The Journal of Neuroscience : The Official Journal of the Society for Neuroscience*, *32*, 4959–4971.

Ghaeli, P., Nikvarz, N., Alaghband-Rad, J., Alimadadi, A., & Tehrani-Doost, M. (2014). Effects of risperidone on core symptoms of autistic disorder based on childhood autism rating scale: an open label study. *Indian Journal of Psychological Medicine*, *36*, 66–70.

Goldman-Rakic, P S, Muly E.C, I. I. I., & Williams, G. V. (2000). D1 receptors in prefrontal cells and circuits. *Brain Research Reviews*, *31*, 295–301.

Goldman-Rakic, Patricia S, & Brown, R. M. (1982). Postnatal development of monoamine content and synthesis in the cerebral cortex of rhesus monkeys. *Developmental Brain Research*, *4*, 339–349.

Gorelova, N., Seamans, J. K., & Yang, C. R. (2002). Mechanisms of dopamine activation of fast-spiking interneurons that exert inhibition in rat prefrontal cortex. *Journal of Neurophysiology*, *88*, 3150–3166.

Gressens, P. (2000). Mechanisms and Disturbances of Neuronal Migration. *Pediatric Research*, *48*, 725–730.

Guiard, B. P., & Giovanni, G. Di. (2015). Central serotonin-2A (5-HT2A) receptor dysfunction in depression and epilepsy: the missing link? *Frontiers in Pharmacology*, *6*. Retrieved from https://www.frontiersin.org/journals/pharmacology/articles/10.3389/fphar.2015.00046

Gulledge, A. T., & Jaffe, D. B. (1998). Dopamine decreases the excitability of layer V pyramidal cells in the rat prefrontal cortex. *The Journal of Neuroscience*, Vol. 18, pp. 9139–9151. Jaffe, David B.: Division of Life Sciences, University of Texas at San Antonio, 6900 North Loop 1604 West, San Antonio, TX, US, 78249: Society for Neuroscience.

Gulledge, A. T., & Jaffe, D. B. (2001). Multiple Effects of Dopamine on Layer V Pyramidal Cell Excitability in Rat Prefrontal Cortex. *Journal of Neurophysiology*, *86*, 586–595.

Hamilton, P. J., Campbell, N. G., Sharma, S., Erreger, K., Herborg Hansen, F., Saunders,

C., … Consortium, N. I. H. A. A. S. (2013). De novo mutation in the dopamine transporter gene associates dopamine dysfunction with autism spectrum disorder. *Molecular Psychiatry*, *18*, 1315–1323.

Hauptman, J. S., & Mathern, G. W. (2012). Surgical treatment of epilepsy associated with cortical dysplasia: 2012 update. *Epilepsia*, *53*, 98–104.

Ho, C. S. H., Dubeau, F., Séguin, R., & Ducharme, S. (2019). Prevalence of neuropsychiatric symptoms associated with malformations of cortical development. *Epilepsy & Behavior*, *92*, 306–310.

Hoelz, H., Coppenrath, E., Hoertnagel, K., Roser, T., Tacke, M., Gerstl, L., & Borggraefe, I. (2018). Childhood-Onset Epileptic Encephalopathy Associated With Isolated Focal Cortical Dysplasia and a Novel TSC1 Germline Mutation. *Clinical EEG and Neuroscience*, *49*, 187–191.

Hoops, D., & Flores, C. (2017). Making Dopamine Connections in Adolescence. *Trends in Neurosciences*, *40*, 709–719.

Huttenlocher, P. R., de Courten, C., Garey, L. J., & Van der Loos, H. (1982). Synaptogenesis in human visual cortex — evidence for synapse elimination during normal development. *Neuroscience Letters*, *33*, 247–252.

Iffland, P. H., & Crino, P. B. (2017). Focal Cortical Dysplasia: Gene Mutations, Cell Signaling, and Therapeutic Implications. *Annual Review of Pathology: Mechanisms of Disease*, *12*, 547–571.

Inoki, K., Li, Y., Xu, T., & Guan, K.-L. (2003). Rheb GTPase is a direct target of TSC2 GAP activity and regulates mTOR signaling. *Genes & Development*, *17*, 1829–1834.

Inoki, K., Li, Y., Zhu, T., Wu, J., & Guan, K.-L. (2002). TSC2 is phosphorylated and inhibited by Akt and suppresses mTOR signalling. *Nature Cell Biology*, *4*, 648–657.

Islam, K. U. S., & Blaess, S. (2024). The impact of the mesoprefrontal dopaminergic system on the maturation of interneurons in the murine prefrontal cortex. *Frontiers in Neuroscience*, *18*. Retrieved from

https://www.frontiersin.org/journals/neuroscience/articles/10.3389/fnins.2024.1403402

Islam, K. U. S., Meli, N., & Blaess, S. (2021). The Development of the Mesoprefrontal Dopaminergic System in Health and Disease. *Frontiers in Neural Circuits*, *15*, 103.

Iversen, L., Iversen, S., Dunnett, S., & Bjorklund, A. (Eds.). (2009, October 16). *Dopamine Handbook*. Oxford University Press.

Iyer, A., Zurolo, E., Spliet, W. G. M., van Rijen, P. C., Baayen, J. C., Gorter, J. A., & Aronica, E. (2010). Evaluation of the innate and adaptive immunity in type I and type II focal cortical dysplasias. *Epilepsia*, *51*, 1763–1773.

Jesus-Ribeiro, J., Pires, L. M., Melo, J. D., Ribeiro, I. P., Rebelo, O., Sales, F., … Melo, J. B. (2021). Genomic and Epigenetic Advances in Focal Cortical Dysplasia Types I and II: A Scoping Review. *Frontiers in Neuroscience*, *14*, 1–13.

Jiang, M., Jang, S. E., & Zeng, L. (2023). The Effects of Extrinsic and Intrinsic Factors on Neurogenesis. *Cells*, *12*, 1–30.

Jones, B. E., Halaris, A. E., McIlhany, M., & Moore, R. Y. (1977). Ascending projections of the locus coeruleus in the rat. I. axonal transport in central noradrenaline neurons. *Brain Research*, *127*, 1–21.

Jones, B. E., & Moore, R. Y. (1977). Ascending projections of the locus coeruleus in the rat. II. Autoradiographic study. *Brain Research*, *127*, 23–53.

Kabanova, A., Pabst, M., Lorkowski, M., Braganza, O., Boehlen, A., Nikbakht, N., … Blaess, S. (2015). Function and developmental origin of a mesocortical inhibitory circuit. *Nature Neuroscience*, *18*, 872–882.

Kalsbeek, A., Voorn, P., Buijs, R. M., Pool, C. W., & Uylings, H. B. M. (1988). Development of the dopaminergic innervation in the prefrontal cortex of the rat. *Journal of Comparative Neurology*, *269*, 58–72.

Khoo, A., de Tisi, J., Foong, J., Bindman, D., O'Keeffe, A. G., Sander, J. W., … Duncan,

J. S. (2022). Long-term seizure, psychiatric and socioeconomic outcomes after frontal lobe epilepsy surgery. *Epilepsy Research*, *186*, 106998.

Kim, D. W., Lee, S. K., Chu, K., Park, K. I., Lee, S. Y., Lee, C. H., … Kim, J. Y. (2009). Predictors of surgical outcome and pathologic considerations in focal cortical dysplasia. *Neurology*, *72*, 211–216.

Kim, J. K., Cho, J., Kim, S. H., Kang, H.-C., Kim, D.-S., Kim, V. N., & Lee, J. H. (2019). Brain somatic mutations in MTOR reveal translational dysregulations underlying intractable focal epilepsy. *The Journal of Clinical Investigation*, *129*, 4207–4223.

Kim, Y. H., Kang, H.-C., Kim, D.-S., Kim, S. H., Shim, K.-W., Kim, H. D., & Lee, J. S. (2011). Neuroimaging in identifying focal cortical dysplasia and prognostic factors in pediatric and adolescent epilepsy surgery. *Epilepsia*, *52*, 722–727.

Kloss, S., Pieper, T., Pannek, H., Holthausen, H., & Tuxhorn, I. (2002). Epilepsy surgery in children with focal cortical dysplasia (FCD): results of long-term seizure outcome. *Neuropediatrics*, *33*, 21–26.

Kolk, S. M., Gunput, R.-A. F., Tran, T. S., van den Heuvel, D. M. A., Prasad, A. A., Hellemons, A. J. C. G. M., … Pasterkamp, R. J. (2009). Semaphorin 3F Is a Bifunctional Guidance Cue for Dopaminergic Axons and Controls Their Fasciculation, Channeling, Rostral Growth, and Intracortical Targeting. *The Journal of Neuroscience*, *29*, 12542 LP – 12557.

Kolk, S. M., & Rakic, P. (2022). Development of prefrontal cortex. *Neuropsychopharmacology*, *47*, 41–57.

Krsek, P, Maton, B., Jayakar, P., Dean, P., Korman, B., Rey, G., … Duchowny, M. (2009). Incomplete resection of focal cortical dysplasia is the main predictor of poor postsurgical outcome. *Neurology*, *72*, 217–223.

Krsek, Pavel, Kudr, M., Jahodova, A., Komarek, V., Maton, B., Malone, S., … Duchowny, M. (2013). Localizing value of ictal SPECT is comparable to MRI and EEG in children with focal cortical dysplasia. *Epilepsia*, *54*, 351–358.

Kwan, K. Y., Šestan, N., & Anton, E. S. (2012). Transcriptional co-regulation of neuronal migration and laminar identity in the neocortex. *Development*, *139*, 1535–1546.

Kwon, C.-H., Zhu, X., Zhang, J., & Baker, S. J. (2003). mTor is required for hypertrophy of Pten-deficient neuronal soma in vivo. *Proceedings of the National Academy of Sciences*, *100*, 12923–12928.

Lammel, S., Hetzel, A., Häckel, O., Jones, I., Liss, B., & Roeper, J. (2008). Unique Properties of Mesoprefrontal Neurons within a Dual Mesocorticolimbic Dopamine System. *Neuron*, *57*, 760–773.

Lapish, C. C., Kroener, S., Durstewitz, D., Lavin, A., & Seamans, J. K. (2007). The ability of the mesocortical dopamine system to operate in distinct temporal modes. *Psychopharmacology*, *191*, 609–625.

Laplante, F., Zhang, Z.-W., Huppé-Gourgues, F., Dufresne, M. M., Vaucher, E., & Sullivan, R. M. (2012). Cholinergic depletion in nucleus accumbens impairs mesocortical dopamine activation and cognitive function in rats. *Neuropharmacology*, *63*, 1075–1084.

Laplante, M., & Sabatini, D. M. (2009). mTOR signaling at a glance. *Journal of Cell Science*, *122*, 3589–3594.

Laplante, M., & Sabatini, D. M. (2012). mTOR Signaling in Growth Control and Disease. *Cell*, *149*, 274–293.

Larsen, B., & Luna, B. (2018). Adolescence as a neurobiological critical period for the development of higher-order cognition. *Neuroscience and Biobehavioral Reviews*, *94*, 179–195.

Laubach, M., Amarante, L. M., Swanson, K., & White, S. R. (2018). What, If Anything, Is Rodent Prefrontal Cortex? *Eneuro*, *5*, ENEURO.0315-18.2018.

Lauder, J. M., & Bloom, F. E. (1974). Ontogeny of monoamine neurons in the locus coeruleus, raphe nuclei and substantia nigra of the rat. I. Cell differentiation. *Journal of Comparative Neurology*, *155*, 469–481.

Lavin, A., & Grace, A. A. (2001). Stimulation of D1-type dopamine receptors enhances excitability in prefrontal cortical pyramidal neurons in a state-dependent manner. *Neuroscience*, *104*, 335–346.

Lawlor, M. A., & Alessi, D. R. (2001). PKB/Akt: a key mediator of cell proliferation, survival and insulin responses? *Journal of Cell Science*, *114*, 2903–2910.

Lee, J. H., Huynh, M., Silhavy, J. L., Kim, S., Dixon-Salazar, T., Heiberg, A., … Gleeson, J. G. (2012). De novo somatic mutations in components of the PI3K-AKT3-mTOR pathway cause hemimegalencephaly. *Nature Genetics*, *44*, 941–945.

Legland, D., Arganda-Carreras, I., & Andrey, P. (2016). MorphoLibJ: Integrated library and plugins for mathematical morphology with ImageJ. *Bioinformatics*, *32*, 3532–3534.

Lerner, J. T., Salamon, N., Hauptman, J. S., Velasco, T. R., Hemb, M., Wu, J. Y., … Mathern, G. W. (2009). Assessment and surgical outcomes for mild type i and severe type II cortical dysplasia: A critical review and the UCLA experience. *Epilepsia*, *50*, 1310–1335.

Leslie, C. A., Robertson, M. W., Cutler, A. J., & Bennett, J. P. (1991). Postnatal development of D 1 dopamine receptors in the medial prefrontal cortex, striatum and nucleus accumbens of normal and neonatal 6-hydroxydopamine treated rats: a quantitative autoradiographic analysis. *Developmental Brain Research*, *62*, 109–114.

Leventer, R. J., Scerri, T., Marsh, A. P. L., Pope, K., Gillies, G., Maixner, W., … Lockhart, P. J. (2015). Hemispheric cortical dysplasia secondary to a mosaic somatic mutation in MTOR. *Neurology*, *84*, 2029–2032.

Levitt, P, & Moore, R. Y. (1979). Development of the noradrenergic innervation of neocortex. *Brain Research*, *162*, 243–259.

Levitt, Pat, & Moore, R. Y. (1978). Noradrenaline neuron innervation of the neocortex in the rat. *Brain Research*, *139*, 219–231.

Li, N., Lee, B., Liu, R.-J., Banasr, M., Dwyer, J. M., Iwata, M., … Duman, R. S. (2010).

mTOR-Dependent Synapse Formation Underlies the Rapid Antidepressant Effects of NMDA Antagonists. *Science*, *329*, 959–964.

Li, N., Liu, R.-J., Dwyer, J. M., Banasr, M., Lee, B., Son, H., … Duman, R. S. (2011). Glutamate N-methyl-D-aspartate Receptor Antagonists Rapidly Reverse Behavioral and Synaptic Deficits Caused by Chronic Stress Exposure. *Biological Psychiatry*, *69*, 754–761.

Lidov, H. G. W., Grzanna, R., & Molliver, M. E. (1980). The serotonin innervation of the cerebral cortex in the rat-an immunohistochemical analysis. *Neuroscience*, *5*, 207–227.

Lidov, H. G. W., & Molliver, M. E. (1982). An immunohistochemical study of serotonin neuron development in the rat: Ascending pathways and terminal fields. *Brain Research Bulletin*, *8*, 389–430.

Lidow, M. S., & Rakic, P. (1992). Scheduling of monoaminergic neurotransmitter receptor expression in the primate neocortex during postnatal development. *Cerebral Cortex (New York, N.Y. : 1991)*, *2*, 401–416.

Lim, J. S., Gopalappa, R., Kim, S. H., Ramakrishna, S., Lee, M., Kim, W., … Lee, J. H. (2017). Somatic Mutations in TSC1 and TSC2 Cause Focal Cortical Dysplasia. *The American Journal of Human Genetics*, *100*, 454–472.

Lim, J. S., Kim, W. Il, Kang, H. C., Kim, S. H., Park, A. H., Park, E. K., … Lee, J. H. (2015). Brain somatic mutations in MTOR cause focal cortical dysplasia type II leading to intractable epilepsy. *Nature Medicine*, *21*, 395–400.

Lin, R., Learman, L. N., Na, C.-H., Renuse, S., Chen, K. T., Chen, P. Y., … Worley, P. F. (2021). Persistently Elevated mTOR Complex 1-S6 Kinase 1 Disrupts DARPP-32–Dependent D1 Dopamine Receptor Signaling and Behaviors. *Biological Psychiatry*, *89*, 1058–1072.

Loewith, R., Jacinto, E., Wullschleger, S., Lorberg, A., Crespo, J. L., Bonenfant, D., … Hall, M. N. (2002). Two TOR Complexes, Only One of which Is Rapamycin Sensitive,

Have Distinct Roles in Cell Growth Control. *Molecular Cell*, *10*, 457–468.

López-Meraz, M.-L., González-Trujano, M.-E., Neri-Bazán, L., Hong, E., & Rocha, L. L. (2005). 5-HT1A receptor agonists modify epileptic seizures in three experimental models in rats. *Neuropharmacology*, *49*, 367–375.

Ma, X. M., & Blenis, J. (2009). Molecular mechanisms of mTOR-mediated translational control. *Nature Reviews. Molecular Cell Biology*, *10*, 307–318.

Malik, S., Vinukonda, G., Vose, L. R., Diamond, D., Bhimavarapu, B. B. R., Hu, F., … Ballabh, P. (2013). Neurogenesis continues in the third trimester of pregnancy and is suppressed by premature birth. *Journal of Neuroscience*, *33*, 411–423.

Manitt, C., Eng, C., Pokinko, M., Ryan, R. T., Torres-Berrío, A., Lopez, J. P., … Flores, C. (2013). Dcc orchestrates the development of the prefrontal cortex during adolescence and is altered in psychiatric patients. *Translational Psychiatry*, *3*, 1–13.

Manitt, Colleen, Mimee, A., Eng, C., Pokinko, M., Stroh, T., Cooper, H. M., … Flores, C. (2011). The Netrin Receptor DCC Is Required in the Pubertal Organization of Mesocortical Dopamine Circuitry. *The Journal of Neuroscience*, *31*, 8381 LP – 8394.

Mastwal, S., Li, X., Stowell, R., Manion, M., Zhang, W., Kim, N. S., … Wang, K. H. (2023). Adolescent neurostimulation of dopamine circuit reverses genetic deficits in frontal cortex function. *ELife*, *12*. https://doi.org/10.7554/eLife.87414

McCracken, J. T., McGough, J., Shah, B., Cronin, P., Hong, D., Aman, M. G., … McMahon, D. (2002). Risperidone in children with autism and serious behavioral problems. *The New England Journal of Medicine*, *347*, 314–321.

McDougle, C. J., Scahill, L., Aman, M. G., McCracken, J. T., Tierney, E., Davies, M., … Vitiello, B. (2005). Risperidone for the core symptom domains of autism: results from the study by the autism network of the research units on pediatric psychopharmacology. *The American Journal of Psychiatry*, *162*, 1142–1148.

Meikle, L., Talos, D. M., Onda, H., Pollizzi, K., Rotenberg, A., Sahin, M., … Kwiatkowski, D. J. (2007). A Mouse Model of Tuberous Sclerosis: Neuronal Loss of Tsc1 Causes

Dysplastic and Ectopic Neurons, Reduced Myelination, Seizure Activity, and Limited Survival. *The Journal of Neuroscience*, *27*, 5546–5558.

Meli, N., Sheran, K., Pitsch, J., Krabbe, S., Borger, V., Baumgartner, T., … Blaess, S. (2025). Alterations in dopaminergic innervation and receptors in focal cortical dysplasia. *Brain*, awaf080.

Miner, L. H., Schroeter, S., Blakely, R. D., & Sesack, S. R. (2003). Ultrastructural Localization of the Norepinephrine Transporter in Superficial and Deep Layers of the Rat Prelimbic Prefrontal Cortex and Its Spatial Relationship to Probable Dopamine Terminals. *Journal of Comparative Neurology*, *466*, 478–494.

Mingote, S., Chuhma, N., Kusnoor, S. V, Field, B., Deutch, A. Y., & Rayport, S. (2015). Functional Connectome Analysis of Dopamine Neuron Glutamatergic Connections in Forebrain Regions. *The Journal of Neuroscience*, *35*, 16259 LP – 16271.

Mirzaa, G. M., Campbell, C. D., Solovieff, N., Goold, C., Jansen, L. A., Menon, S., … Dobyns, W. B. (2016). Association of MTOR Mutations With Developmental Brain Disorders, Including Megalencephaly, Focal Cortical Dysplasia, and Pigmentary Mosaicism. *JAMA Neurology*, *73*, 836–845.

Missale, C., Nash, S. R., Robinson, S. W., Jaber, M., & Caron, M. G. (1998). Dopamine Receptors: From Structure to Function. *Physiological Reviews*, *78*, 189–225.

Mohapatra, A. N., & Wagner, S. (2023). The role of the prefrontal cortex in social interactions of animal models and the implications for autism spectrum disorder. *Frontiers in Psychiatry*, *14*. Retrieved from https://www.frontiersin.org/journals/psychiatry/articles/10.3389/fpsyt.2023.1205199

Moore, A. R., Zhou, W.-L., Potapenko, E. S., Kim, E.-J., & Antic, S. D. (2011). Brief dopaminergic stimulations produce transient physiological changes in prefrontal pyramidal neurons. *Brain Research*, *1370*, 1–15.

Morón, J. A., Brockington, A., Wise, R. A., Rocha, B. A., & Hope, B. T. (2002). Dopamine Uptake through the Norepinephrine Transporter in Brain Regions with Low Levels of

the Dopamine Transporter: Evidence from Knock-Out Mouse Lines. *The Journal of Neuroscience*, *22*, 389 LP – 395.

Mühlebner, A., Bongaarts, A., Sarnat, H. B., Scholl, T., & Aronica, E. (2019). New insights into a spectrum of developmental malformations related to mTOR dysregulations: challenges and perspectives. *Journal of Anatomy*, *235*, 521–542.

Muzykewicz, D. A., Newberry, P., Danforth, N., Halpern, E. F., & Thiele, E. A. (2007). Psychiatric comorbid conditions in a clinic population of 241 patients with tuberous sclerosis complex. *Epilepsy & Behavior*, *11*, 506–513.

Najm, I., Lal, D., Alonso Vanegas, M., Cendes, F., Lopes-Cendes, I., Palmini, A., … Blümcke, I. (2022). The ILAE consensus classification of focal cortical dysplasia: An update proposed by an ad hoc task force of the ILAE diagnostic methods commission. *Epilepsia*, *63*, 1899–1919.

Nakagawa, J. M., Donkels, C., Fauser, S., Schulze-Bonhage, A., Prinz, M., Zentner, J., & Haas, C. A. (2017). Characterization of focal cortical dysplasia with balloon cells by layer-specific markers: Evidence for differential vulnerability of interneurons. *Epilepsia*, *58*, 635–645.

Nakamura, S., Ito, Y., Shirasaki, R., & Murakami, F. (2000). Local Directional Cues Control Growth Polarity of Dopaminergic Axons Along the Rostrocaudal Axis. *The Journal of Neuroscience*, *20*, 4112 LP – 4119.

Naneix, F., Marchand, A. R., Di Scala, G., Pape, J. R., & Coutureau, E. (2012). Parallel maturation of goal-directed behavior and dopaminergic systems during adolescence. *Journal of Neuroscience*, *32*, 16223–16232.

Neale, B. M., Kou, Y., Liu, L., Ma'ayan, A., Samocha, K. E., Sabo, A., … Daly, M. J. (2012). Patterns and rates of exonic de novo mutations in autism spectrum disorders. *Nature*, *485*, 242–245.

Nguyen, L. H., & Bordey, A. (2021). Convergent and Divergent Mechanisms of Epileptogenesis in mTORopathies. *Frontiers in Neuroanatomy*, *15*.

https://doi.org/10.3389/fnana.2021.664695

Nguyen, L. H., Mahadeo, T., & Bordey, A. (2019). mTOR Hyperactivity Levels Influence the Severity of Epilepsy and Associated Neuropathology in an Experimental Model of Tuberous Sclerosis Complex and Focal Cortical Dysplasia. *The Journal of Neuroscience*, *39*, 2762 LP – 2773.

Noctor, S. C., Flint, A. C., Weissman, T. A., Dammerman, R. S., & Kriegstein, A. R. (2001). Neurons derived from radial glial cells establish radial units in neocortex. *Nature*, *409*, 714–720.

O'Donnell, P. (2010). Adolescent Maturation of Cortical Dopamine. *Neurotoxicity Research*, *18*, 306–312.

Pachitariu, M., & Stringer, C. (2022). Cellpose 2.0: how to train your own model. *Nature Methods*, *19*, 1634–1641.

Panchaud, N., Péli-Gulli, M.-P., & De Virgilio, C. (2013). Amino Acid Deprivation Inhibits TORC1 Through a GTPase-Activating Protein Complex for the Rag Family GTPase Gtr1. *Science Signaling*, *6*, ra42–ra42.

Park, S. M., Lim, J. S., Ramakrishina, S., Kim, S. H., Kim, W. K., Lee, J., … Lee, J. H. (2018). Brain Somatic Mutations in MTOR Disrupt Neuronal Ciliogenesis, Leading to Focal Cortical Dyslamination. *Neuron*, *99*, 83-97.e7.

Pavăl, D. (2017). A Dopamine Hypothesis of Autism Spectrum Disorder. *Developmental Neuroscience*, *39*, 355–360.

Pavăl, Denis, & Micluția, I. V. (2021). The Dopamine Hypothesis of Autism Spectrum Disorder Revisited: Current Status and Future Prospects. *Developmental Neuroscience*, *43*, 73–83.

Pérez-López, J. L., Contreras-López, R., Ramírez-Jarquín, J. O., & Tecuapetla, F. (2018). Direct Glutamatergic Signaling From Midbrain Dopaminergic Neurons Onto Pyramidal Prefrontal Cortex Neurons. *Frontiers in Neural Circuits*, *12*, 1–10.

Petanjek, Z., Judaš, M., Šimić, G., Rašin, M. R., Uylings, H. B. M., Rakic, P., & Kostović, I. (2011). Extraordinary neoteny of synaptic spines in the human prefrontal cortex. *Proceedings of the National Academy of Sciences*, *108*, 13281–13286.

Peter R., H. (1979). Synaptic density in human frontal cortex — Developmental changes and effects of aging. *Brain Research*, *163*, 195–205.

Peters, K. Z., & Naneix, F. (2022). The role of dopamine and endocannabinoid systems in prefrontal cortex development: Adolescence as a critical period. *Frontiers in Neural Circuits*, *16*. https://doi.org/10.3389/fncir.2022.939235

Petese, A., Fries, F. L., Broske, B., Stumm, R., & Blaess, S. (2022). Lineage Analysis of Cxcr4-Expressing Cells in the Developing Midbrain Suggests That Progressive Competence Restriction in Dopaminergic Progenitor Cells Contributes to the Establishment of Dopaminergic Neuronal Diversity. *ENeuro*, *9*. https://doi.org/10.1523/ENEURO.0052-22.2022

Pham, T. H., & Gardier, A. M. (2019). Fast-acting antidepressant activity of ketamine: highlights on brain serotonin, glutamate, and GABA neurotransmission in preclinical studies. *Pharmacology & Therapeutics*, *199*, 58–90.

Plummer, N. W., Scappini, E. L., Smith, K. G., Tucker, C. J., & Jensen, P. (2017). Two Subpopulations of Noradrenergic Neurons in the Locus Coeruleus Complex Distinguished by Expression of the Dorsal Neural Tube Marker Pax7. *Frontiers in Neuroanatomy*, *11*. https://doi.org/10.3389/fnana.2017.00060

Poduri, A., Evrony, G. D., Cai, X., Elhosary, P. C., Beroukhim, R., Lehtinen, M. K., … Walsh, C. A. (2012). Somatic Activation of AKT3 Causes Hemispheric Developmental Brain Malformations. *Neuron*, *74*, 41–48.

Potter, C. J., Pedraza, L. G., & Xu, T. (2002). Akt regulates growth by directly phosphorylating Tsc2. *Nature Cell Biology*, *4*, 658–665.

Powell, J. M., Plummer, N. W., Scappini, E. L., Tucker, C. J., & Jensen, P. (2019). DEFiNE: A method for enhancement and quantification of fluorescently labeled

axons. *Frontiers in Neuroanatomy*, *12*, 1–11.

Rácz, A., Becker, A. J., Quesada, C. M., Borger, V., Vatter, H., Surges, R., & Elger, C. E. (2021). Post-Surgical Outcome and Its Determining Factors in Patients Operated on With Focal Cortical Dysplasia Type II—A Retrospective Monocenter Study. *Frontiers in Neurology*, *12*. https://doi.org/10.3389/fneur.2021.666056

Raghanti, M. A., Stimpson, C. D., Marcinkiewicz, J. L., Erwin, J. M., Hof, P. R., & Sherwood, C. C. (2008). Cortical dopaminergic innervation among humans, chimpanzees, and macaque monkeys: a comparative study. *Neuroscience*, *155*, 203–220.

Rakic, P, & Lombroso, P. J. (1998). Development of the cerebral cortex: I. Forming the cortical structure. *Journal of the American Academy of Child and Adolescent Psychiatry*, *37*, 116–117.

Rakic, Pasko. (1972). Mode of cell migration to the superficial layers of fetal monkey neocortex. *Journal of Comparative Neurology*, *145*, 61–83.

Rakic, Pasko. (1978). Neuronal migration and contact guidance in the primate telencephalon. *Postgraduate Medical Journal*, *54*, 25 – 40.

Rakic, Pasko. (1995). Corticogenesis in human and nonhuman primates. In *The cognitive neurosciences.* (pp. 127–145). Cambridge, MA, US: The MIT Press.

Rakic, Pasko, Cameron, R. S., & Komuro, H. (1994). Recognition, adhesion, transmembrane signaling and cell motility in guided neuronal migration. *Current Opinion in Neurobiology*, *4*, 63–69.

Ransdell, J. L., Faust, T. B., & Schulz, D. J. (2010). Correlated levels of mRNA and soma size in single identified neurons: Evidence for compartment-specific regulation of gene expression. *Frontiers in Molecular Neuroscience*, *3*, 1–9.

Reader, T. A. (1981). Distribution of catecholamines and serotonin in the rat cerebral cortex: Absolute levels and relative proportions. *Journal of Neural Transmission*, *50*, 13–27.

Rey, R., Suaud-Chagny, M.-F., Bohec, A.-L., Dorey, J.-M., d'Amato, T., Tamouza, R., & Leboyer, M. (2020). Overexpression of complement component C4 in the dorsolateral prefrontal cortex, parietal cortex, superior temporal gyrus and associative striatum of patients with schizophrenia. *Brain, Behavior, and Immunity*, *90*, 216–225.

Reynolds, L. M., & Flores, C. (2021). Mesocorticolimbic Dopamine Pathways Across Adolescence: Diversity in Development. *Frontiers in Neural Circuits*, *15*, 1–17.

Reynolds, L. M., Pokinko, M., Torres-Berrío, A., Cuesta, S., Lambert, L. C., Del Cid Pellitero, E., … Flores, C. (2018). DCC Receptors Drive Prefrontal Cortex Maturation by Determining Dopamine Axon Targeting in Adolescence. *Biological Psychiatry*, *83*, 181–192.

Ribierre, T., Deleuze, C., Bacq, A., Baldassari, S., Marsan, E., Chipaux, M., … Baulac, S. (2018). *Second-hit mosaic mutation in mTORC1 repressor DEPDC5 causes focal cortical dysplasia – associated epilepsy*. *128*.

Robbins, T. W., & Arnsten, A. F. T. (2009). The neuropsychopharmacology of fronto-executive function: Monoaminergic modulation. *Annual Review of Neuroscience*, *32*, 267–287.

Robertson, S. D., Plummer, N. W., de Marchena, J., & Jensen, P. (2013). Developmental origins of central norepinephrine neuron diversity. *Nature Neuroscience*, *16*, 1016–1023.

Rocha, L., Alonso-Vanegas, M., Villeda-Hernández, J., Mújica, M., Cisneros-Franco, J. M., López-Gómez, M., … Borsodi, A. (2012). Dopamine abnormalities in the neocortex of patients with temporal lobe epilepsy. *Neurobiology of Disease*, *45*, 499–507.

Rosenberg, D. R., & Lewis, D. A. (1994). Changes in the dopaminergic innervation of monkey prefrontal cortex during late postnatal development: A tyrosine hydroxylase immunohistochemical study. *Biological Psychiatry*, *36*, 272–277.

Rosenberg, D. R., & Lewis, D. A. (1995). Postnatal maturation of the dopaminergic

innervation of monkey prefrontal and motor cortices: a tyrosine hydroxylase immunohistochemical analysis. *The Journal of Comparative Neurology*, *358*, 383–400.

Rotaru, D. C., Lewis, D. A., & Gonzalez-Burgos, G. (2007). Dopamine D1 receptor activation regulates sodium channel-dependent EPSP amplification in rat prefrontal cortex pyramidal neurons. *The Journal of Physiology*, *581*, 981–1000.

Rothmond, D. A., Weickert, C. S., & Webster, M. J. (2012). Developmental changes in human dopamine neurotransmission: cortical receptors and terminators. *BMC Neuroscience*, *13*, 18.

Santana, N., & Artigas, F. (2017). Laminar and Cellular Distribution of Monoamine Receptors in Rat Medial Prefrontal Cortex. *Frontiers in Neuroanatomy*, *11*, 87.

Santana, N., Mengod, G., & Artigas, F. (2009). Quantitative analysis of the expression of dopamine D1 and D2 receptors in pyramidal and GABAergic neurons of the rat prefrontal cortex. *Cerebral Cortex*, *19*, 849–860.

Schambra, U. B., Duncan, G. E., Breese, G. R., Fornaretto, M. G., Caron, M. G., & Fremeau Jr, R. T. (1994). Ontogeny of D_{1a} and D_2 dopamine receptor subtypes in rat brain using in situ hybridization and receptor binding. *Neuroscience*, *62*, 65–85.

Schur, S., Allen, V., White, A., Mirsky, D., Stence, N., O'Neill, B., … Laoprasert, P. (2018). Significance of FDG-PET Hypermetabolism in Children with Intractable Focal Epilepsy. *Pediatric Neurosurgery*, *53*, 153–162.

Seamans, J. K., & Yang, C. R. (2004). The principal features and mechanisms of dopamine modulation in the prefrontal cortex. *Progress in Neurobiology*, *74*, 1–58.

Séguéla, P., Watkins, K. C., & Descarries, L. (1988). Ultrastructural features of dopamine axon terminals in the anteromedial and the suprarhinal cortex of adult rat. *Brain Research*, *442*, 11–22.

Seifer, G., Blenkmann, A., Princich, J. P., Consalvo, D., Papayannis, C., Muravchik, C., &

Kochen, S. (2012). Noninvasive Approach to Focal Cortical Dysplasias: Clinical, EEG, and Neuroimaging Features. *Epilepsy Research and Treatment*, *2012*, 736784.

Shaw, P., Eckstrand, K., Sharp, W., Blumenthal, J., Lerch, J. P., Greenstein, D., … Rapoport, J. L. (2007). Attention-deficit/hyperactivity disorder is characterized by a delay in cortical maturation. *Proceedings of the National Academy of Sciences*, *104*, 19649–19654.

Sidman, R. L., & Rakic, P. (1973). Neuronal migration, with special reference to developing human brain: a review. *Brain Research*, *62*, 1–35.

Sierra-Marcos, A., Maestro, I., Falcón, C., Donaire, A., Setoain, J., Aparicio, J., … Bargalló, N. (2013). Ictal EEG-fMRI in localization of epileptogenic area in patients with refractory neocortical focal epilepsy. *Epilepsia*, *54*, 1688–1698.

Siuta, M. A., Robertson, S. D., Kocalis, H., Saunders, C., Gresch, P. J., Khatri, V., … Galli, A. (2010). Dysregulation of the Norepinephrine Transporter Sustains Cortical Hypodopaminergia and Schizophrenia-Like Behaviors in Neuronal Rictor Null Mice. *PLOS Biology*, *8*, e1000393.

Staal, W. G. (2015). Autism, DRD3 and repetitive and stereotyped behavior, an overview of the current knowledge. *European Neuropsychopharmacology*, *25*, 1421–1426.

Steinbusch, H. W. M. (1981). Distribution of serotonin-immunoreactivity in the central nervous system of the rat—Cell bodies and terminals. *Neuroscience*, *6*, 557–618.

Strac, D. S., Pivac, N., Smolders, I. J., Fogel, W. A., De Deurwaerdere, P. D., & Di Giovanni, G. (2016). Monoaminergic mechanisms in epilepsy may offer innovative therapeutic opportunity for monoaminergic multi-target drugs. *Frontiers in Neuroscience*, *10*, 1–26.

Stringer, C., Wang, T., Michaelos, M., & Pachitariu, M. (2021). Cellpose: a generalist algorithm for cellular segmentation. *Nature Methods*, *18*, 100–106.

Subramanian, L., Calcagnotto, M. E., & Paredes, M. F. (2020). Cortical Malformations: Lessons in Human Brain Development. *Frontiers in Cellular Neuroscience*, *13*, 1–17.

Szczurkowska, J., Cwetsch, A. W., Dal Maschio, M., Ghezzi, D., Ratto, G. M., & Cancedda, L. (2016). Targeted in vivo genetic manipulation of the mouse or rat brain by in utero electroporation with a triple-electrode probe. *Nature Protocols*, *11*, 399–412.

Szot, P., Lester, M., Laughlin, M. L., Palmiter, R. D., Liles, L. C., & Weinshenker, D. (2004). The anticonvulsant and proconvulsant effects of alpha2-adrenoreceptor agonists are mediated by distinct populations of alpha2A-adrenoreceptors. *Neuroscience*, *126*, 795–803.

Tarazi, F. I., & Baldessarini, R. J. (2000). Comparative postnatal development of dopamine D1, D2 and D4 receptors in rat forebrain. *International Journal of Developmental Neuroscience*, *18*, 29–37.

Team, R. C. (2020). *R: A Language and Environment for Statistical Computing*. Vienna, Austria: R Foundation for Statistical Computing.

Tee, A. R., Manning, B. D., Roux, P. P., Cantley, L. C., & Blenis, J. (2003). Tuberous sclerosis complex gene products, Tuberin and Hamartin, control mTOR signaling by acting as a GTPase-activating protein complex toward Rheb. *Current Biology : CB*, *13*, 1259–1268.

Torres-Berrío, A., Hernandez, G., Nestler, E. J., & Flores, C. (2020). The Netrin-1/DCC Guidance Cue Pathway as a Molecular Target in Depression: Translational Evidence. *Biological Psychiatry*, *88*, 611–624.

Trantham-Davidson, H., Kröner, S., & Seamans, J. K. (2008). Dopamine modulation of prefrontal cortex interneurons occurs independently of DARPP-32. *Cerebral Cortex (New York, N.Y. : 1991)*, *18*, 951–958.

Trantham-Davidson, H., Neely, L. C., Lavin, A., & Seamans, J. K. (2004). Mechanisms Underlying Differential D1 versus D2 Dopamine Receptor Regulation of Inhibition in Prefrontal Cortex. *The Journal of Neuroscience*, *24*, 10652–10659.

Tripathi, P. P., & Bozzi, Y. (2015). The role of dopaminergic and serotonergic systems in

neurodevelopmental disorders: A focus on epilepsy and seizure susceptibility. *BioImpacts*, *5*, 97–102.

Tritsch, N. X., & Sabatini, B. L. (2012). Dopaminergic Modulation of Synaptic Transmission in Cortex and Striatum. *Neuron*, *76*, 33–50.

Trottier, S., Evrard, B., Biraben, A., & Chauvel, P. (1994). Altered patterns of catecholaminergic fibers in focal cortical dysplasia in two patients with partial seizures. *Epilepsy Research*, *19*, 161–179.

Trottier, S., Evrard, B., Vignal, J. P., Scarabin, J. M., & Chauvel, P. (1996). The serotonergic innervation of the cerebral cortex in man and its changes in focal cortical dysplasia. *Epilepsy Research*, *25*, 79–106.

Tseng, K. Y., & O'Donnell, P. (2004). Dopamine-glutamate interactions controlling prefrontal cortical pyramidal cell excitability involve multiple signaling mechanisms. *The Journal of Neuroscience : The Official Journal of the Society for Neuroscience*, *24*, 5131–5139.

Veersema, T. J., van Schooneveld, M. M. J., Ferrier, C. H., van Eijsden, P., Gosselaar, P. H., van Rijen, P. C., … Braun, K. P. J. (2019). Cognitive functioning after epilepsy surgery in children with mild malformation of cortical development and focal cortical dysplasia. *Epilepsy & Behavior*, *94*, 209–215.

Verney, C. (1999). Distribution of the Catecholaminergic Neurons in the CentralNervous System of Human Embryos and Fetuses. *MICROSCOPY RESEARCH AND TECHNIQUE*.

Verney, Catherine, Milosevic, A., Alvarez, C., & Berger, B. (1993). Immunocytochemical evidence of well-developed dopaminergic and noradrenergic innervations in the frontal cerebral cortex of human fetuses at midgestation. *The Journal of Comparative Neurology*, *336*, 331–344.

Vincent, S. L., Khan, Y., & Benes, F. M. (1993). Cellular distribution of dopamine D1 and D2 receptors in rat medial prefrontal cortex. *The Journal of Neuroscience*, *13*, 2551

LP – 2564.

Vitalis, T., Ansorge, M. S., & Dayer, A. G. (2013). Serotonin homeostasis and serotonin receptors as actors of cortical construction: Special attention to the 5-HT3A and 5-HT6 receptor subtypes. *Frontiers in Cellular Neuroscience*, *7*, 1–20.

Vosberg, D. E., Leyton, M., & Flores, C. (2020). The Netrin-1/DCC guidance system: dopamine pathway maturation and psychiatric disorders emerging in adolescence. *Molecular Psychiatry*, *25*, 297–307.

Wallace, J. A., & Lauder, J. M. (1983). Development of the serotonergic system in the rat embryo: An immunocytochemical study. *Brain Research Bulletin*, *10*, 459–479.

Waterhouse, B. D., & Chandler, D. J. (2016). Heterogeneous organization and function of the central noradrenergic system. *Brain Research*, *1641*, v–x.

Weickert, C. S., Webster, M. J., Gondipalli, P., Rothmond, D., Fatula, R. J., Herman, M. M., … Akil, M. (2007). Postnatal alterations in dopaminergic markers in the human prefrontal cortex. *Neuroscience*, *144*, 1109–1119.

Weinshenker, D., Szot, P., Miller, N. S., & Palmiter, R. D. (2001). α₁ and β₂ Adrenoreceptor Agonists Inhibit Pentylenetetrazole-Induced Seizures in Mice Lacking Norepinephrine. *Journal of Pharmacology and Experimental Therapeutics*, *298*, 1042 LP – 1048.

Wu, J., Xiao, H., Sun, H., Zou, L., & Zhu, L.-Q. (2012). Role of Dopamine Receptors in ADHD: A Systematic Meta-analysis. *Molecular Neurobiology*, *45*, 605–620.

Wu, X., Sosunov, A. A., Lado, W., Teoh, J. J., Ham, A., Li, H., … Tang, G. (2022). Synaptic hyperexcitability of cytomegalic pyramidal neurons contributes to epileptogenesis in tuberous sclerosis complex. *Cell Reports*, *40*. https://doi.org/10.1016/j.celrep.2022.111085

Yang, C. R., & Seamans, J. K. (1996). Dopamine D1 receptor actions in layers V-VI rat prefrontal cortex neurons in vitro: modulation of dendritic-somatic signal integration. *The Journal of Neuroscience : The Official Journal of the Society for Neuroscience*,

16, 1922–1935.

Yokokura, M., Takebasashi, K., Takao, A., Nakaizumi, K., Yoshikawa, E., Futatsubashi, M., … Ouchi, Y. (2021). In vivo imaging of dopamine D1 receptor and activated microglia in attention-deficit/hyperactivity disorder: a positron emission tomography study. *Molecular Psychiatry*, *26*, 4958–4967.

Zecevic, N., & Verney, C. (1995). Development of the catecholamine neurons in human embryos and fetuses, with special emphasis on the innervaton of the cerebral cortex. *Journal of Comparative Neurology*, *351*, 509–535.

Zhang, Z.-W., Burke, M. W., Calakos, N., Beaulieu, J.-M., & Vaucher, E. (2010). Confocal analysis of cholinergic and dopaminergic inputs onto pyramidal cells in the prefrontal cortex of rodents. *Frontiers in Neuroanatomy*, *4*. Retrieved from https://www.frontiersin.org/journals/neuroanatomy/articles/10.3389/fnana.2010.00021

Zhang, Z.-W., Kang, J. Il, & Vaucher, E. (2011). Axonal Varicosity Density as an Index of Local Neuronal Interactions. *PLOS ONE*, *6*, e22543.

Zhou, M., Li, W., Huang, S., Song, J., Kim, J. Y., Tian, X., … Silva, A. J. (2013). mTOR Inhibition Ameliorates Cognitive and Affective Deficits Caused by Disc1 Knockdown in Adult-Born Dentate Granule Neurons. *Neuron*, *77*, 647–654.

Zoncu, R., Efeyan, A., & Sabatini, D. M. (2011). mTOR: from growth signal integration to cancer, diabetes and ageing. *Nature Reviews Molecular Cell Biology*, *12*, 21–35.

9. Acknowledgements

I would like to express my deepest gratitude to everyone who supported me throughout this thesis. Their help has been invaluable, and this work would not have been possible without them.

First and foremost, I am immensely grateful to my supervisors, Prof. Dr. Sandra Blaess and Prof. Dr. Albert Becker, for trusting me with this exciting research project. I am especially thankful to Sandra for her continuous support, insightful guidance, and patience over the years. Her passion for research and knowledge has been truly inspiring and has encouraged my own enthusiasm for the world of science. I am also deeply thankful to Albert for his guidance and valuable insights, particularly in the analysis of human biopsies. The support from both of you during professional and personal challenges has been invaluable, and I cannot thank you enough.

I would like to extend my gratitude to Prof. Dr. Rainer Surges and Prof. Premsyl Jiruska, MD, PhD for agreeing to be on my thesis committee.

A heartfelt thanks to the members of the AG Becker/Schoch group, especially Dr. Silvia Cases Cunillera and Idil Uyan Ariöz, for teaching me the technique of *in utero* electroporation and for always being available to offer support during these experiments. I am also particularly grateful to Dr. Julika Pitsch for her meticulous work on the TVAs and her invaluable assistance. Special thanks to Dr. Hannes Beckert and the microscopy core facility at the Medical Faculty of the University of Bonn for their support with imaging.

To my former and current colleagues in the AG Blaess group, thank you for creating such an incredible working environment. I am especially grateful to Dr. Marianna Tolve, Alessandro Petese, Adrián López Fernández, Dr. Ushna Islam, Philipp Grunwald, Rui Lois Tan, Catarina Pacheco, Lena Fahrbach, Paula Siebrecht, Daniel Pliev, Anneke Fuß, and Dr. Yuko Shida for their support, encouragement, and the memories we shared during lab outings, drinking sessions, and karaoke nights. I am especially grateful to Marianna for her help during the initial phase of my PhD and to Ushna, whose unwavering support and companionship from the very beginning have been a constant source of strength, sharing countless meaningful moments with me throughout this journey. I am deeply grateful to

Anneke, whose warmth, encouragement, and support during the final stages of my PhD brought comfort and made the final days in the lab truly memorable. I am also thankful to Annika Diebels for her technical help in this thesis and personal support. I am deeply grateful to Katherine Sheran from AG Krabbe for her crucial contributions to the pipeline analysis and her dedicated support throughout the troubleshooting process. I would also like to extend my gratitude to the student assistants throughout the years — Alesja, Julian, Antonia, Jonathan, Jannika, Annika, Martin, and Katrin — their dedication and efforts in keeping the lab running efficiently.

To my family, I owe everything to my parents, Agim and Vjollca, whose unconditional love and encouragement have been my foundation. To my siblings, Orgesa and Olsi, your steadfast emotional support has given me strength throughout this process. I am also grateful to my grandmother, whose loving presence I have always felt. I hope I have made you all proud.

I would also like to thank my dear friends — Karo, Olta, Klea, and Emma — for their committed friendship. Sharing laughs, drinks, and support with you made this journey far more enjoyable and manageable.

Finally, my deepest gratitude is reserved for my fiancé, Eckard. From the very beginning of my journey in Bonn and throughout this PhD, he has been my biggest cheerleader during tough times and my partner in every sense. His love, support, and delicious meals have been the best part of coming home after long days of work.

To all of you, **faleminderit!**